

Photo-Physical Characterization of Flavin-Pyrene-Phenothiazine Molecular Photonic Complexes



Dissertation
zur Erlangung des Doktorgrades
der Naturwissenschaften
(Dr. rer. nat.)
der Fakultät Physik
der Universität Regensburg

vorgelegt von
Javid Shirdel
aus Tabriz, Iran

Regensburg 2007

Diese Arbeit wurde angeleitet von Prof. Dr. A. Penzkofer.

Das Promotionsgesuch wurde am 12. März 2007 eingereicht.

Prüfungsausschuß:

Vorsitzender: Prof. Dr. I. Morgenstern

1. Gutachter: Prof. Dr. A. Penzkofer

2. Gutachter: Prof. Dr. J. Zweck

weiterer Prüfer: Prof. Dr. C. Strunk

*To my Parents
and Sarah*

Contents:

1. Introduction	1
2. Photophysical and Photochemical Fundamentals	5
2.1 Absorption	5
2.1.1 Classification of molecular orbitals	5
2.1.2 Classification of electronic states	7
2.1.3 Beer-Lambert law	8
2.1.4 Selection rules	8
2.1.5 The Franck-Condon Principle	9
2.2 Deactivation of excited molecules	10
2.2.1 Internal conversion	11
2.2.2 Fluorescence	12
2.2.3 Intersystem crossing and phosphorescence	13
2.3 Fluorescence lifetime and quantum yield	14
2.4 Stimulated emission cross-section and radiative lifetime	15
2.5 Degree of fluorescence polarisation and molecular reorientation time	16
2.6 Energy transfer	17
2.6.1 Förster-type energy transfer	19
2.7 Electron Transfer	21
3. Experimental	25
3.1 Investigated dyes	25
3.2 Absorption detection	29
3.3 Fluorescence spectra	30
3.4 The fluorescence lifetimes	33
3.4.1 Single-shot real time detection	33

3.4.2	Fluorescence up-conversion	34
3.5	Ground state absorption recovery	36
3.6	Photo-degradation	37
3.7	Mass spectroscopy	38
4.	Results and discussion	39
4.1	Phenyl-isoalloxazines dye IAE and BrPF	39
4.1.1	Results	39
4.1.2	Discussion	56
4.2	Pyrene and 1-methylpyrene	62
4.2.1	Results	62
4.2.2	Discussion	68
4.3	Heptyl-phenothiazine and heptyl-phenyl-phenothiazine	71
4.3.1	Results	71
4.3.2	Discussion	76
4.4	Pyrene-flavin dyad (PFD)	78
4.4.1	Results	78
4.4.2	Discussion	85
4.5	Phenothiazine-flavin dyad (PTFD)	91
4.5.1	Results	91
4.5.2	Discussion	97
4.6	Pyrene-flavin-phenothiazine triad (PYFPT)	107
4.6.1	Results	107
4.6.2	Discussion	114
5.	Comparative discussion	120
6.	Conclusions	126
7.	References	128

8. Acknowledgements

1. Introduction

Information technology has revolutionized daily life in the last decades. The continuously increasing amount of data to be stored at high speed stimulated the search for molecular devices of ultra-fast response. Molecular electronic is one of the fields which deal with this problem. Molecular electronics constitutes a multidisciplinary research area focusing on the potential utilization of molecular scale systems and molecular materials for electronics or optoelectronics. The study of molecular electronics has an ambitious but realistic goal: the use of synthesis and assembly on a molecular level to achieve a huge density of devices molecular wires, switches, rectifiers, transistors and memories. It foresees applications not only in standard electronics but also some unique to molecular systems, for instance sensors based on molecular recognition, and molecular interfaces with biological systems [Fer01, Jor97, Car88, Mah96].

Molecular switches are active components of molecular electronic devices capable of inducing chemical and physical changes in response to external stimuli such as electrical current, light, and biological impulses. An optoelectronic molecular switch is a molecular system which possesses electronic properties that can be triggered or controlled with the aid of light or electrochemical potential. The most interesting natural process assisted by a photonic switch is the phenomenon of vision in living systems. Thereby rhodopsin undergoes changes in geometry upon optical excitation, altering from the cis to the trans conformation on a subpicosecond time scale, and this is responsible for the various switching processes in vision. Over recent years there have been several attempts to design molecular switches with the goal of developing molecular electronic devices, expected to be a key technology of the future. Photoresponsive molecular electronic switches in particular are of great interest, since use of light as an external stimulus allows rapid and clean interconversions of distinctly

1. Introduction

different states. Several classes of photoresponsive molecular switches are known, operating through various processes like reversible bond formation and breaking, cis-trans isomerization, photoinduced electron transfer and energy transfer. Photoinduced electron transfer and energy transfer are the most interesting rapid switching mechanisms. Since energy and electron transfer processes can occur on a subpicosecond timescale, it is possible to produce devices that respond with equal rapidity. Fluorescence emission is perhaps the most widely exploited property in the design of photoinduced electron transfer molecular switches, since it is extremely sensitive to various perturbations such as solvent polarity, donor-acceptor interactions, and the presence of metal ions. Several systems have been used in the design of logic gates and molecular sensors [Fer01, Jor97].

Covalently linked molecules of electron donor and acceptor chromophore can be used to perform switching operations. It is possible to tune both the optical and electrochemical properties of a multicomponent system by selecting the appropriate electron donors and acceptors. Generally, these systems consist of an acceptor chromophore (A), a bridging group (B), and a donor chromophore (D). Absorption of a photon in a donor-acceptor system results in one of two processes: photoinduced electron transfer from donor to acceptor, resulting in a charge-separated state, or energy (excitation) transfer from donor to acceptor.

In this thesis an absorption and emission spectroscopic characterisation of a pyrene-isoalloxazine dyad, a phenothiazine-isoalloxazine dyad, and a pyrene-isoalloxazine-phenothiazine triad is undertaken. For an understanding of the electron transfer and energy transfer processes in these dyads and the triad a detailed knowledge of the photo-physical behaviour of the constituents is necessary.

Isoalloxazine dyes covalently linked to other dyes in donor acceptor systems with bridges, antennas, and mediators are artificial model systems for biological counterparts [Kön97, She03, She02, Tri05]. They gain importance in photo-voltaic systems, molecular switching devices, and molecular logics applications [Jor97, Car88, Mah96].

1. Introduction

Isoalloxazine forms the building block of the huge family of flavins [Hol05, Kam71, Yag94, Ste97] with rich redox chemistry [Mül92, Pal97], photochemistry [Hee82], and biochemical activity in enzymes [Mül92, Pal97, Fri88] and photoreceptors [Bat03, Bri05, Häd06]. The optical spectroscopy of isoalloxazine dyes (flavins) is reviewed in [She03, Mül92, Hee82, Hee91, Son71]. 10-phenyl-isoalloxazine dyes, which are applied in the dyads and the triad studied here, were investigated in [Kir95, Kna76, Kna74, Kir96, Pro04, Shi06].

Pyrene is an important polycyclic aromatic hydrocarbon [Ber71, Mur93, Win93, Vul05]. It is frequently used for fluorescence labelling of water-soluble polymers [Win93], silicas, aluminas, clays, and zeolites [Ram91, Kra91]. It is also an important fluorescence label in DNA research and molecular sensing [Wag05, Str04, Str02, Car93]. Optical spectroscopic data on pyrene are found in [Ber71, Mur93, Win93, Bir70, Har80, Kar95, Nak73, Van98]. Environmental effects on the absorption strength and on the fluorescence behaviour of pyrene [Kal77, Lia79, Lan83, Kar95] opens the application of pyrene in local environmental sensing. The pyrene derivative 1-methylpyrene, which is a constituent of the studied pyrene-isoalloxazine dyad, reduces the high symmetry of pyrene and thereby increases the absorption strength of the symmetry-forbidden S_0 - S_1 transition [Lia80, Zeg84].

Phenothiazine derivatives are a pharmaceutically important class of heterocycles, known as pharmacophores in sedatives, tranquilizers, antiepileptics, antituberculotics, antipyretics, antitumor agents, bactericides, and parasiticides [Sai06, Bod68]. The phenothiazine chemistry is described in [Bod68, Sai98, Sai84]. Optical spectroscopic data on phenothiazine are found in [Rag64, Dom77, Kaw86, Kaw86b, Bau01]. 3-phenyl-phenothiazine (constituent in investigated phenothiazine-flavin dyad) is considerably stronger absorbing than phenothiazine [She03, Pro04].

The next chapter of this dissertation treats photophysical and photochemical fundamentals such as photo-excitation and relaxation, energy transfer and electron transfer.

1. Introduction

In the chapter 3, first the investigated organic molecules are introduced and then the different experimental setups and methods are discussed which have been applied for measurements of absorption cross-sections, fluorescence quantum distributions and quantum yields, fluorescence lifetimes, absorption transients, photo-degradations, and mass spectra.

In the chapter 4, the experimental results are presented and discussed.

Some overall discussion is presented in chapter 5, and conclusions are given at the end.

2. Photophysical and Photochemical Fundamentals

2.1 Absorption

An electronic transition consists of the promotion of an electron from one occupied orbital of a molecule to another unoccupied orbital. The transition may be caused by the absorption of a photon. Generally the molecule is initially in its electronic ground state and light absorption brings it to an excited state.

2.1.1 Classification of Molecular Orbitals

A σ orbital can be formed either from two s atomic orbitals, or from one s and one p atomic orbital, or from two p atomic orbitals having a collinear axis of symmetry. The bond formed in this way is called a σ bond. A π orbital is formed from two p atomic orbitals overlapping laterally. The resulting bond is called a π bond (Figure 2.1). For example in ethylene ($CH_2 = CH_2$), the two carbon atoms are linked by one σ and one π bond. Absorption of a photon of appropriate energy can promote one of the π electrons to an antibonding orbital denoted by π^* . The transition is then called $\pi \rightarrow \pi^*$. A molecule may also possess non-bonding electrons located on heteroatoms such as oxygen or nitrogen. The corresponding molecular orbitals are called n orbitals. Promotion of a non-bonding electron to an antibonding orbital is possible and the associated transition is denoted by $n \rightarrow \pi^*$ [Bal65, Alb85].

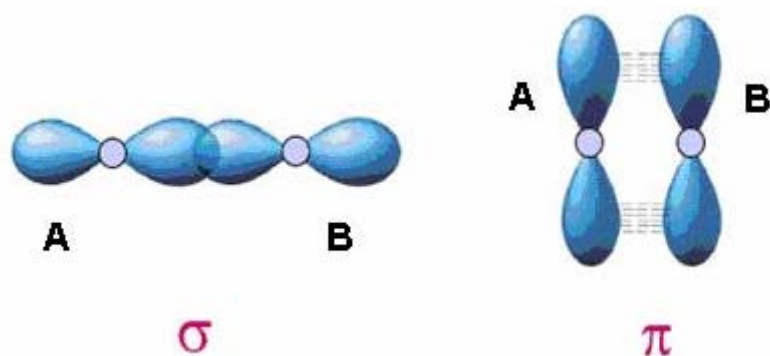


Figure 2.1: Illustration of σ and π orbital by two p atomic orbitals of A and B.

To illustrate the orbital energy levels, Figure 2.2 shows the formaldehyde (CH_2O) molecule as an example, with all possible transitions. In absorption and fluorescence spectroscopy, two important types of orbitals are considered: the Highest Occupied Molecular Orbitals (HOMO) and the Lowest Unoccupied Molecular Orbitals (LUMO).

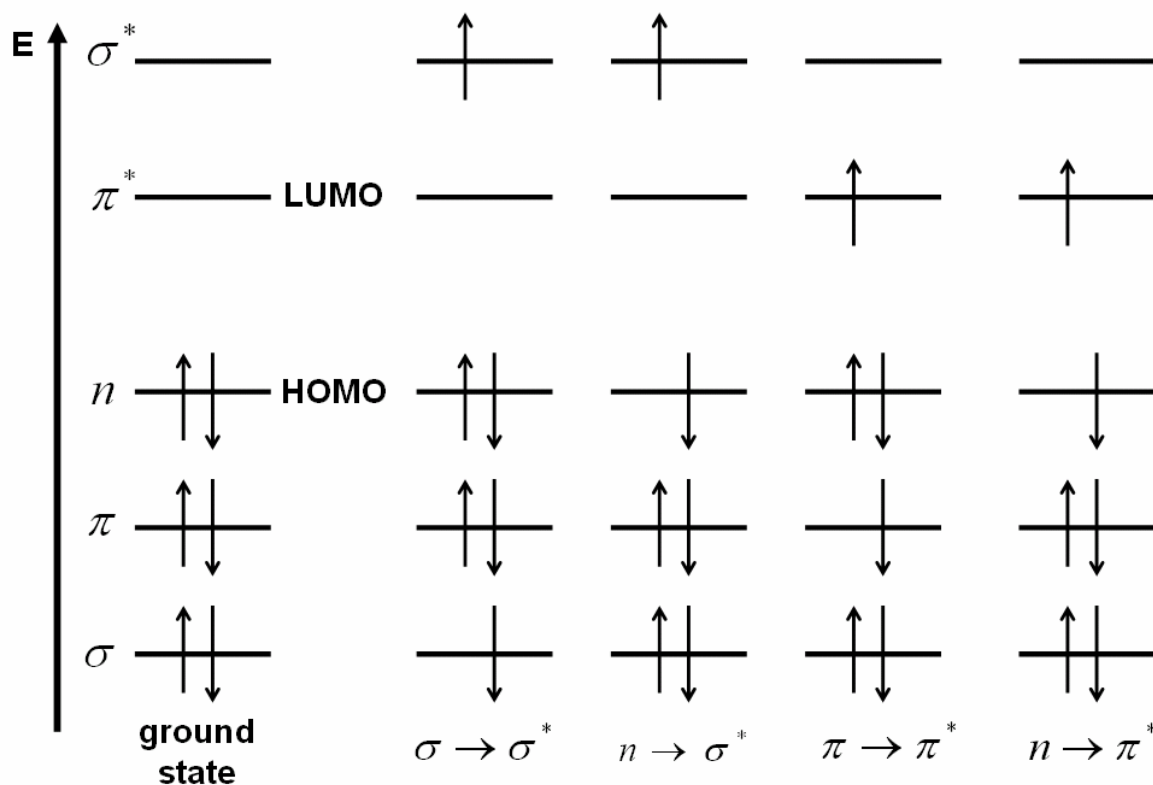


Figure 2.2: Energy level of molecular orbitals in formaldehyde (HOMO: Highest Occupied Molecular orbitals; LUMO: Lowest Unoccupied Molecular Orbitals) and possible electronic transitions [Val02].

2.1.2 Classification of Electronic States

The electronic state of a molecule is characterized by its total spin and the degree of excitation. In the ground state for most molecules the total spin is $S=0$, here, all electrons (each of them with $S=1/2$) are paired with anti-parallel spin. When exciting a single electron, the two resulting unpaired electrons can either be parallel ($S=1$) or anti-parallel ($S=0$). According to the resulting multiplicity of the states (number of potential realizations with the same total energy) the $S=0$ and $S=1$ states are called singlet (S) and triplet (T) states, respectively. The level of excitation is indicated by subscript numbers, 0 is the ground state and 1 and 2,... are excited states with increasing energy (Figure 2.3). The triplet state has a lower energy than the singlet state of the same configuration due to the exchange interaction, [Val02].

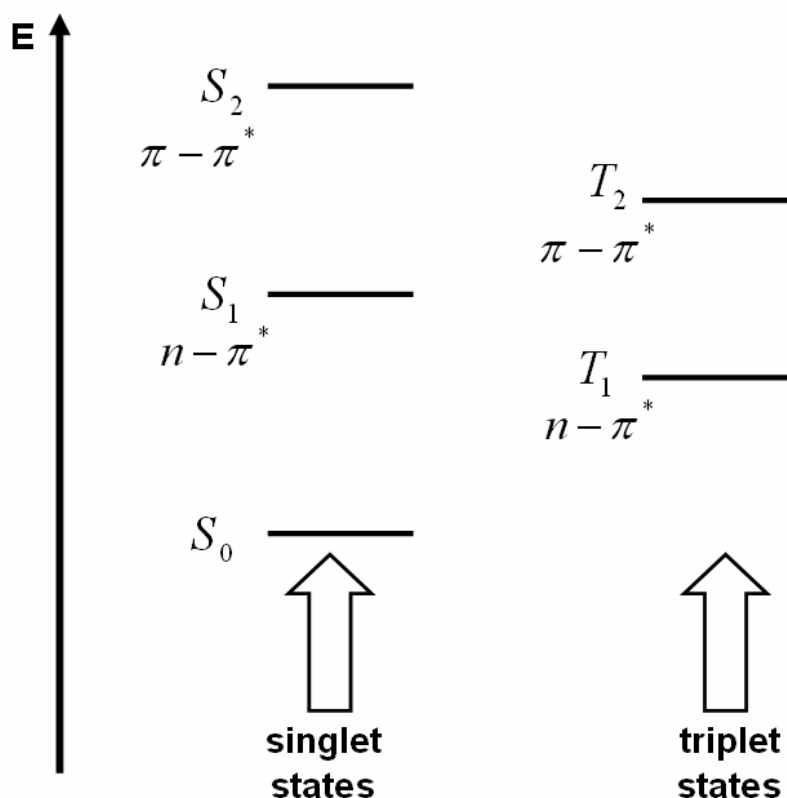


Figure 2.3: Distinction between singlet and triplet states, using formaldehyde as an example

2.1.3 Beer-Lambert law

The efficiency of light absorption at a wavelength λ of an absorbing medium may be described by the transmission $T(\lambda)$:

$$T(\lambda) = \frac{I}{I_0} \quad (2.1)$$

Where I_0 and I are the light intensities of the beam entering and leaving the absorbing medium, respectively. According to Beer-Lambert Law the transmission depends on the absorption coefficient $\alpha(\lambda)$ and the absorption cross-section $\sigma_a(\lambda)$ in the following way:

$$T(\lambda) = e^{-\alpha(\lambda)l} = e^{-N\sigma_a(\lambda)l} = e^{-N_A\sigma_a(\lambda)cl} \quad (2.2)$$

where l is the sample length, N is the number density of dye molecules, N_A is Avogadro constant and C is the molar concentration. The absorption cross-section $\sigma_a(\lambda)$ characterizes the photon-capture area of a molecule. Rewriting of Equation 2.2 gives

$$\sigma_a(\lambda) = \frac{\alpha(\lambda)}{N} = -\frac{\ln(T)}{Nl} \quad (2.3)$$

2.1.4 Selection rules

The transition dipole moment $\vec{\mu}$ is determined by the displacement of charges between initial state $|a\rangle$ and final state $|b\rangle$ of an excitation, i.e. $\vec{\mu} = \langle a|er|b\rangle$. Molecules with their absorption transition moment parallel to the electric field vector of a linearly polarized incident light are preferentially excited.

There are some rules for electronic transitions: transitions between states of equal spin multiplicities are allowed and between different spin multiplicities are forbidden, i.e. singlet-singlet and triplet-triplet transitions are allowed, but singlet-triplet or triplet-singlet transitions are forbidden by electric dipole interaction. However, there is always a weak interaction between the wavefunctions of different multiplicities via spin-orbit coupling. This leads to a

small but non-negligible absorption and emission between a singlet state and a triplet state or vice versa. A transition can be forbidden for symmetry reasons (cancellation of transition matrix element). Also symmetry-forbidden transitions may be observed weakly because the molecular vibrations cause some departure from perfect symmetry (vibronic coupling) [Atk97].

2.1.5 The Franck-Condon Principle

The motion of electrons is much more rapid than that of the nuclei (i.e. the molecular vibrations) [Atk97]. Promotion of an electron to an antibonding molecular orbital upon excitation takes about 10^{-15} s, which is very quick compared to the characteristic time for molecular vibration (10^{-10} – 10^{-12} s). This situation is the basis of the Frank-Condon principle: an electronic transition occurs without changes of the position of the nuclei in the molecular entity and its environment. The resulting state is called a Frank-Condon state, and the transition is called Frank-Condon transition (Figure 2.4).

At room temperature, most of the molecules are in the lowest vibrational level of the ground state (level population according to Boltzmann distribution). Excitation from the ground state potential energy minimum to the excited state potential energy surface occurs fast (no change in configuration coordinate system). The absorption of the vibrational levels in the excited state is determined by the overlap of ground state and excited state wavefunction (Franck-Condon integral $S = \langle i | f \rangle$ where $|i\rangle$ is the electronic wavefunction in the ground state and $|f\rangle$ is the electronic wavefunction in the excited state). There are several vibronic transitions whose interaction strength depends on the relative position and shape of the potential energy curves (Figure 2.4) [Val02].

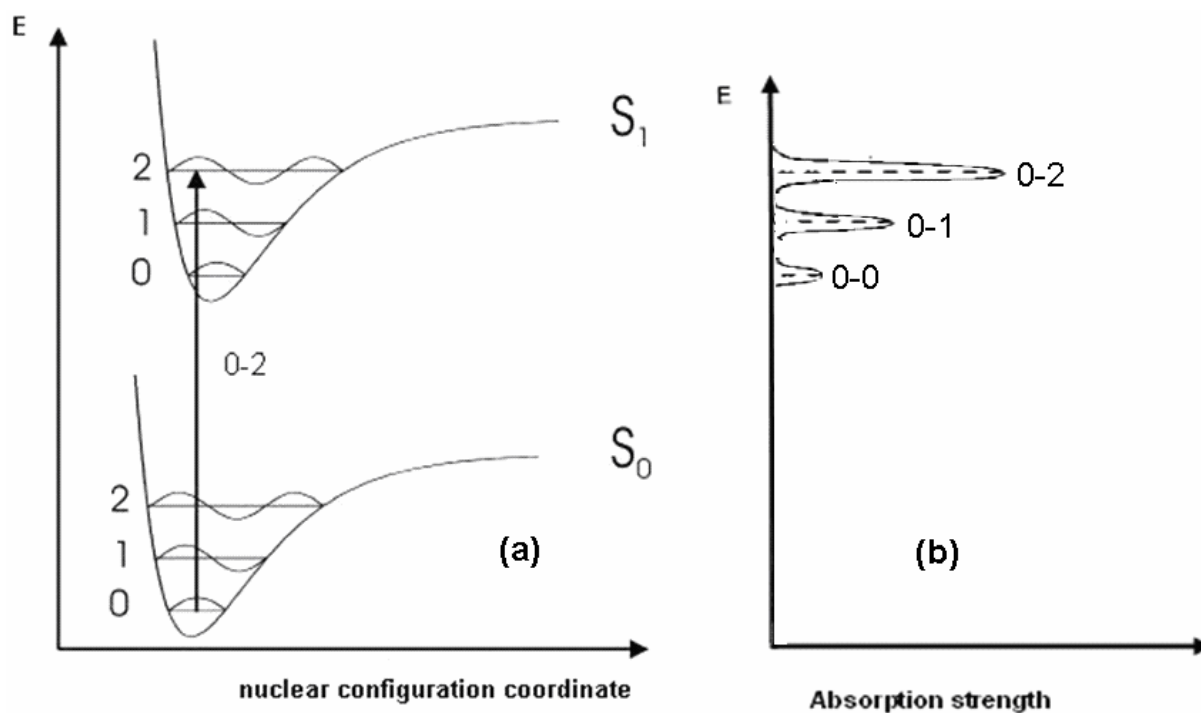


Figure 2.4: Potential energy diagram with vertical transition (Franck-Condon principle) (a) and illustration of absorption strength (b).

2.2 Deactivation of excited molecules

Excited molecules lose their excess energy by different chemical and physical processes. The Perrin-Jablonski diagram (Figure 2.5) is often used to visualize the physical processes of excitation and deactivation: photon absorption, internal conversion (IC), fluorescence, intersystem crossing (ISC), and phosphorescence. The various deactivation processes are discussed in the following.

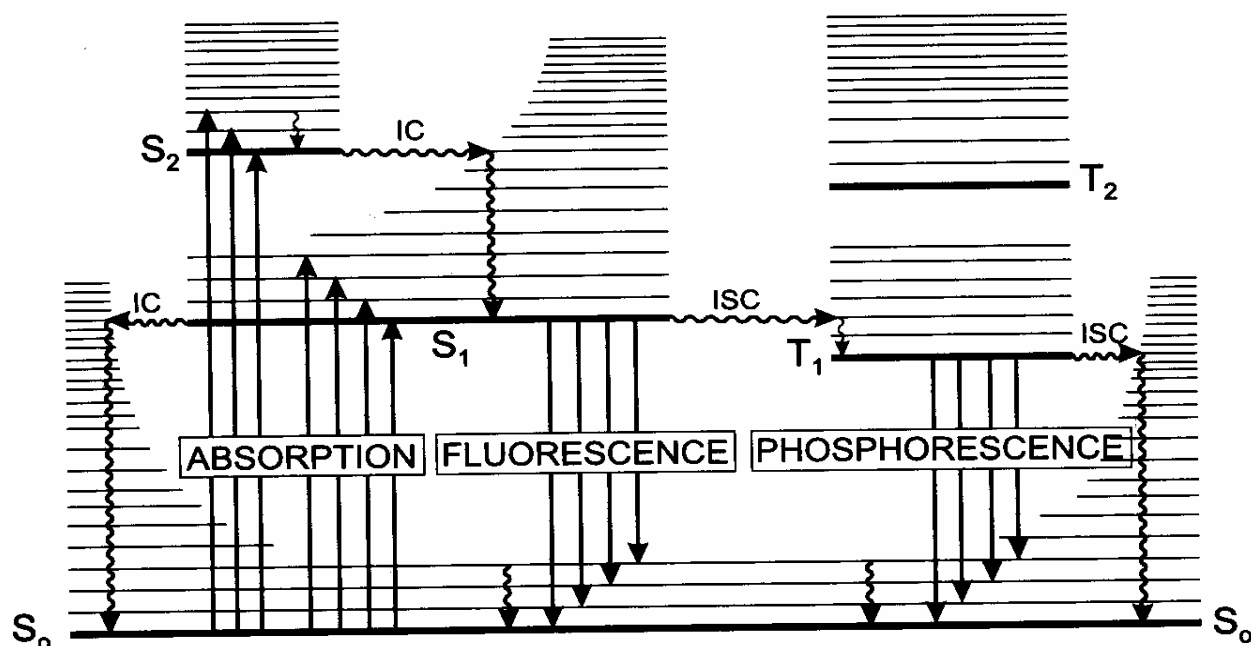


Figure 2.5: Perrin-Jablonski diagram showing the photo physical processes during deactivation of excited molecules [Val02, Lak99].

2.2.1 Internal conversion

Internal conversion is an isoenergetic non-radiative transition between two electronic states of the same spin multiplicity (e.g. $S_2 \rightarrow S_1$ or $S_1 \rightarrow S_0$). This process is followed by a vibrational relaxation towards the lowest vibrational level of the final electronic state on a time scale of $10^{-13} - 10^{-11}$ s [Val02]. When a molecule is excited to an energy level higher than the lowest vibrational level of the electronic state S_n , additional to internal conversion vibrational relaxation may bring the excited molecule towards the 0 vibrational level of the S_n singlet state, and then internal conversion may make the transition from $S_n(v=0)$ to $S_{n-1}(v)$ and so on.

2.2.2 Fluorescence

Spontaneous emission of photons accompanying the $S_1 \rightarrow S_0$ relaxation is called fluorescence. Normally fluorescence emission occurs from S_1 and therefore its characteristics (except polarization) do not depend on the excitation wavelength. According to Stokes Law the fluorescence spectrum is located at longer wavelengths than the absorption spectrum because of the energy loss in the excited state due to vibrational relaxation (see Figure 2.5). Normally long wavelength part of the absorption spectrum overlaps with the short wavelength part of the fluorescence spectrum because at room temperature, a small fraction of molecules are in vibrational levels higher than 0 vibrational level, in the ground state as well as in the excited state. The fluorescence spectrum often resembles the first absorption band (mirror image rule), since the vibrational levels are similar in the ground and excited states. The gap wavelength between the maximum of the first absorption band and the maximum of fluorescence is called Stokes shift. Emission of a photon through fluorescence is as fast as absorption of a photon (10^{-15} s). However, excited molecules stay in the S_1 state for a certain time before emitting a photon or undergoing other de-excitation processes. Thus, after excitation of molecules with a very short pulse of light (shorter than fluorescence lifetime), the fluorescence intensity decrease exponentially with a characteristic time, reflecting the average lifetime of the molecules in the S_1 excited state (excited state fluorescence lifetime).

2.2.3 Intersystem crossing and phosphorescence

Intersystem crossing is a non-radiative transition between isoenergetic vibrational levels belonging to electronic states of different multiplicities. For example, an excited molecule in the 0 vibrational level of the singlet S_1 state may move to the isoenergetic vibrational level of the triplet state T_1 ; and then relax vibrationally to the lowest vibrational level of T_1 . Crossing between states of different multiplicity is spin forbidden, but spin-orbit coupling overcomes the selection rule partly.

Radiative de-excitation through $T_1 \rightarrow S_0$ emission is called phosphorescence. In fact, the transition $T_1 \rightarrow S_0$ is spin forbidden, thus the phosphorescence radiative rate constant is very low. During the slow process of radiative $T_1 \rightarrow S_0$ emission, numerous collisions with solvent molecules favour $T_1 \rightarrow S_0$ intersystem crossing and subsequent vibrational relaxation in the S_0 singlet state. In liquid solution of dye molecules at room temperature, non-radiative de-excitation from the triplet state T_1 , is generally predominant over phosphorescence. At low temperature and/or in a rigid medium, non-radiative relaxation is less efficient and phosphorescence may become observable. Under these conditions, the triplet state lifetime may increase up to minutes.

Reverse intersystem crossing $T_1 \rightarrow S_1$ may occur when the energy difference between S_1 and T_1 is small and when the life time of T_1 is long enough. This results in emission with the same spectral distribution as normal fluorescence, but with a much longer decay time constant. This fluorescence emission is thermally activated and is called delayed fluorescence.

2.3 Fluorescence lifetime and quantum yield

Excited molecule in the first excited singlet state depopulate generally exponentially after excitation. The intensity of the fluorescence signal $S_F(t)$ (spontaneous emission) is proportional to the S_1 -state level population. It decays exponentially after end of excitation according to

$$S_F(t) = S_{F,0} \exp(-t / \tau_F) \quad (2.4)$$

where t is the time, τ_F is the fluorescence lifetime of excited state S_1 . The fluorescence lifetime τ_F is equal to the S_1 -state lifetime τ_{S_1} . It is the inverse of the total de-excitation rate of the excited state, k_{tot} i.e.

$$\tau_F = \frac{1}{k_{tot}} \quad (2.5)$$

The total de-excitation rate consists of radiative, k_{rad} and non-radiative, k_{nr} de-excitation contribution. The non-radiative relaxation rate includes internal conversion, (rate k_{ic}) and intersystem crossing, (rate k_{isc}). Therefore it is

$$k_{tot} = k_{rad} + k_{ic} + k_{isc} = k_{rad} + k_{nr} \quad (2.6)$$

whereby

$$k_{nr} = k_{ic} + k_{isc} \quad (2.7)$$

The radiative lifetime τ_{rad} is defined by

$$\tau_{rad} = \frac{1}{k_{rad}} \quad (2.8)$$

The fluorescence quantum yield ϕ_F is the fraction of excited molecules which return to the ground state S_0 by emission of photons. It is given by

$$\phi_F = \frac{k_{rad}}{k_{rad} + k_{nr}} = \frac{\tau_F}{\tau_{rad}} \quad (2.9)$$

In other words, the fluorescence quantum yield ϕ_F is the ratio of the number of emitted photons, $n_{ph,em}$ to the number of absorbed photons, $n_{ph,abs}$, and is given by

$$\phi_F = \frac{n_{ph,em}}{n_{ph,abs}} = \frac{\int S_I(\lambda) d\lambda}{W_{L,abs} / h\nu_L} = \int E_F(\lambda) d\lambda \quad (2.10)$$

$E_F(\lambda)$ is the fluorescence quantum distribution and is defined by

$$E_F(\lambda) = \frac{S_I(\lambda)}{n_{ph,abs}} = \frac{S_I(\lambda)}{W_{L,abs} / h\nu_L} \quad (2.11)$$

where $S_I(\lambda)$ is the intrinsic spectral fluorescence photon density distribution, $W_{L,abs}$ is the absorbed input energy and ν_L the frequency of the input light [Hol99].

2.4 Stimulated emission cross-section and radiative lifetime

The S_1 - S_0 stimulated emission cross-section spectrum, $\sigma_{em}(\lambda)$, of dyes can be extracted from the absorption cross-section spectrum, $\sigma_a(\lambda)$, and the fluorescence quantum distribution, $E_F(\lambda)$, by the relation [Spe87, Gra00, Pet71]

$$\sigma_{em}(\lambda) = \frac{\lambda^4 n_F}{n_A} \frac{E_F(\lambda)}{\int_{em} \lambda'^3 E_F(\lambda') d\lambda'} \int_{abs} \frac{\sigma_a(\lambda')}{\lambda'} d\lambda', \quad (2.12)$$

Where n_A and n_F are the average refractive indices of the solution in the S_0 - S_1 absorption region and the S_1 - S_0 emission region, respectively. The integrals extend over the S_0 - S_1 absorption band and the S_1 - S_0 emission band (*em*). The stimulated emission cross-section characterizes the light amplification property of a medium [Bir69]. Equation 2.12 is derived from the equivalence of the absorption and stimulated emission according to the Einstein B-coefficient.

Experimentally accessible is the radiative lifetime τ_{rad} by measurement of the fluorescence lifetime and the fluorescence quantum yield, according to

$$\tau_{rad} = \frac{\tau_F}{\phi_F} \quad (2.13)$$

The radiative lifetime, τ_{rad} is the inverse of the rate of spontaneous emission, k_{rad} . The spontaneous emission rate is equal to the rate of stimulated emission caused by quantum fluctuations. The radiative lifetime is the inverse of the Einstein A-coefficient which is fixed related to the Einstein B coefficient and subsequently to the absorption cross-section. As a result the radiative lifetime, τ_{rad} is related to the absorption spectrum by the Strickler-Berg formula [Str62]

$$\tau_{rad} = \left[\frac{8\pi c_0 n_F^3 \int_{em} E_F(\lambda) d\lambda}{n_A \int_{em} E_F(\lambda) \lambda^3 d\lambda} \int_{abs} \frac{\sigma_a(\lambda) d\lambda}{\lambda} \right]^{-1} \quad (2.14)$$

Rewriting of Equation 2.12 with the aid of Equation 2.14 allow to express the stimulated emission cross-section as a function of the radiative lifetime

$$\sigma_{em}(\lambda) = \frac{\lambda^4}{8\pi n_F^2 c_0 \tau_{rad}} \frac{E_F(\lambda)}{\int_{em} E_F(\lambda') d\lambda'} \quad (2.15)$$

2.5 Degree of fluorescence polarisation and molecular reorientation time

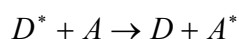
The degree of fluorescence polarization [Dör66], $P_F = (S_{F,\parallel} - S_{F,\perp}) / (S_{F,\parallel} + S_{F,\perp})$, can be determined by measuring the fluorescence signal polarized parallel ($S_{F,\parallel}$) and polarized perpendicular ($S_{F,\perp}$) to the excitation light. The degree of fluorescence polarisation, P_F , is related to the reorientation time, $\tau_{or,\mu}$ of the transition dipole moment, μ , by the Perrin formula [Par68, Per29, Wei95]

$$\tau_{or,\mu} = \frac{1/P_0 - 1/3}{1 - P_F/P_0} P_F \tau_F, \quad (2.16)$$

where $P_0 = 0.5$. In diluted solutions (no electronic energy transfer) the reorientation time of the transition dipole moments, $\tau_{or,\mu}$, is equal to the molecular reorientation time, $\tau_{or,m}$.

2.6 Energy transfer

Transfer of the excited-state energy from the initially excited donor (D) to an acceptor (A) according to



is called energy transfer. One distinguishes the radiative and the non-radiative energy transfer [Val02]. Radiative transfer is a two-step process: a photon emitted by a donor (D) is absorbed by an acceptor (A). It is the process of absorption of the fluorescence of the donor by the acceptor.



Such a transfer does not require any interaction between the partners; it depends only on the spectral overlap of the emission spectrum of the donor with the absorption spectrum of the acceptor. The higher the concentration of the acceptor the more fluorescence light is reabsorbed. The process is illustrated in Figure 2.6.

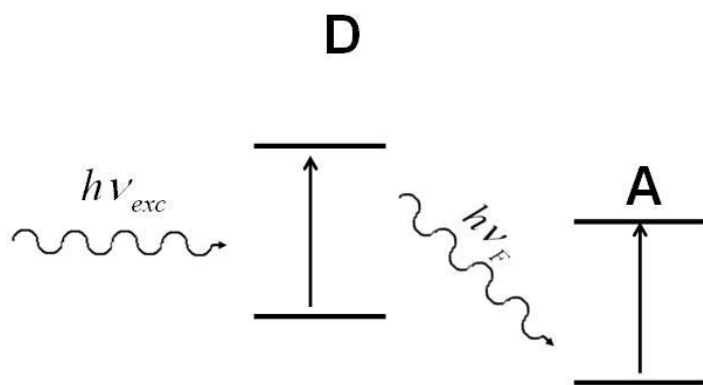


Figure 2.6: Illustration of radiative energy transfer (absorption of fluorescence of donor by acceptor) (from [Val02, Lak99]).

Non-radiative energy transfer occurs without emission of photons at distances less than the wavelength. It occurs if the emission spectrum of the donor overlaps with the absorption spectrum of the acceptor.

Non-radiative energy transfer results from different interaction mechanisms. The interactions may be of Coulombic nature or of quantum mechanical wavefunctional nature. The Coulombic interactions consist of dipole-dipole interactions (Förster's mechanisms) and multi-polar interactions (between donor and acceptor molecules). The energy transfer due to electron exchange under charge resonance condition (Dexter's mechanism), occur only if the involved wavefunctions overlap spatially (donor and acceptor molecule in near contact). The Förster-type energy transfer (excitation transfer) is shown in Figure 2.7. The Dexter-type energy transfer (excitation transfer) is illustrated in Figure 2.8.

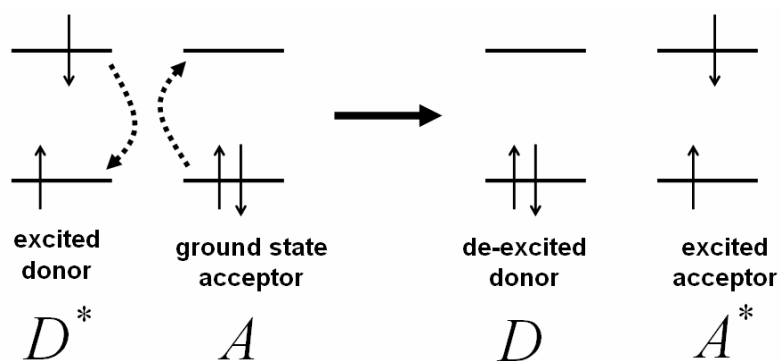


Figure 2.7: Schematic representation of the Förster-type energy transfer (from [Häd99]).

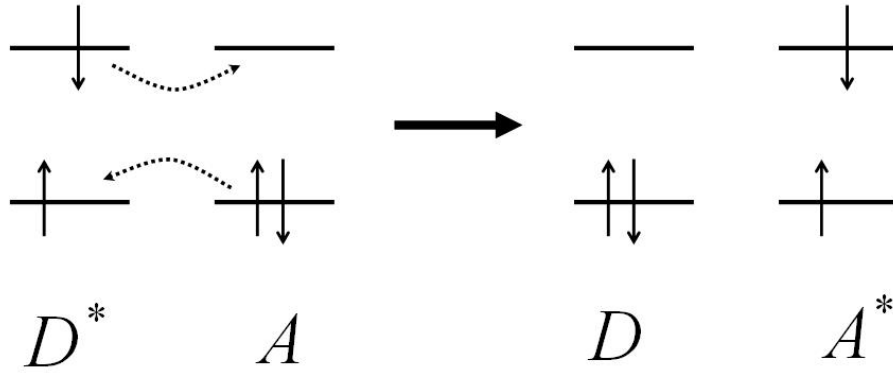


Figure 2.8: Illustration of Dexter-type energy transfer (from [Häd99]).

2.6.1 Förster-type energy transfer

Förster derived the energy transfer rate constant (k_{FT}) due to dipole-dipole coupling and got the following results [För51, Fle86]

$$k_{FT} = k_{F,0,d} \left(\frac{R_0}{R_d} \right)^6 = \frac{1}{\tau_{F,0,D}} \left(\frac{R_0}{R_d} \right)^6 \quad (2.17)$$

Where $k_{F,0,d} = 1/\tau_{F,0,D}$ is the emission rate constant of the donor, in the absence of energy transfer, R_d is the distance between the donor and the acceptor, (distance of the transition dipoles) and R_0 is the critical Förster distance, i.e. the distance at which the energy transfer rate and the rate of spontaneous decay of the excited donor are equal ($k_{FT} = k_{F,0,d}$).

R_0 , is give by [För51, Fle86, Amm95]

$$R_0^6 = \frac{9\kappa^2}{128\pi^5 n^4} \int E_{F,D}(\lambda) \sigma_a(\lambda) \lambda^4 d\lambda \quad (2.18)$$

where n in the average refractive index in the overlap region of absorption and emission (Figure 2.9), $E_{F,D}(\lambda)$ is the fluorescence quantum distribution of the donor, and $\sigma_a(\lambda)$ is the absorption cross-section of the acceptor. The orientation factor κ is determined by the orientation of the transition dipole moments of the interacting molecules d (donor) and a (acceptor) according to [Fle86]

$$\kappa = \cos(\varphi_{da}) - 3\cos(\varphi_d)\cos(\varphi_a), \quad (2.19)$$

where φ_d and φ_a are the angles of the donor and acceptor transition dipole moments to the connection line between d and a , and φ_{da} is the mutual angle between the transition dipole moments (Figure 2.10). Depending on the orientation of transition dipole moments κ may vary between 0 and 2. For a statistical isotropic orientation of the transition dipole moments it is $\overline{\kappa^2} = 2/3$ [Fle86].

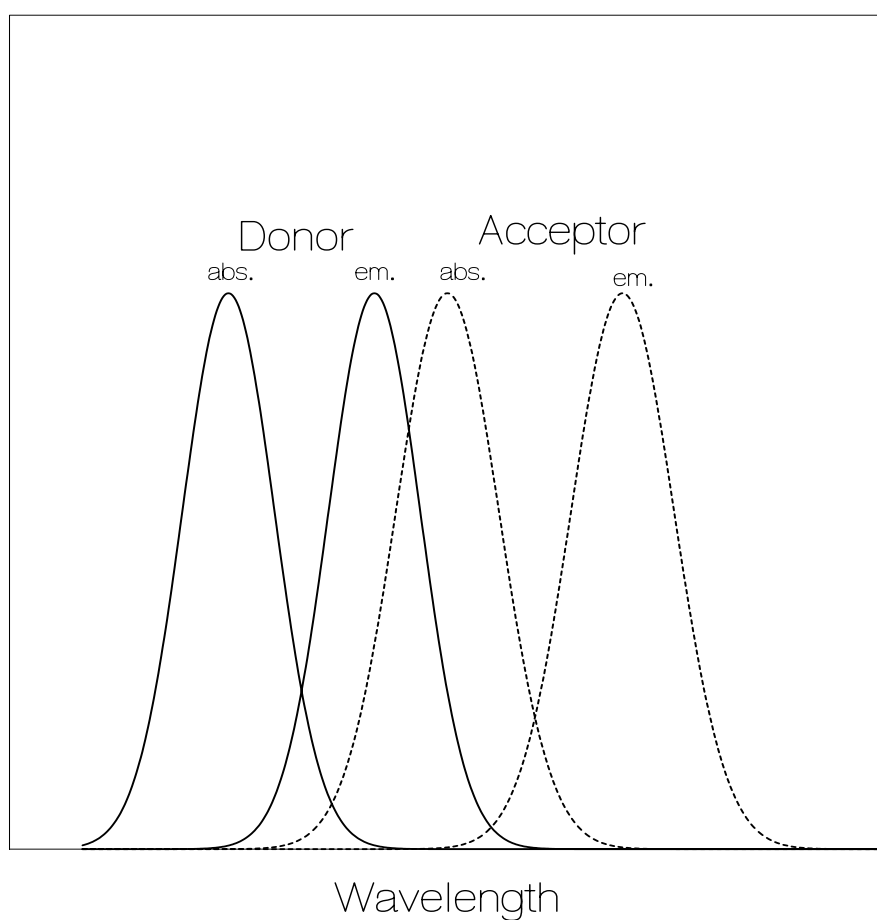


Figure 2.9: Illustration of the integral overlap between the emission spectrum of the donor and the absorption of the acceptor.

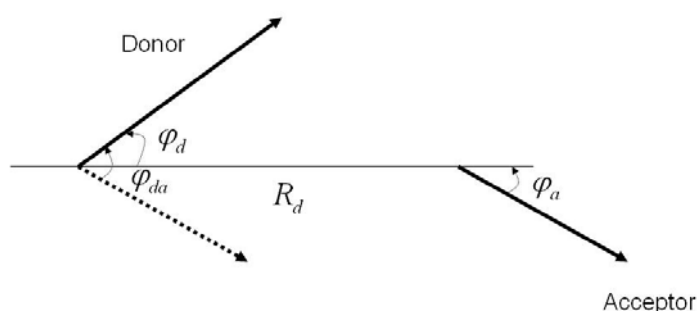


Figure 2.10: Angles involved in the definition of the orientation factor κ .

The quantum efficiency of Förster-type energy transfer, ϕ_{FT} is given by

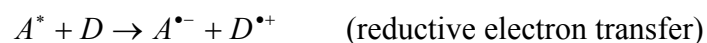
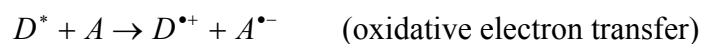
$$\phi_{FT} = \frac{k_{FT}}{k_{tot}} = \frac{k_{FT}}{k_{FT} + k_{F,0,d}} \quad (2.20)$$

which is the ratio of the energy transfer rate to the total decay rate of the donor.

2.7 Electron Transfer

Electron transfer (ET) is the process where an electron moves from one atom or molecule to an adjacent atom or molecule [Lak99]. In donor-acceptor system photo-excitation may cause adiabatic electron transfer, called optical electron transfer, in the case of strong coupling between electron donor and electron acceptor or non-adiabatic (diabatic) electron transfer, called photo-induced electron transfer, in the case of weak coupling [Che06]. If the excited molecule (D^* , excited electron donor) leaves an electron to the adjacent ground-state molecule (A, electron acceptor) then one speak of oxidative electron transfer. If the excited molecule (A^* , excited electron acceptor) gets an electron from the adjacent ground state molecule (D, electron donor) then one speak of reductive electron transfer. In both cases the fluorescence emission of the excited molecule is quenched.

Oxidative and reductive photoinduced electron transfer processes occurring according to the following reactions



are schematically illustrated in Figure 2.11.

Photoinduced electron transfer is involved in many organic photochemical reactions. It plays a major role in photosynthesis and in artificial systems for the conversion of solar energy to charge separation [Val02, Lak99].

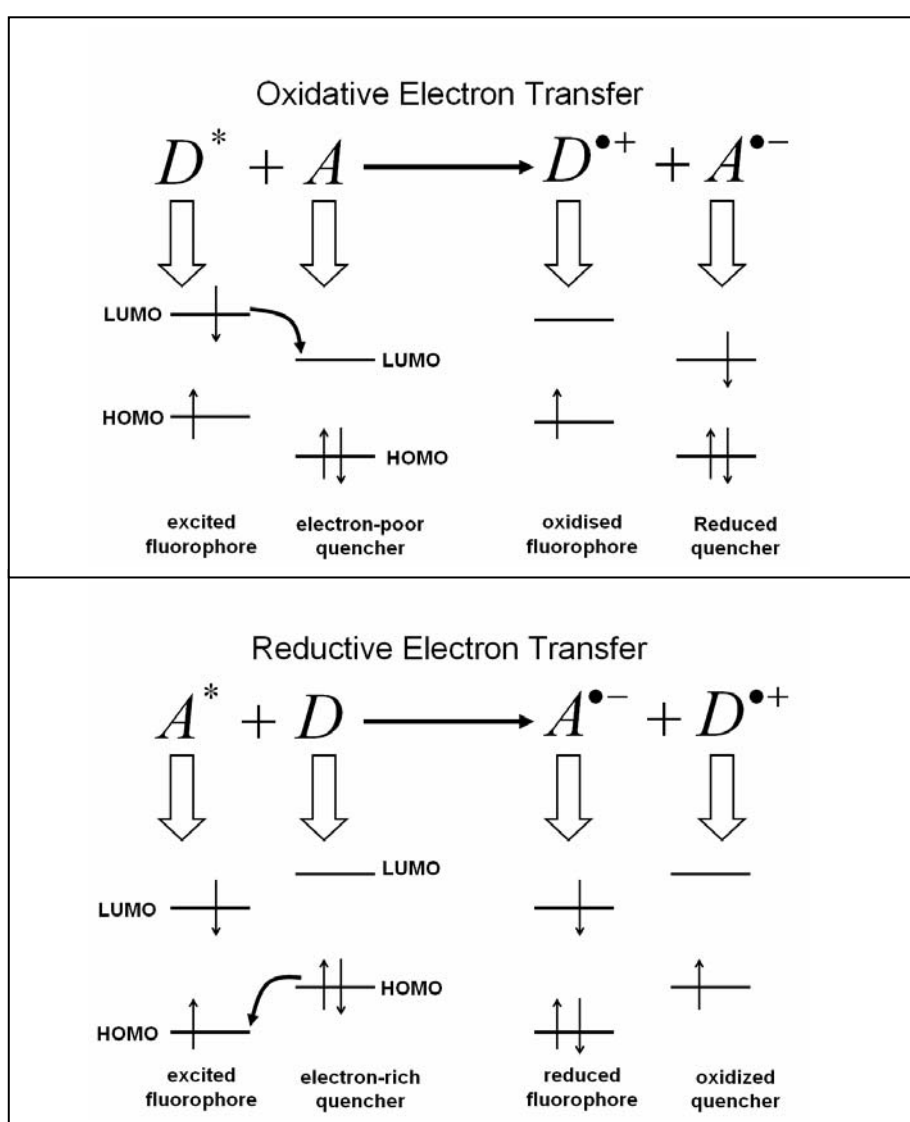


Figure 2.11: Reductive and oxidative electron transfer (from [Val02]).

The photo-induced electron transfer is described theoretically by the Marcus theory [Jor76, Hop74, Mar56, Mar85, Lev77, Hus61]. It involves three parameters, the donor-acceptor coupling constant, V_0^2 (square of wavefunction overlap integral, V_0 , of donor and acceptor state), the free enthalpy $\Delta G^0 = G^0(\text{acceptor}) - G^0(\text{donor})$ of the reaction, and the reorganisation energy $\lambda = G^0(\text{acceptor}, x_D) - G^0(\text{acceptor}, x_A)$, where x_D is the reaction coordinate equilibrium position of the donor, and x_A is the reaction coordinate equilibrium position of the acceptor. The donor-acceptor coupling constant depends exponentially on the edge to edge distance, R , between donor and acceptor, i.e. $V_0^2(R) = V_0^2(0)\exp(-\beta R)$, with distance coefficient β of about 0.14 nm^{-1} [Mos92] (see Figure 2.12). Depending on the magnitude of the reorganisation energy relative to the standard free enthalpy difference three regions are distinguished: i) the normal region for $\lambda > -\Delta G^0$, ii) the activation-energy-free position $\lambda = -\Delta G^0$ (optimal region), and iii) the inverse region $\lambda < -\Delta G^0$ (see Figure 2.13)

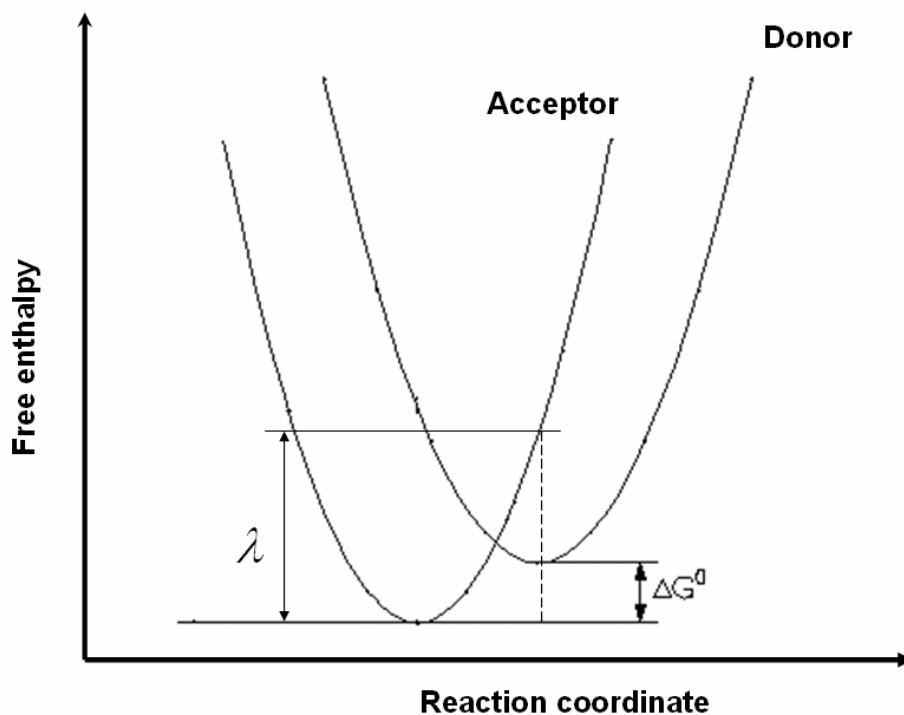


Figure 2.12: Representation of the potential energy Marcus-parabola curve used in electron transfer theory. The reorganisation energy (λ), and the free enthalpy ΔG^0 are indicated (from [Häd99]).

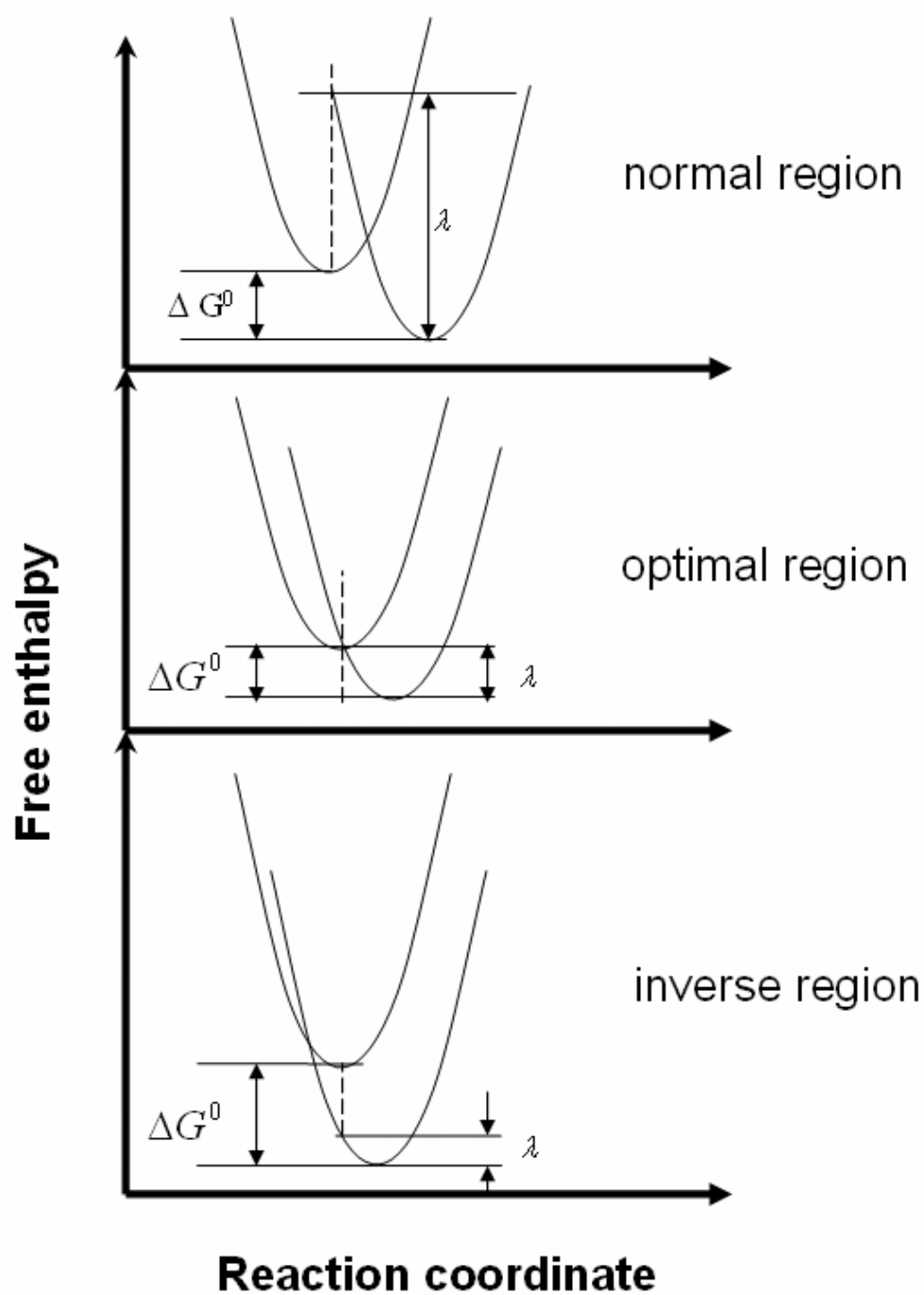


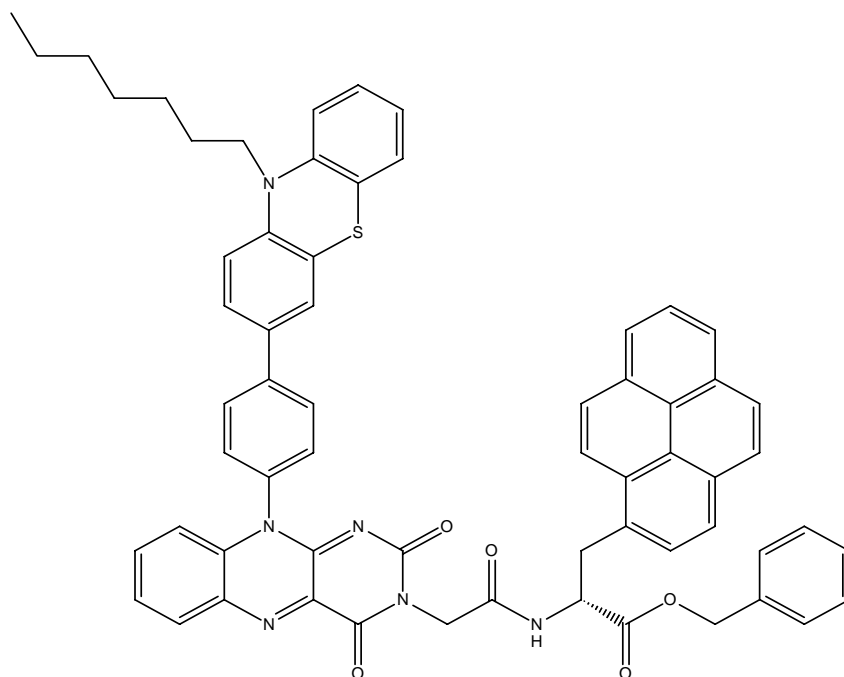
Figure 2.13: The different regions in the Marcus theory of electron transfer, together with the representations of the free energy ΔG^0 change, and the reorganization energy (λ) (from Häd99)].

3. Experimental

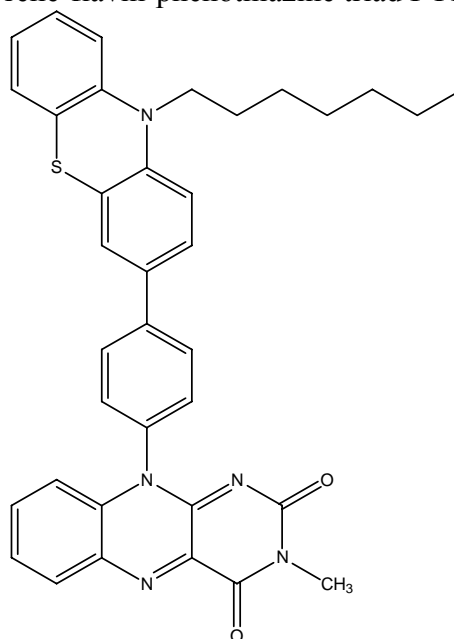
3.1 Investigated dyes

In this dissertation a pyrene – flavin (isoalloxazine) dyad (abbreviated by PFD), a phenothiazine-phenyl-isoalloxazine dyad, (called PTFD, short-writing of phenothiazine-flavin dyad), and a pyrene-flavin-phenothiazine triad (abbreviated by PYFPT) are investigated. Their structural formulae are given in Figure 3.1. In order to understand the complex electron transfer and energy transfer processes in these dyads and the triad, a detailed knowledge of the photo-physical behaviour of their constituents, the flavoquinone molecules isoalloxazine acetic acid ethyl ester (IAE) and bromo-phenyl-isoalloxazine (BrPF), the pyrene molecules pyrene, 1-methylpyrene, and the phenothiazine molecules heptyl-phenothiazine (HPT), heptyl-phenyl-phenothiazine (HPPT), are needed. Their structural formulae are given in Figure 3.2.

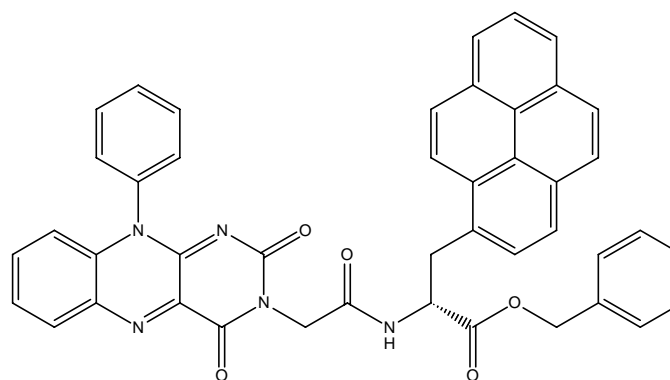
The dyes PFD, PTFD, PYFPT, IAE, BrPF, HPT, HPPT, were synthesized by Dr. R. Procházka from the group of Prof. J. Daub in the Institute für Organische Chemie, Universität Regensburg, Germany. The dyes pyrene, 1-methylpyrene, solvents dichloromethane, acetonitrile and methanol, were purchased from Sigma-Aldrich, Taufkirchen, Germany and were used without further purification.



Pyrene-flavin-phenothiazine triad PYFPT



Phenothiazine-flavin dyad PTFD

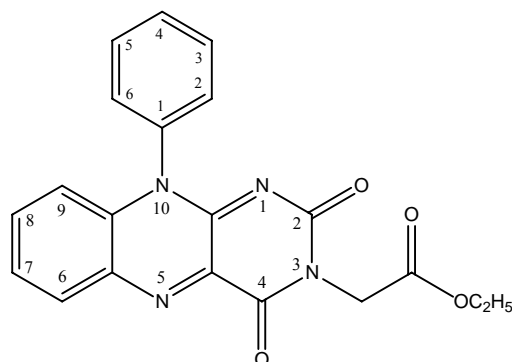


Pyrene-flavin dyad PFD

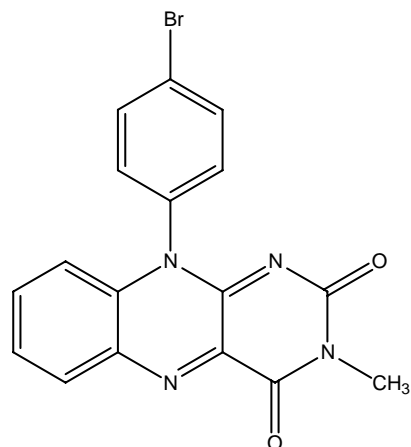
Figure 3.1: Structural formulae of investigated dyads and triad. PFD: Full name: 1-Pyrenepropanoic acid, α -[[4,10-dihydro-2,4-dioxo-10-phenylbenzo[g]pteridin-3(2H)-yl]acetyl]amino]-, phenylmethyl ester, (α R) - (9Cl). Formula: $C_{44}H_{31}N_5O_5$. Molar mass: $709.75 \text{ g mol}^{-1}$.

PTFD: Full name: 10 [4-(10-heptyl-10H-phenothiazine-3-yl)-phenyl]-3-methyl-10H-benzo[g]pteridine-2,4-dione. Formula: $C_{36}H_{33}N_5O_2S$. Molar mass: $599.75 \text{ g mol}^{-1}$.

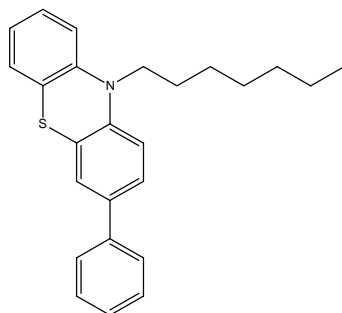
PYFPT: Full name: 2(2-{10-[4-(10-heptyl-10H-phenothiazin-3-yl)-phenyl]-2,4-dioxy-4,10-dihydro-2H-beno[g]pteridin-3-yl}-acetylamino)-3-pyren-1-yl-propionic acid benzyl ester. Formula: $C_{63}H_{52}N_6O_5S$. Molar mass: $1005.19 \text{ g mol}^{-1}$.



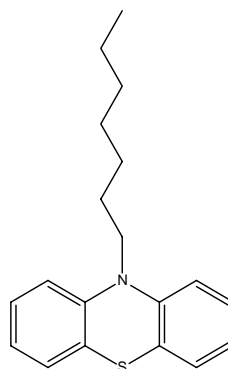
Dye IAE



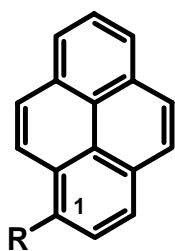
Dye BrPF



Heptyl-phenothiazine HPT



Heptyl-phenyl-phenothiazine HPPT



R = H pyrene

R = CH₃ 1-methylpyrene

Figure 3.2: Structural formulae of investigated constituents of PFD, PTFD dyads and PYFPT triad. IAE: Full name: (2,4-dioxo-10-phenyl-4,10-dihydro-2H-benzo[g]pteridin-3-yl)-acetic acid ethyl ester, Formula: C₂₀H₁₆N₄O₄, Molar mass: 376.37 g mol⁻¹. BrPF: Full name: 10-(4-bromo-phenyl)-3-methyl-10H-benzo[g]pteridine-2,4-dione, Formula: C₁₇H₁₁BrN₄O₂, Molar mass: 383.20 g mol⁻¹. Pyrene: Formula: C₁₆H₁₀, Molar mass: 202.25 g mol⁻¹. 1-methylpyrene: Formula: C₁₇H₁₂, Molar mass: 216.25 g mol⁻¹. HPT: Full name: 10-Heptyl-10H-phenothiazine, Formula: C₁₉H₂₅NS, Molar mass: 299.47 g mol⁻¹. HPPT: Full name: 10-Heptyl-3-phenyl-10H-phenothiazine, Formula: C₂₅H₂₇NS, Molar mass: 373.55 g mol⁻¹.

3. Experimental

The dyes were dissolved in dichloromethane (CH_2Cl_2), acetonitrile (CH_3CN), or methanol (CH_3OH). The measurements were performed at room temperature (ca. 22 °C). Air-saturated samples were used. Some characteristics of the applied solvents and dyes are shown in Table 3.1 and Table 3.2 respectively.

Table 3.1: Some characteristics of the applied solvents (from Merck catalog)

solvent	Boiling point	Freezing point	Dielectric constant	Electrical dipole moment Debye)
Dichloromethan	40°C	-95°C	.91	1.6 D
e				
Acetonitrile	82°C	-46°C	3.75	3.44 D
Methanol	65°C	-98°C	3.26	1.7 D

Table 3.2: Characteristic parameters of the applied dyes (from [Pro04])

dye	Formula	Molar mass g mol^{-1}	Melting point
IAE	$\text{C}_{20}\text{H}_{16}\text{N}_4\text{O}_4$	376.37	290°C
BrPF	$\text{C}_{17}\text{H}_{11}\text{BrN}_4\text{O}_2$	383.20	>300°C
Pyrene	$\text{C}_{16}\text{H}_{10}$	202.25	148°C
1-methylpyrene	$\text{C}_{17}\text{H}_{12}$	216.25	74°C
HPT	$\text{C}_{19}\text{H}_{25}\text{NS}$	299.47	<0°C
HPPT	$\text{C}_{25}\text{H}_{27}\text{NS}$	373.55	<0°C
PFD	$\text{C}_{44}\text{H}_{31}\text{N}_5\text{O}_5$	709.75	285-289°C
PTFD	$\text{C}_{36}\text{H}_{33}\text{N}_5\text{O}_2\text{S}$	599.75	238-240°C
PYFPT	$\text{C}_{63}\text{H}_{52}\text{N}_6\text{O}_5\text{S}$	1005.19	262-263°C

The synthesis and chemical characteristics of the applied flavoquinone dyes IAE and BrPF are found in [She03, Pro04]. A brief description is given in [Shi06]. The synthesis and chemical characters of pyrene – flavin – dyad are found in [She03, Pro04]. A short description is given in [Shi07a]. The pyrene – flavin (isoalloxazine) dyad (abbreviated by PFD) is made up of a phenyl-isoalloxazine derivative and of 1-methylpyrene, in which both chromophores are linked via an enantiomerically pure dipeptide bridge of R-configuration (Figure 3.1). The phenothiazine-phenyl-isoalloxazine dyad, (called PTFD, short-writing of phenothiazine-flavin dyad) is made up of the approximate constituents of the dyad, 10-heptyl-10*H*-phenothiazine (abbreviated by HPT), or 10-heptyl-3-phenyl-10*H*-phenothiazine (abbreviated by HPPT), and 10 (4-bromo-phenyl)-3-methyl-10*H*-benzo[g]pteridine-2,4-dione (called BrPF, short-writing of bromo-phenyl-flavin) (Figures 3.1 and 3.2). The synthesis and chemical characteristics of PTFD are given in [She03, Pro04]. A short synthesis route is given [Shi07b]. The pyrene-flavin-phenothiazine triad, (abbreviated by PYFPT), is made up of the approximate constituents of the triad, 10-heptyl-10*H*-phenothiazine (abbreviated by HPT), or 10-heptyl-3-phenyl-10*H*-phenothiazine (abbreviated by HPPT), and 10 (4-bromo-phenyl)-3-methyl-10*H*-benzo[g]pteridine-2,4-dione (called BrPF, short-writing of bromo-phenyl-flavin) and of 1-methylpyrene (Figures 3.1 and 3.2). The synthesis of the triad PYFPT is described in [Pro04].

3.2 Absorption detection

Absorption measurements were carried out with a commercial double beam UV-VIS-IR spectrophotometer (Beckman type ACTA M IV) by measuring transmission spectra $T(\lambda)$. The absorption coefficient spectra, $\alpha_a(\lambda)$ and the absorption cross-section spectra, $\sigma_a(\lambda)$ were extracted from the transmission spectra, $T(\lambda)$, by the Equations 2.2 and 2.3 respectively.

3.3 Fluorescence spectra

Fluorescence measurements were carried out with the experimental setup schematically shown in Figure 3.3. The setup consists of an excitation path and a detection path. In the excitation path a high-pressure mercury lamp in combination with an interference filter and a polarizer is used as excitation source. The vertical polarized excitation light is focused to the sample S by lens L2. In the detection path the fluorescence emission is gathered by lens L3 and directed to the spectrometer SP by lens L4 under magic angle direction (polarizer transmission under an angle of 54.7° to the vertical) [Dör66], the dispersed fluorescence spectrum is registered by a silicon diode array detection multi-channel analyser system (Tracor DARRS system) and the data are transferred to a computer for analysis.

In experiments the absolute intrinsic fluorescence quantum distribution, $E_F(\lambda)$, and fluorescence quantum yields, ϕ_F were determined by calibration to reference dyes of known fluorescence quantum yield [Hol99, För51].

For excitation in the blue and violet spectral range the dye coumarin 314T in ethanol was used as reference (fluorescence quantum yield $\phi_F = 0.87$ according to technical data sheet of Kodak). In the case of near UV excitation the dye quinine-sulphate dihydrate in 1N H_2SO_4 was used as reference ($\phi_F = 0.546/(1+14.5 C)$ where C is the dye concentration in $mol\ dm^{-3}$ [Mel61]). In the case of excitation in the green spectral range the dye rhodamine 101 in ethanol ($\phi_F = 1.0$ [Kar80]) was used as reference. The absorption cross-section spectra and the fluorescence emission spectra of these reference dyes are shown in Figure 3.4 and Figure 3.5 respectively.

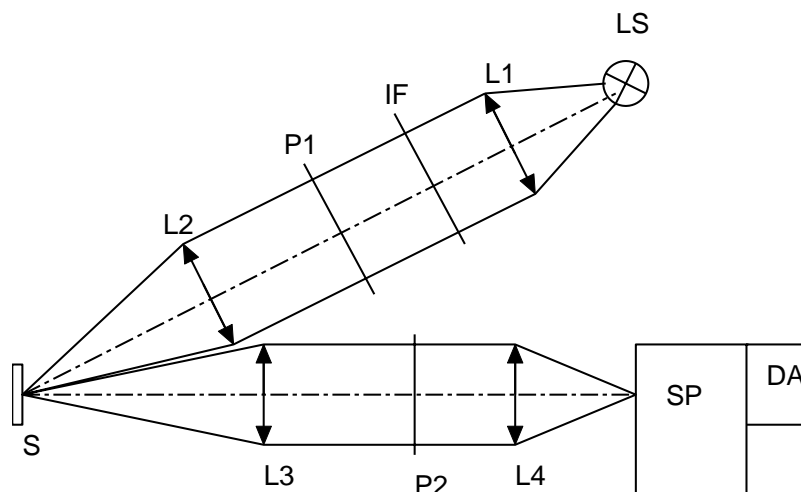


Figure 3.3: Experimental setup for fluorescence measurements. LS, light source (high pressure mercury lamp). IF, interference filter. L1-L4, lenses. P1, P2, polariser's. S, sample. SP, spectrometer. DA, diode-array detection system.

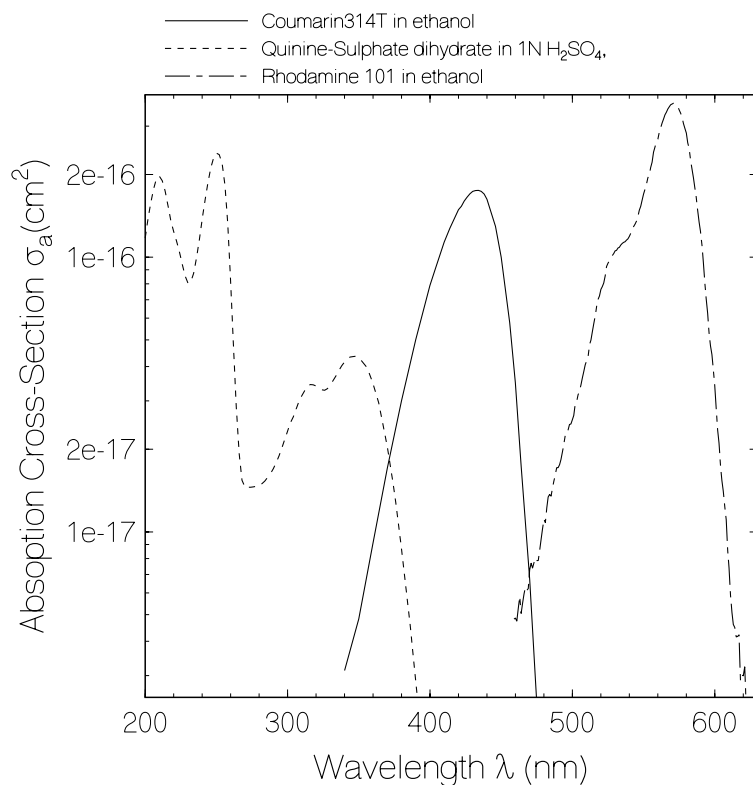


Figure 3.4: Absorption cross-sections of applied reference dyes.

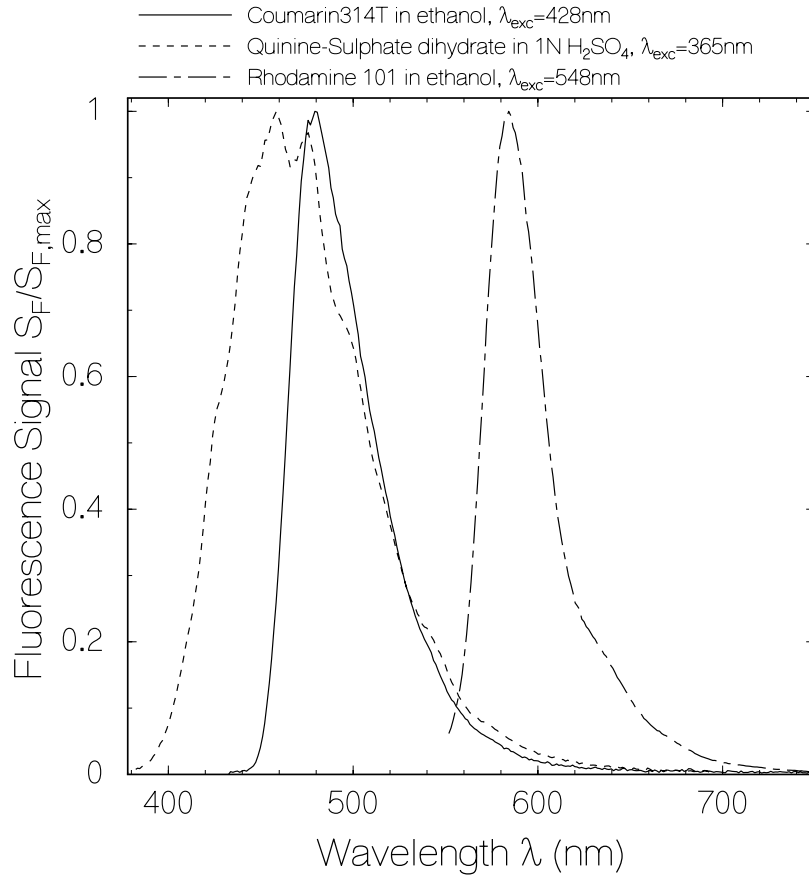


Figure 3.5: Fluorescence spectra of applied reference dyes.

The degree of fluorescence polarization [Dör66], P_F was determined by measuring the fluorescence signal polarized parallel ($S_{F,\parallel}$) and polarized perpendicular ($S_{F,\perp}$) to the excitation light and by using the relation

$$P_F = (S_{F,\parallel} - S_{F,\perp}) / (S_{F,\parallel} + S_{F,\perp}) \quad (3.1)$$

3.4 The fluorescence lifetimes

3.4.1 Single-shot real time detection

Fluorescence lifetime measurements of samples in the time range between the sub-nanoseconds and nanoseconds were carried out with the experimental setup depicted in Figure 3.6. The samples were excited by a vertical polarized picosecond laser pulses. For detection the fluorescence was gathered by lens L1 and directed to a micro-channel-plate photomultiplier (Hamamatsu, type R1564-U01) by lens L2 under magic angle direction (polarizer transmission under an angle of 54.7° to the vertical) [Dör66]. The photomultiplier signal was recorded with a high-speed digital oscilloscope (LeCroy, type DSO 9362). In the fluorescence path edge filters (F) were used to cut unwanted excitation light.

The samples were excited at wavelength $\lambda_L = 400$ nm, with second harmonic pulses of a Ti:sapphire femtosecond oscillator-amplifier laser system (Hurricane from Spectra-Physics) with pulses of $\Delta t_L \approx 4$ ps (FWHM) duration.

In the case of excitation at wavelength $\lambda_L = 347.15$ nm, second harmonic pulses of a mode-locked ruby laser system with pulse duration of $\Delta t_L \approx 35$ ps (FWHM) were used [Wei93].

For excitation at wavelength $\lambda_L = 527$ nm, second harmonic pulses of a mode-locked Nd-phosphate:glass laser system [Sch90] with pulse duration of $\Delta t_L \approx 6$ ps FWHM were used .

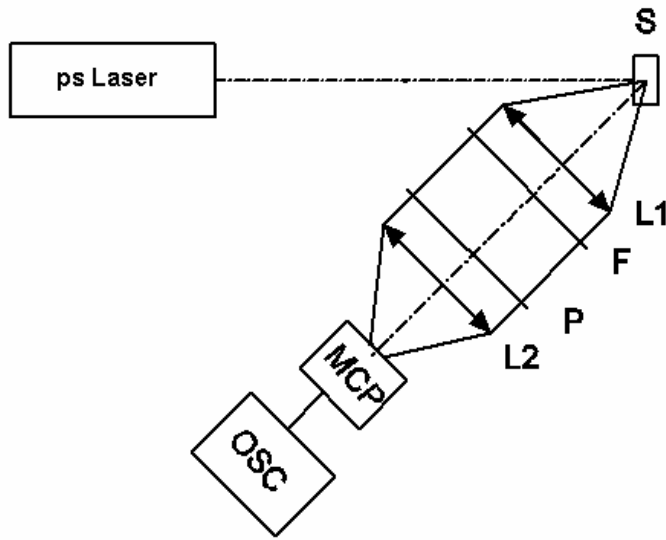


Figure 3.6: Experimental setup for fluorescence lifetime measurements. S, sample. L1-L2, lenses. P, polarizer. F, Schott type filter. MCP, micro-channel-plate photomultiplier. OSC, digital oscilloscope.

3.4.2 Fluorescence up-conversion

The temporal fluorescence behaviour of dyes in the sub-picosecond to picosecond region, was studied by fluorescence up-conversion with a Ti:sapphire femtosecond oscillator - amplifier system (laser system Hurricane from Spectra-Physics) [Shi07a, Sch01, Val02]. The experimental setup is shown in figure 3.7. The laser was operated with a pulse-duration of 110 fs at 800nm. The samples were excited with frequency doubled femtosecond pulses at 400 nm, and the generated fluorescence signals (frequency ν_F) were frequency up-converted with the fundamental laser pulses at 800 nm (frequency ν_L) in a non-linear optical crystal (BBO crystal of 0.2 mm thickness[Dmi91]) by non-collinear type-II phase-matched sum-frequency generation according to $\nu_F(e) + \nu_L(o) \rightarrow \nu_{up}(e)$, (o: ordinary polarized light, e: extraordinary polarized light [Dmi91], ν_F is the frequency of the fluorescence light, ν_L is the frequency of the fundamental laser light, and ν_{up} is the frequency of the up-converted light). For time resolution the gating fundamental laser pulse was time-delayed relative to the second-harmonic excitation pulse with a stepper-motor driven linear translation stage. The up-

3. Experimental

converted fluorescence signal passed through a broad band filter (Schott glass UG11 of 10 mm thickness, transmission range from 270 to 380 nm) and was detected with a photomultiplier tube (Valvo, type PM2254B) and a high-speed digital oscilloscope (LeCroy, type DSO 9362). The laser was operated at 1 Hz repetition rate.

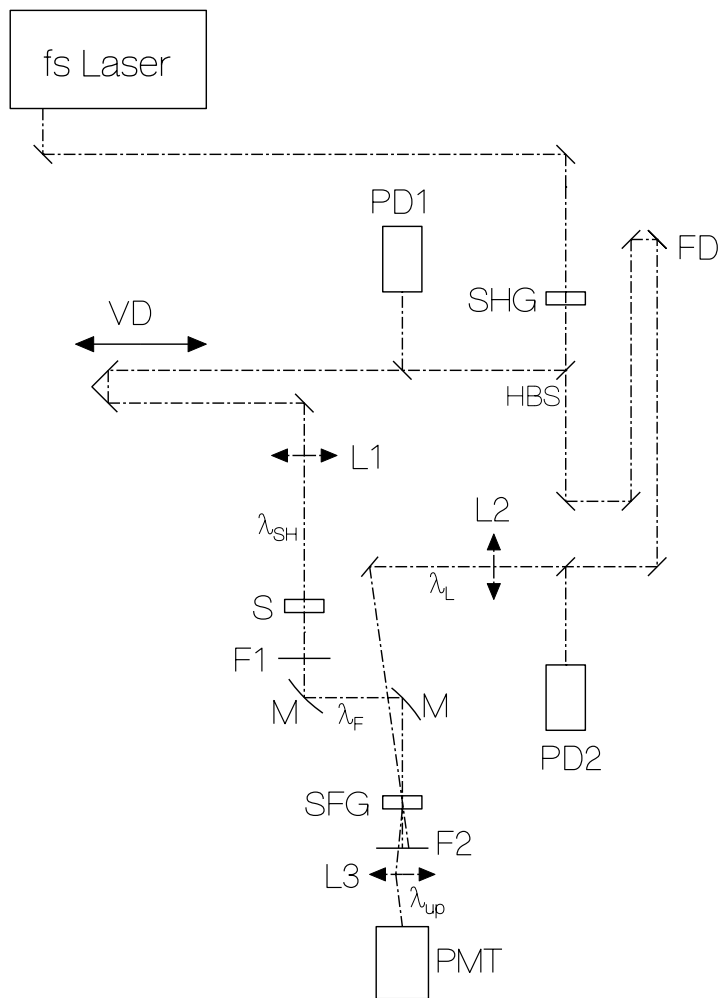


Figure 3.7: Scheme of experimental setup for fluorescence up-conversion. fs-Laser: femtosecond oscillator-amplifier system. SHG: BBO crystal for second harmonic generation. HBS: harmonic beam splitter. VD: variable delay-line. FD: fixed delay line. L1 - L3: lenses. S: sample. M: parabolic mirrors. PD1, PD2: photo-detectors. F1, F2: filters. SFG: BBO crystal for sum-frequency generation. PMT: photomultiplier tube.

3.5 Ground state absorption recovery

The ground-state absorption recovery of PFD was determined by pump and probe transmission measurement with the Hurricane laser system (applied pulse duration: 1.4 ps, wavelength 400 nm, and pulse energy 200 μJ) [Shi07a]. The experimental arrangement is shown in Figure 3.8. The pump pulse passes through a variable delay-line, and is focused to the sample (dye in a 1 mm glass cell) with a 50 cm lens in 46 cm distance from the sample. The probe pulse (applied pulse duration: 1.4 ps, wavelength 400 nm, pulse energy ca. 20 μJ) is split-off from the pulse (10 % of pump pulse) and is focused (focal length 50 cm, distance 46 cm) to the sample in opposite direction. The optical delay is varied with a stepper motor. The pump pulse transmission is measured with the photo-detectors PD1 and PD3, while the probe pulse transmission is measured with the photo-detectors PD1 and PD2.

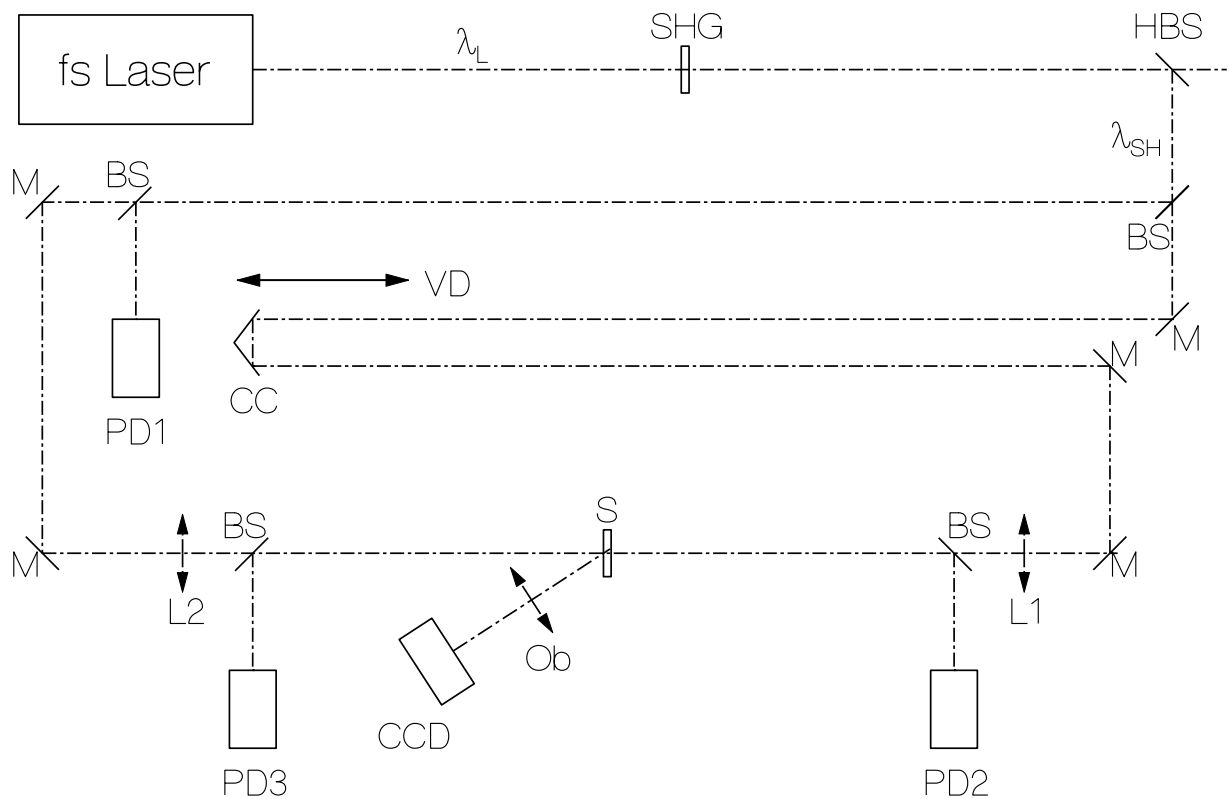


Figure 3.8: Scheme of experimental setup for pump-probe measurements. M: beam steering mirrors. BS: beam splitters. L1, L2: lenses. PD1-PD3: photo-detectors. Ob: camera objective. CCD: CCD camera

3.6 Photo-degradation

The photo-degradation measurements were carried out with the experimental arrangement shown in Figure 3.9. The setup consists of three parts: the excitation part, the detection part, and the probe part. In the excitation path a high-pressure mercury lamp or a high-pressure xenon lamp in combination with an interference filter is used as excitation source. In the photo-degradation experiments a small-volume sample cell were exposed to the excitation light. During light exposure transmission spectra were recorded at several times by passing the white light of an attenuated tungsten lamp or light of a deuterium lamp (in the case of UV degradation study) through the samples and measuring their spectral distributions with a spectrometer-diode array detection system (TRACOR DARRS).

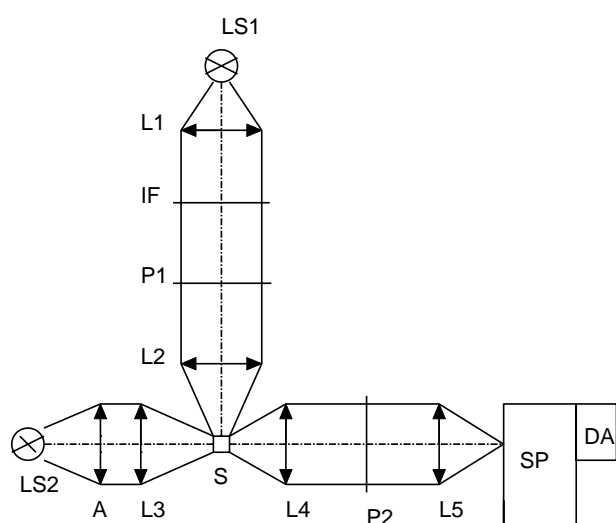


Figure 3.9: Experimental setup for photo-degradation measurements. LS1, light source (high pressure mercury lamp or high pressure Xenon lamp). LS2, tungsten lamp or deuterium lamp. IF, interference filter. L1-L5, lenses. P1, P2, polarisers. S, sample. SP, spectrometer. DA, diode-array detection system.

Quantum yield of photo-degradation is defined as the ratio of the length-integrated number density of degraded molecules (ΔN_D) to the number density of absorbed excitation photons by the un-destroyed molecules ($\Delta n_{ph,abs}$). Calculation of the quantum yields of photo-degradation as a function of the exposed energy density to the samples done by the relations:

$$\phi_D = \frac{\Delta N_D}{\Delta n_{ph,abs}}, \quad (3.2)$$

$$\Delta N_D = -\frac{\ln[T(w_1, \lambda_{pr})] - \ln[T(w_2, \lambda_{pr})]}{\sigma_a(\lambda_{pr})}, \quad (3.3)$$

and

$$\Delta n_{ph,abs} = \frac{w_2 - w_1}{h\nu_{exc}} \left(1 - \frac{T(w_1, \lambda_{exc}) + T(w_2, \lambda_{exc})}{2} \right). \quad (3.4)$$

ΔN_D is the length-integrated number density of degraded molecules (in cm^{-2}), and $\Delta n_{ph,abs}$ is the number density of absorbed excitation photons by the un-destroyed molecules (in cm^{-2}). $\sigma_a(\lambda_{pr})$ is the absorption cross-section of the un-destroyed molecules at the probe wavelength (photo-product absorption at λ_{pr} and λ_{exc} are neglected).

3.7 Mass spectroscopy

For identification of the produced photoproducts, mass spectra have been determined for dye IAE and BrPF, before and after some time of light exposure, by the work group of Prof. R. Deutzmann, Institut für Biochemie I, Universität Regensburg Germany, using an ion-trap mass-spectrometer (Bruker Esquire LC) with a nano-ESI (electro-spray-ionization) source. The spectra were recorded in the positive ion mode, and selected ions were fragmented for identification. The samples were infused in a 1:1 volume mixture of methanol/water containing 0.5 vol-% acetic acid (IAE and BrPF in acetonitrile, methanol) or in methanol with 1 vol-% acetic acid (IAE and BrPF in dichloromethane).

4. Results and discussion

In this chapter, absorption and emission spectroscopic results of the investigated dyads, the triad and their constituents: the phenyl-isoalloxazine IAE and BrPF, pyrene and 1-methylpyrene, heptyl-phenothiazine (HPT) and heptyl-phenyl-phenothiazine (HPPT) are given.

4.1 Phenyl-isoalloxazines dye IAE and BrPF

4.1.1 Results

The phenyl-isoalloxazine dye IAE and BrPF approximate the flavin constituents in the investigated dyads and triad. To understand the behaviour of the full compounds later, the photo-physics of the flavin compound is given in this section [Shi06]. The absorption cross-section spectra of IAE in dichloromethane, acetonitrile, and methanol are shown in Figure 4.1. The S_0 - S_1 absorption bands (extending up to $\lambda_u \approx 370$ nm) show a well resolved vibronic structures with peak absorption of the $S_0(\nu = 0)$ to $S_1(\nu = 1)$ transition at 442 nm for dichloromethane, and at 437 nm for acetonitrile. The vibronic structure in methanol is smeared out, and the S_0 - S_1 absorption peak is at 438 nm. Long-wavelength absorption shoulders are present around 550 nm in all three solvents. They are thought to be due to a small amount of impurity. The absorption tails remained unchanged by reducing the dye concentration a factor of ten (tested for acetonitrile) as well as by measuring at 10 °C and 30 °C (tested for all three solvents). These findings exclude the presence of physically bound ground-state dimers, since their absorption contribution should decrease with decreasing dye concentration and with increasing temperature [Her74, McR64, Kop81, Pen86].

The absorption cross-section spectra of BrPF in dichloromethane, acetonitrile, and methanol are shown in Figure 4.2. The S_0 - S_1 absorption bands (extending up to $\lambda_u \approx 370$ nm)

in acetonitrile and dichloromethane again show a well resolved vibronic structure with peak absorption at 442 nm for dichloromethane and at 437 nm for acetonitrile, while in methanol again the vibronic structure of the S_0 - S_1 band is smeared out. Well resolved long-wavelength absorption shoulders are present at around 550 nm, which are thought to be caused by some small amount of an unidentified impurity (absorption cross-section independent of concentration).

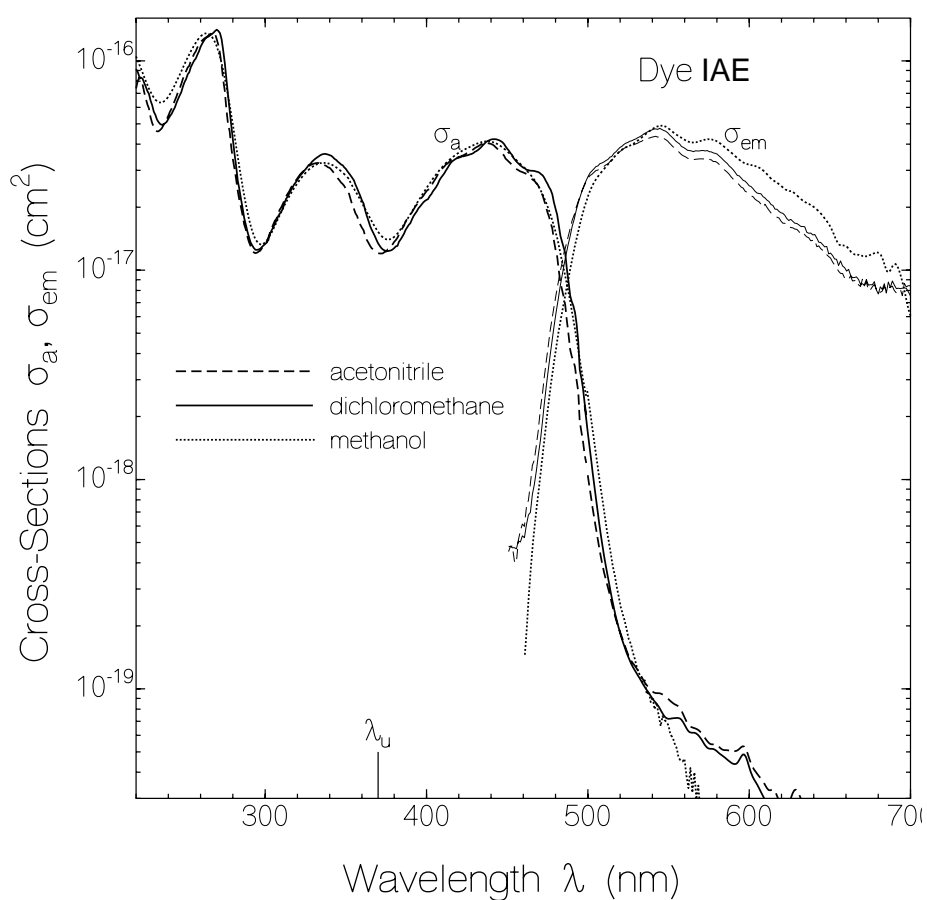


Figure 4.1: Absorption and stimulated emission cross-section spectra of IAE in dichloromethane (solid curves, concentration $C = 1.17 \times 10^{-3} \text{ mol dm}^{-3}$), acetonitrile (dashed curves, $C = 5.6 \times 10^{-4} \text{ mol dm}^{-3}$), and methanol (dotted curves, $C = 1.3 \times 10^{-4} \text{ mol dm}^{-3}$). λ_u indicates upper wavelength border of S_0 - S_1 transition.

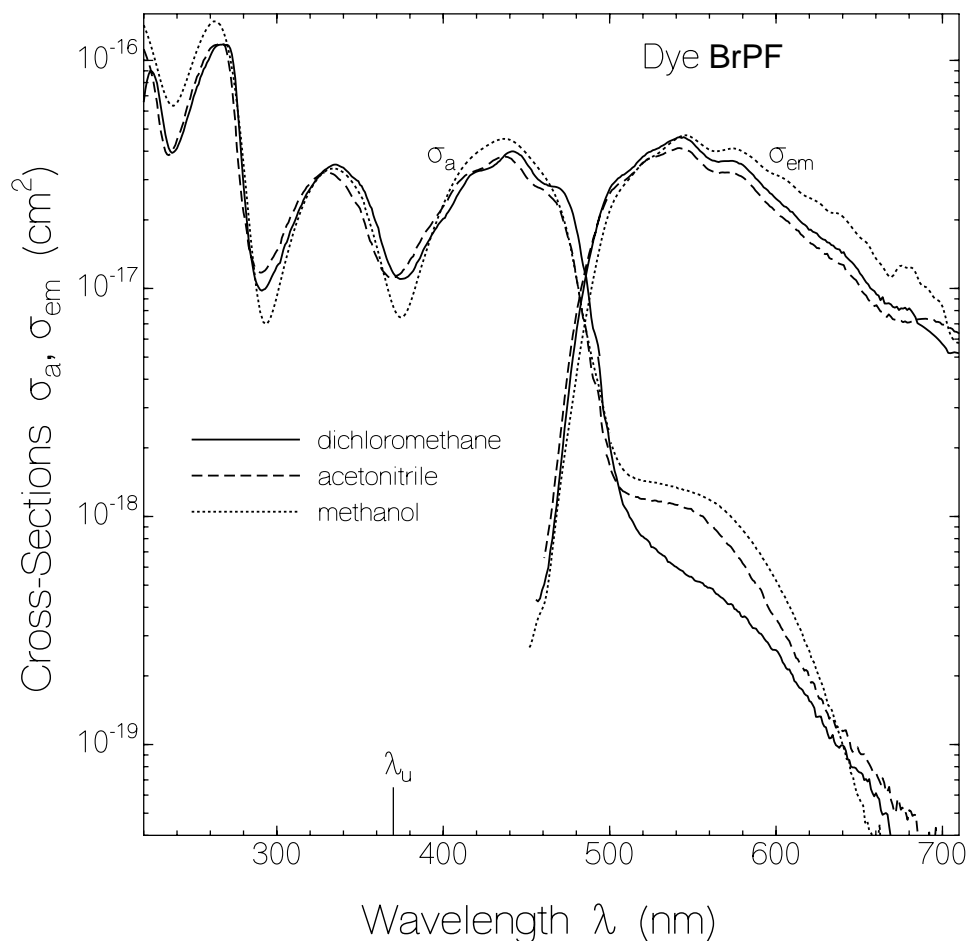


Figure 4.2: Absorption and stimulated emission cross-section spectra of BrPF in dichloromethane (solid curves, concentration $C = 6.1 \times 10^{-4} \text{ mol dm}^{-3}$), acetonitrile (dashed curves, $C = 4.5 \times 10^{-4} \text{ mol dm}^{-3}$), and methanol (dotted curves, $C = 1.3 \times 10^{-4} \text{ mol dm}^{-3}$).

The stimulated emission cross-section spectra of IAE and BrPF are included in Figure 4.1 and Figure 4.2, respectively. For both dyes the peak emission strength for the $S_1 (v = 0)$ to $S_0 (v = 1)$ transition is at 544 nm.

The fluorescence quantum distributions of IAE in dichloromethane (solid curve, $C = 1.4 \times 10^{-4} \text{ mol dm}^{-3}$, $\lambda_{\text{exc}} = 428 \text{ nm}$, viscosity $\eta(15 \text{ }^\circ\text{C}) = 0.449 \text{ cP}$), acetonitrile (dashed curve, $C = 1.1 \times 10^{-4} \text{ mol dm}^{-3}$, $\lambda_{\text{exc}} = 428 \text{ nm}$, $\eta(15 \text{ }^\circ\text{C}) = 0.375 \text{ cP}$), and methanol (dash-dotted curve, $C = 3.79 \times 10^{-4} \text{ mol dm}^{-3}$, $\lambda_{\text{exc}} = 428 \text{ nm}$, $\eta(15 \text{ }^\circ\text{C}) = 0.623 \text{ cP}$) are shown in Figure 4.3. The extracted fluorescence quantum yields (Equation 2.10), $\phi_F = \int_{em} E_F(\lambda) d\lambda$, are $\phi_F(\text{IAE, dichloromethane}) = 0.22$, $\phi_F(\text{IAE, acetonitrile}) = 0.15$, and $\phi_F(\text{IAE, methanol}) = 0.09$. The

4. Results and discussion: Phenyl-isalloxazines dye IAE and BrPF

values are listed in Table 4.1. There is no relation between the fluorescence quantum yield and the solvent viscosity. The fluorescence quantum distribution of IAE in acetonitrile in the case of long-wavelength excitation at $\lambda_{\text{exc}} = 548$ nm (impurity excitation) is included in the top part of Figure 4.3. The approximate fluorescence quantum yield is $\phi_{\text{F}} \approx 0.015$.

The fluorescence polarisation spectra, $P_{\text{F}}(\lambda)$, of IAE in dichloromethane, acetonitrile, and methanol are plotted in lower part of Figure 4.3. ($\lambda_{\text{exc}} = 428$ nm). The average degree of fluorescence polarisation is found to be $P_{\text{F}}(\text{IAE}) \approx 0.05$ for all three solvents.

The fluorescence quantum distributions of BrPF in dichloromethane (solid curve, $C = 1.3 \times 10^{-4}$ mol dm⁻³, $\lambda_{\text{exc}} = 428$ nm), acetonitrile (dashed curve, $C = 9.8 \times 10^{-5}$ mol dm⁻³, $\lambda_{\text{exc}} = 428$ nm), and methanol (dash-dotted curve, $C = 1.98 \times 10^{-4}$ mol dm⁻³, $\lambda_{\text{exc}} = 428$ nm) are shown in top part of Figure 4.4. The extracted fluorescence quantum yields are $\phi_{\text{F}}(\text{BrPF, dichloromethane}) = 0.28$, $\phi_{\text{F}}(\text{BrPF, acetonitrile}) = 0.25$, and $\phi_{\text{F}}(\text{BrPF, methanol}) = 0.17$. The fluorescence quantum distribution of BrPF in acetonitrile in the case of excitation at $\lambda_{\text{exc}} = 548$ nm is included in Figure 4.4. The approximate fluorescence quantum yield is $\phi_{\text{F}} \approx 0.015$.

The fluorescence polarisation spectra, $P_{\text{F}}(\lambda)$, of dye BrPF in dichloromethane, acetonitrile, and methanol are plotted in lower part of Figure 4.4. The average degree of fluorescence polarisation is $P_{\text{F}}(\text{BrPF}) \approx 0.039$ for all three applied solvents.

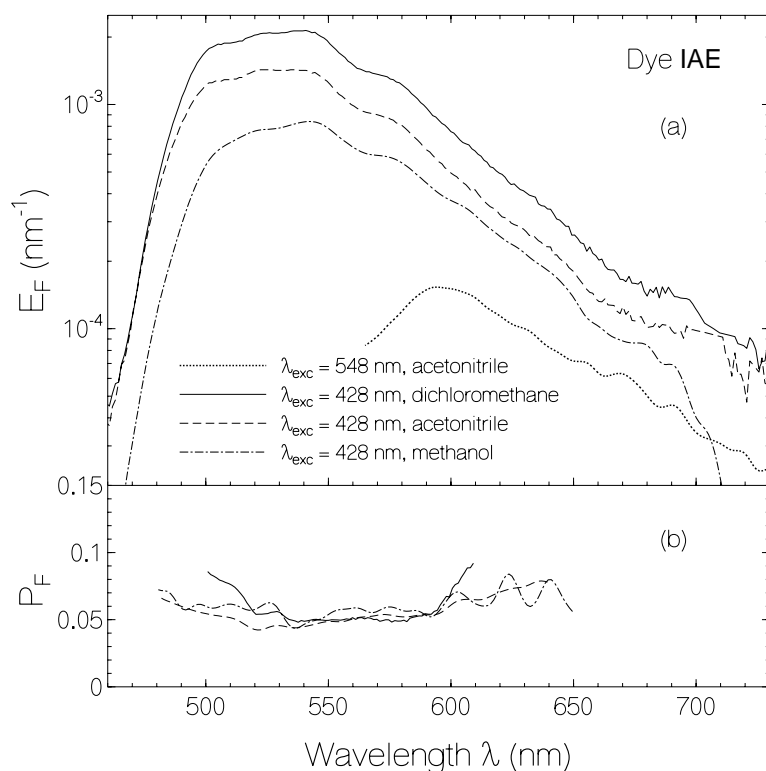


Figure 4.3: (a) Fluorescence quantum distributions, $E_F(\lambda)$, of dye IAE in dichloromethane (solid curve, $\lambda_{\text{exc}} = 428$ nm), acetonitrile (dashed curve, $\lambda_{\text{exc}} = 428$ nm), methanol (dash-dotted curve, $\lambda_{\text{exc}} = 428$ nm), and of impurity in dye IAE in acetonitrile (dotted curve, $\lambda_{\text{exc}} = 548$ nm).

(b) Spectra of degree of fluorescence polarization, $P_F(\lambda)$, of IAE in dichloromethane (solid curve), acetonitrile (dashed curve), and methanol (dash-dotted curve). Excitation wavelength $\lambda_{\text{exc}} = 428$ nm

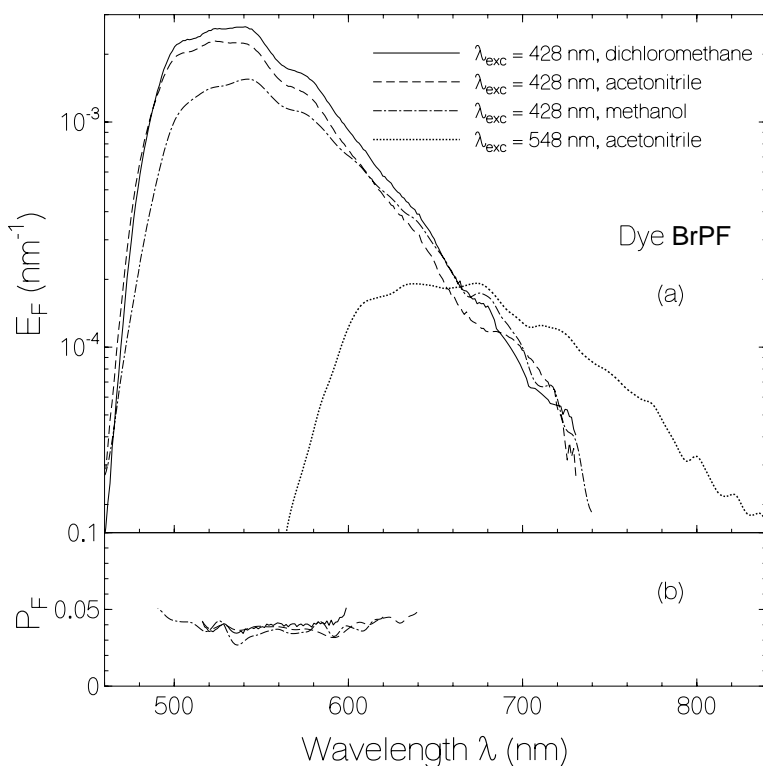


Figure 4.4: (a) Fluorescence quantum distributions, $E_F(\lambda)$, of dye BrPF in dichloromethane (solid curve, $\lambda_{\text{exc}} = 428$ nm), acetonitrile (dashed curve, $\lambda_{\text{exc}} = 428$ nm), methanol (dash-dotted curve, $\lambda_{\text{exc}} = 428$ nm), and of impurity in dye BrPF in acetonitrile (dotted curve, $\lambda_{\text{exc}} = 548$ nm).

(b) Spectra of degree of fluorescence polarisation, $P_F(\lambda)$, of dye BrPF in dichloromethane (solid curve), acetonitrile (dashed curve), and methanol (dash-dotted curve). Excitation wavelength $\lambda_{\text{exc}} = 428$ nm.

Some temporal fluorescence traces are shown in Figure 4.5. The determined fluorescence lifetimes are listed in Table 4.1. The solid curve in part (a) depicts the fluorescence signal of IAE in dichloromethane in the case of excitation at $\lambda_L = 400$ nm (duration $\Delta t_L = 4$ ps) and fluorescence collection in the wavelength range from 500 nm to 610 nm (broad-band interference filter). The dashed curve belongs to IAE in acetonitrile, and the dash-dotted line belongs to IAE in methanol. The fluorescence signals fit well to a single-exponential decay according to (Equation 2.4).

Fluorescence lifetimes of τ_F (IAE, dichloromethane) = 4.4 ns, τ_F (IAE, acetonitrile) = 3.3 ns, and τ_F (IAE, methanol) = 2.1 ns are extracted.

- The fluorescence signal obtained by long-wavelength excitation at $\lambda_L = 527$ nm (pulse duration $\Delta t_L = 6$ ps) and fluorescence detection in the wavelength range from 645 nm to 699 nm (interference filter) is shown by the triple-dotted curve in Figure 4.5. It is composed of two single-exponential contributions (dye IAE and impurity) according to

$$S_F(t) = S_{F,0} [\kappa \exp(-t/\tau_F) + (1 - \kappa) \exp(-t/\tau_{F,im})]. \quad (4.1)$$

where κ gives the dye IAE contribution, and $\tau_{F,im}$ is the fluorescence lifetime of the impurity. The best fitting parameters are $\kappa \approx 0.26$ and $\tau_{F,im} \approx 0.3$ ns (fit curve not shown). The short fluorescence lifetime and finite fluorescence quantum yield ($\tau_{rad,im} = \tau_{F,im}/\phi_{F,im} \approx 20$ ns) excludes a singlet-triplet absorption of dye IAE as origin of the observed the absorption in the 500nm to 600 nm range (radiative lifetime of triplet state would be longer).

Temporal fluorescence signal traces of BrPF in dichloromethane (solid curve), acetonitrile (dashed curve), and methanol (dash-dotted curve) are shown in part (b) of Figure 4.5. The same experimental arrangements have been applied as for dye IAE. Again the fluorescence signals fit well to a single-exponential decay. The obtained fluorescence lifetimes of BrPF in dichloromethane ($\tau_F = 5.3$ ns) and of BrPF in acetonitrile ($\tau_F = 5.5$ ns) are quite similar. For

dye BrPF in methanol a shorter fluorescence lifetime of $\tau_F = 3.8$ ns is measured. The impurity fluorescence lifetime of BrPF in acetonitrile (triple-dotted curve in Figure 4.5b) was found to be $\tau_{F,im} \approx 0.87$ ns (dye BrPF contribution $\kappa \approx 0.11$, $\tau_{rad,im} = \tau_{F,im}/\phi_{F,im} \approx 60$ ns)

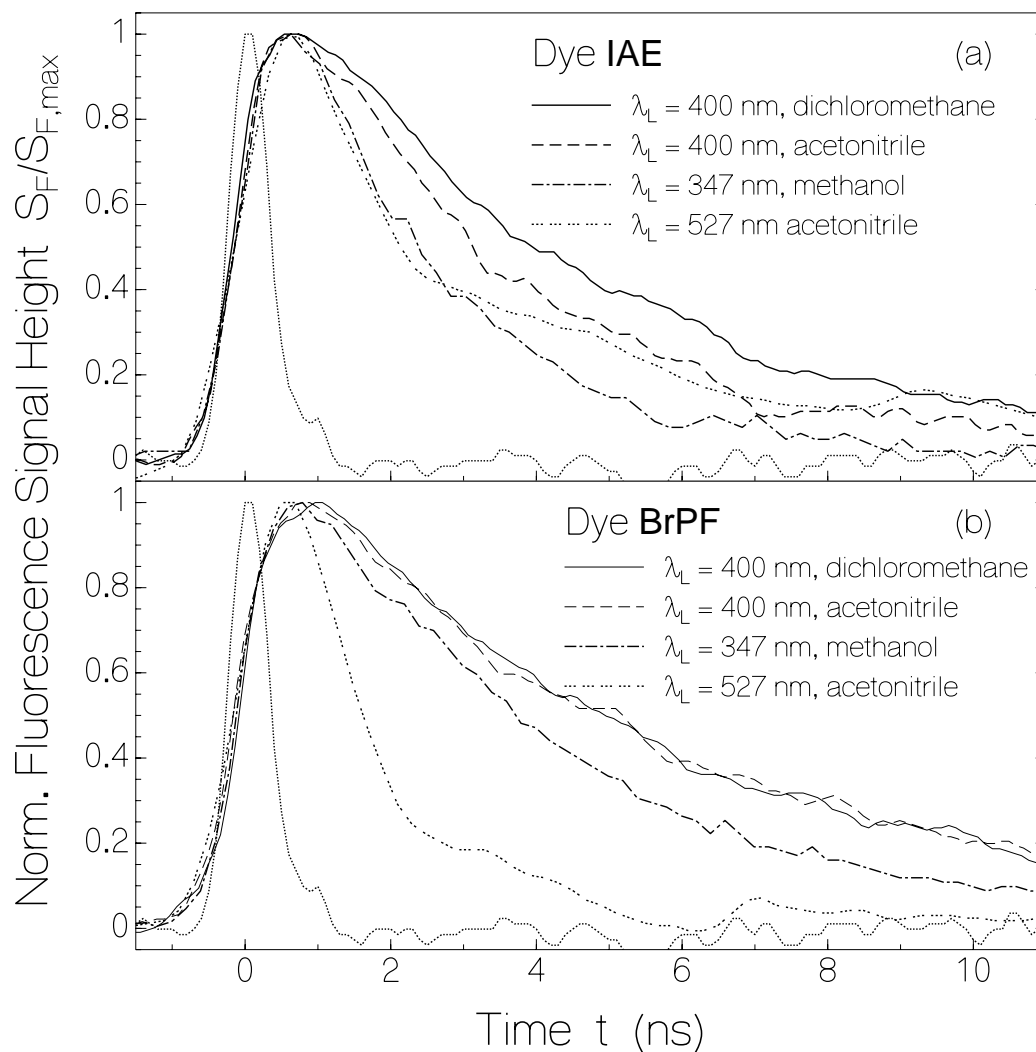


Figure 4.5: Temporal fluorescence signals of dyes IAE and BrPF. Dotted curve is system response function.

a) Dye IAE. Solid line: solvent dichloromethane, excitation wavelength $\lambda_L = 400$ nm, fluorescence lifetime $\tau_F = 4.3$ ns. Dashed line: solvent acetonitrile, $\lambda_L = 400$ nm, $\tau_F = 3.2$ ns. Dash-dotted lines: solvent methanol, $\lambda_L = 347.15$ nm, $\tau_F = 2.1$ ns. Triple-dotted line: solvent acetonitrile, $\lambda_L = 527$ nm.

b) Dye BrPF. Solid line: solvent dichloromethane, $\lambda_L = 400$ nm, $\tau_F = 5.3$ ns. Dashed line: solvent acetonitrile, $\lambda_L = 400$ nm, $\tau_F = 5.5$ ns. Dash-dotted line: solvent methanol, $\lambda_L = 347.15$ nm, $\tau_F = 3.8$ ns. Triple-dotted line: solvent acetonitrile, $\lambda_L = 527$ nm.

4. Results and discussion: Phenyl-isoalloxazines dye IAE and BrPF

Mass spectra are shown in Figure 4.6 top row (dye IAE) and Figure 4.7 top row (dye BrPF). The lower rows were observed after photo-degradation and will be discussed later. They reveal the molar masses of dye IAE (peak indicated by I, dye IAE + H⁺: $m/z = 377.1$, dye IAE + Na⁺: $m/z = 399.1$) and dye BrPF (dye BrPF + H⁺: $m/z = 383.0$ and 385.0 due to Br isotopes, dye BrPF + Na⁺: $m/z = 405.0$ and 407.0). The mass spectra were recorded up to $m/z \approx 800$, but the displayed spectra are restricted $m/z < 490$ nm.

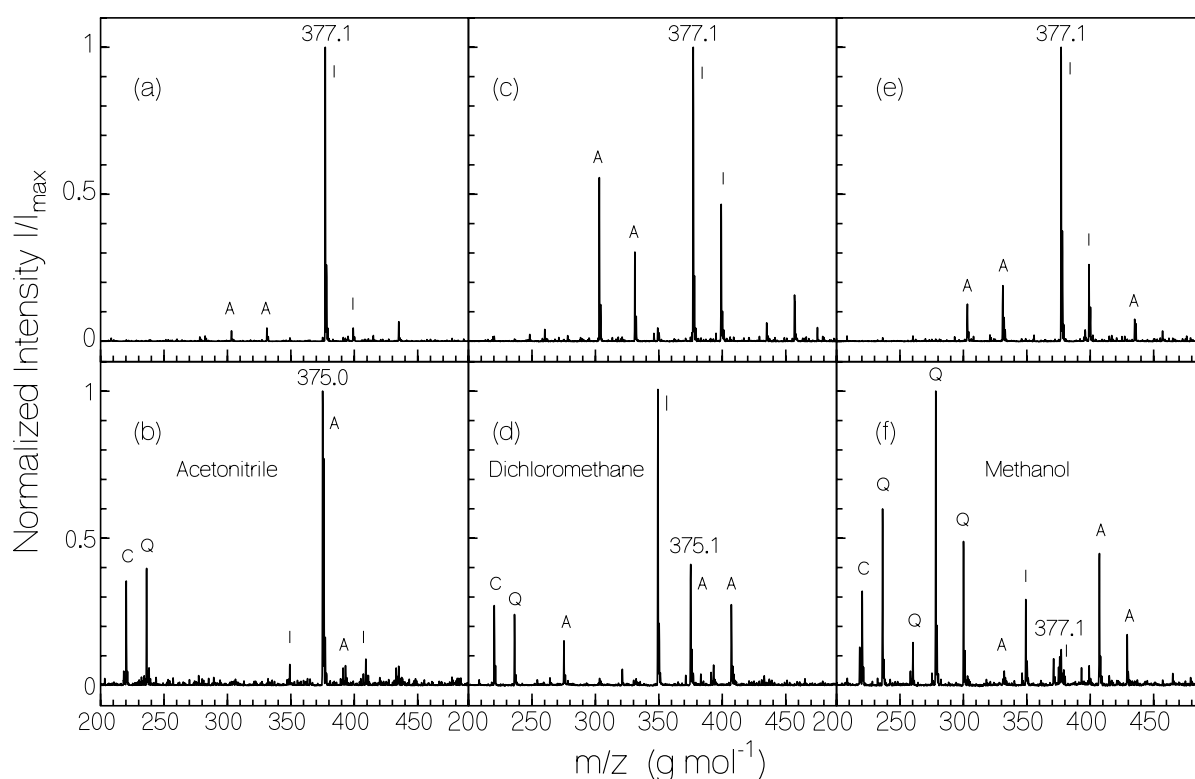


Figure 4.6: Mass spectra of dye IAE in the solvents acetonitrile, dichloromethane, and methanol before (top row) and after light exposure (bottom row). Excitation occurred at 428 nm. The excitation intensities, I_{exc} , and the periods of exposure, t_{exp} , are 0.0175 W cm^{-2} and 50 min for acetonitrile (b), 0.0175 W cm^{-2} and 79 min for dichloromethane (d), 0.0182 W cm^{-2} and 7 min for methanol (f). The peaks are attributed to: 377.1: dye IAE + H⁺; 399.1: dye IAE + Na⁺; 409.1: dye IAE + H⁺ + methanol; 331.1: I + H⁺ with $R_1 = \text{H}$, $R_2 = \text{CH}_2\text{CH}_2\text{CH}_3$; 303.2: I + H⁺ with $R_1 = \text{H}$, $R_2 = \text{CH}_3$; 349.2: I + H⁺ with $R_1 = \text{H}$, $R_2 = \text{CH}_2\text{COOH}$; 375.1: A + H⁺ with $R_1 = \text{H}$, $R_2 = \text{CH}_2\text{COOC}_2\text{H}_5$; 393.1: A + H⁺ + H₂O with $R_1 = \text{H}$, $R_2 = \text{CH}_2\text{COOC}_2\text{H}_5$; 407.2: A + H⁺ + methanol with $R_1 = \text{H}$, $R_2 = \text{CH}_2\text{COOC}_2\text{H}_5$; 429.1: A + Na⁺ + methanol with $R_1 = \text{H}$, $R_2 = \text{CH}_2\text{COOC}_2\text{H}_5$; 435.1: A + H⁺ + acetic acid with $R_1 = \text{H}$, $R_2 = \text{CH}_2\text{COOC}_2\text{H}_5$; 332.1: A + H⁺ with $R_1 = \text{H}$, $R_2 = \text{CH}_2\text{COOH}$; 275.3: A + H⁺ with $R_1 = \text{H}$, $R_2 = \text{H}$; 278.2: Q + H⁺ with $R_1 = \text{H}$, $R_2 = \text{NCHO}$, $R_3 = \text{CH}_2\text{OH}$; 300.1: Q + Na⁺ with $R_1 = \text{H}$, $R_2 = \text{NCHO}$, $R_3 = \text{CH}_2\text{OH}$; 260.2: Q + H⁺ + methanol with $R_1 = \text{H}$, $R_2 = \text{NH}$, $R_3 = \text{CH}_3$; 236.3: Q + H⁺ with $R_1 = \text{H}$, $R_2 = \text{NH}$, $R_3 = \text{CH}_3$; 220.3: C + H⁺ with $R_1 = \text{H}$, $R_2 = \text{NH}$, $R_3 = \text{H}$.

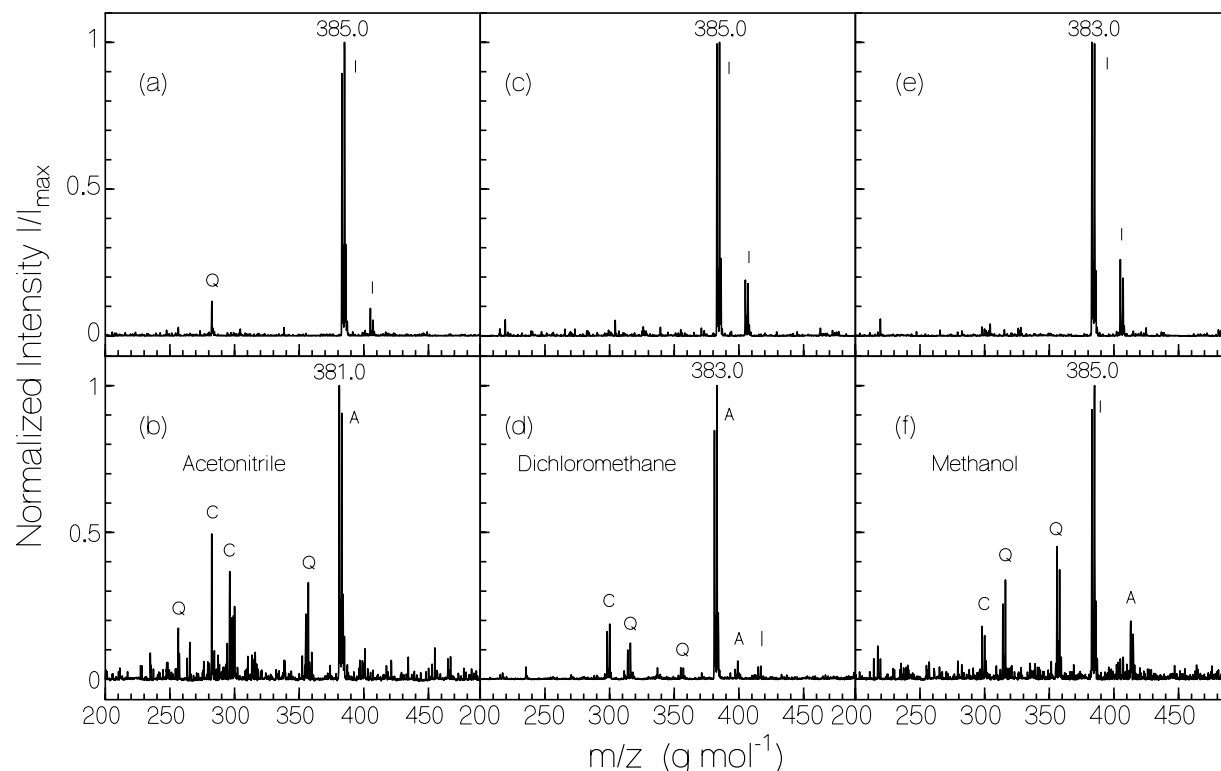


Figure 4.7: Mass spectra of dye BrPF in the solvents acetonitrile, dichloromethane, and methanol before (top row) and after light exposure (bottom row). Excitation occurred at 428 nm. The excitation intensities, I_{exc} , and the periods of exposure, t_{exp} , are 0.0155 W cm^{-2} and 167 min for acetonitrile (b), 0.0175 W cm^{-2} and 54 min for dichloromethane (d), 0.0182 W cm^{-2} and BrPF70 min for methanol (f). The peaks are attributed to: 383.0 and 385.0: dye BrPF + H^+ ; 405.0 and 407.0: dye BrPF + Na^+ ; 412.9 and 414.9: A + H^+ + methanol with $\text{R}_1 = \text{Br}$, $\text{R}_2 = \text{CH}_3$; 355.1 and 357.1: Q + H^+ with $\text{R}_1 = \text{Br}$, $\text{R}_2 = =\text{NCHO}$, $\text{R}_3 = \text{CHO}$; 356.0 and 358.0: Q + H^+ + H (semiquinone form) with $\text{R}_1 = \text{Br}$, $\text{R}_2 = =\text{NCHO}$, $\text{R}_3 = \text{CHO}$; 314.1 and 316.1: Q + H^+ with $\text{R}_1 = \text{Br}$, $\text{R}_2 = =\text{NH}$, $\text{R}_3 = \text{CH}_3$; 304.3: Q + Na^+ with $\text{R}_1 = \text{H}$, $\text{R}_2 = =\text{NCH}_2\text{OH}$, $\text{R}_3 = \text{CH}_2\text{OH}$; 282.4: Q + H^+ with $\text{R}_1 = \text{H}$, $\text{R}_2 = =\text{NCH}_2\text{OH}$, $\text{R}_3 = \text{CH}_2\text{OH}$; 256.4: Q + Na^+ with $\text{R}_1 = \text{H}$, $\text{R}_2 = =\text{NH}$, $\text{R}_3 = \text{CH}_3$; 234.9: Q + H^+ with $\text{R}_1 = \text{H}$, $\text{R}_2 = =\text{NH}$, $\text{R}_3 = \text{CH}_3$; 298.0 + 300.0: C + H^+ with $\text{R}_1 = \text{Br}$, $\text{R}_2 = =\text{NH}$, $\text{R}_3 = \text{H}$; 282.4: C + H^+ + H (semiquinone form) with $\text{R}_1 = \text{H}$, $\text{R}_2 = \text{NHCH}_2\text{OH}$, $\text{R}_3 = \text{CH}_2\text{OH}$;

Dimer mass peaks were observed for dye IAE. Fragmentation of the dimer peak observed for dye IAE gave only the monomer peak without higher m/z components, indicating that no covalently bound dimers were present (should have shown up in fragments).

The absorption changes due to blue-light ($\lambda_{exc} = 428 \text{ nm}$) excitation of IAE in acetonitrile (part a), dichloromethane (part b), and methanol (part c) are shown in Figure 4.8. Absorption coefficient spectra are depicted for different times of light exposure at fixed excitation intensities, I_{exc} . At the longest exposure time practically all original molecules have been

converted to photoproducts, and the remaining spectra belong to the photoproducts. The speed of photo-degradation and the shape of the photoproduct spectra depend somewhat on the solvent. In acetonitrile and dichloromethane the long-wavelength absorption tail is first decreased due to photo-degradation of the impurity, and then a long-wavelength absorption band builds up due to the formation of long-wavelength absorbing photoproducts. After initially slow absorption reduction of the main band around 440 nm, the absorption decrease is speeded-up (see below Figure 4.10). It is thought that the photo-fragments enhance the isoalloxazine degradation. The product formation stops when the excitation light is switched off (this was tested experimentally on dye IAE in acetonitrile by stopping light exposure at certain times of exposure).

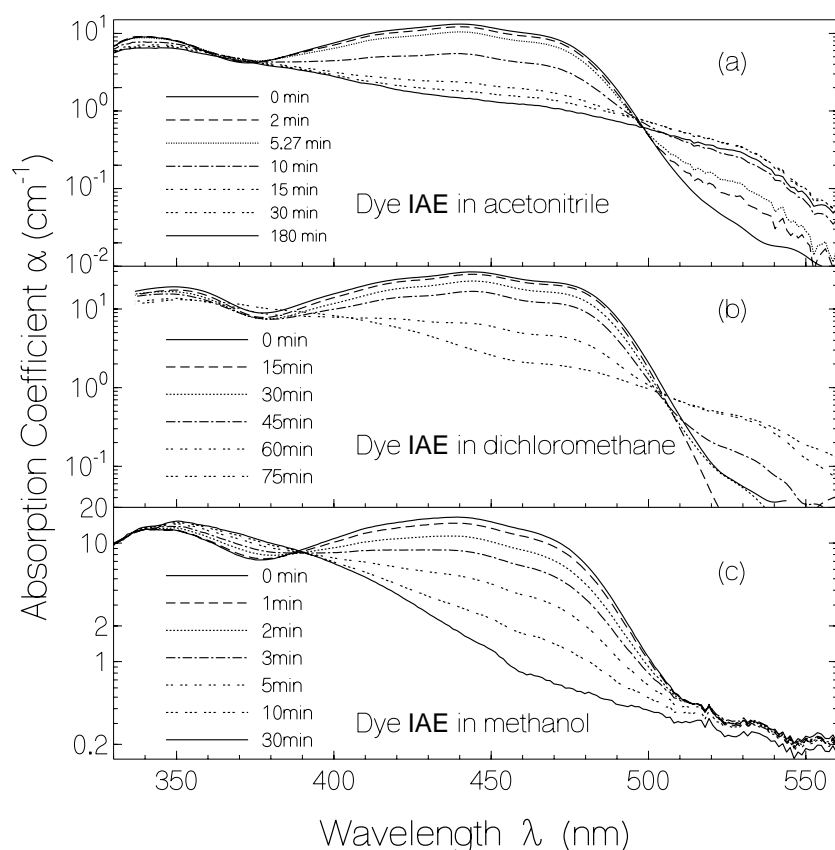


Figure 4.8: Absorption coefficient spectra of dye IAE after several durations of light exposure. Excitation wavelength $\lambda_{\text{exc}} = 428$ nm. Exposure times are listed in legends.
 (a) Solvent acetonitrile. Excitation intensity $I_{\text{exc}} = 0.0368$ W cm^{-2} .
 (b) Solvent dichloromethane. $I_{\text{exc}} = 3.31 \times 10^{-3}$ W cm^{-2} .
 (c) Solvent methanol. $I_{\text{exc}} = 6.85 \times 10^{-3}$ W cm^{-2} .

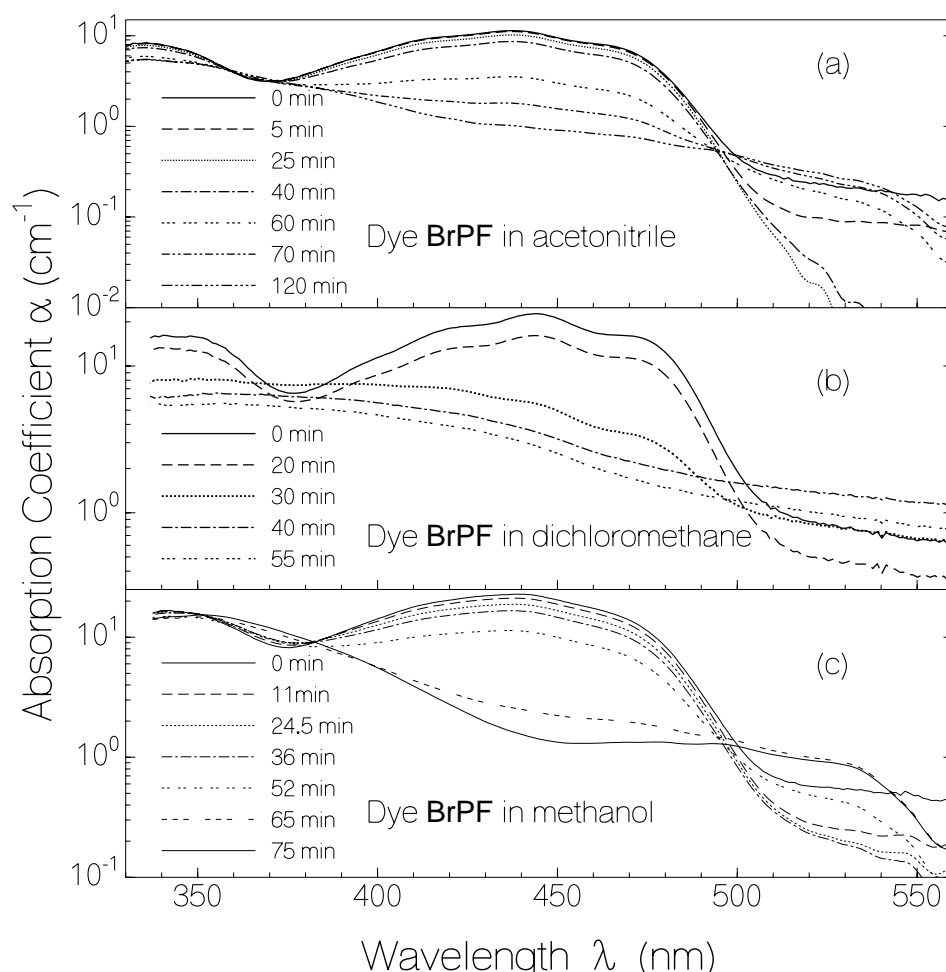


Figure 4.9: Absorption coefficient spectra of dye BrPF after several durations of light exposure. Excitation wavelength $\lambda_{\text{exc}} = 428$ nm. Exposure times are listed in legends.
 (a) Solvent acetonitrile. Excitation intensity $I_{\text{exc}} = 0.0268$ W cm⁻².
 (b) Solvent dichloromethane. $I_{\text{exc}} = 0.0114$ W cm⁻².
 (c) Solvent methanol. $I_{\text{exc}} = 0.0268$ W cm⁻².

The absorption changes due to blue-light ($\lambda_{\text{exc}} = 428$ nm) excitation of dye BrPF in acetonitrile (part a), dichloromethane (part b), and methanol (part c) are shown in Figure 4.9. As in Figure 4.8 absorption coefficient spectra are depicted for different times of light exposure at fixed excitation intensities, I_{exc} . Again the rate of photo-degradation speeds up after some time of exposure (see Figure 4.11), and again the long-wavelength impurity absorption band decreases and a new long-wavelength absorption band is build up by photoproduct formation.

The reduction of absorption at the wavelength position, λ_p , of peak S_0 - S_1 absorption due to light exposure is displayed in Figures 4.10 and 4.11 for dye IAE and dye BrPF, respectively. The data points are taken from Figures 4.8 and 4.9. In all cases the initial absorption decrease is small and then after some time of exposure the absorption decreases faster (enhancement of quantum yield of photo-degradation). The fastening of the photo-degradation is thought to be caused by formed photo-fragments. In the discussion below the experimental exposure dependence will be used to determine rate constants and quantum yields of photo-degradation.

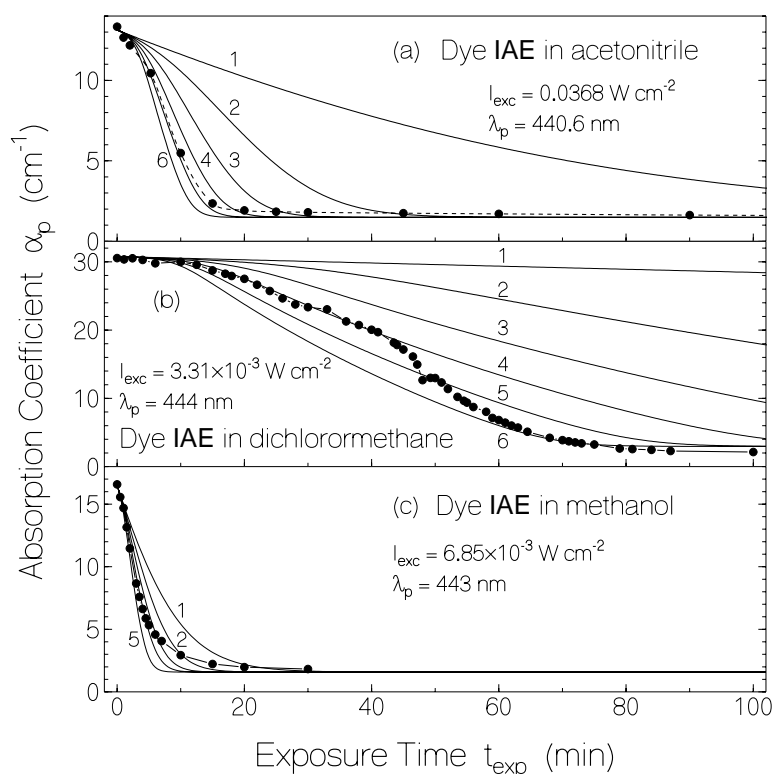


Figure 4.10: Dependence of peak S_0 - S_1 absorption coefficient, α_p , of dye IAE on exposure time at fixed excitation intensity. Excitation wavelength $\lambda_{exc} = 428$ nm. Data are taken from Figure 4.8.

(a) Solvent acetonitrile. Curves are calculated (Equations 14-16) for $k_1 = 5 \times 10^4 \text{ s}^{-1}$ ($\phi_{D,0} = 1.65 \times 10^{-4}$), and (1) $k_2 = 0$, (2) $1 \times 10^{-12} \text{ s}^{-1} \text{ cm}^3$, (3) $2 \times 10^{-12} \text{ s}^{-1} \text{ cm}^3$, (4) $3 \times 10^{-12} \text{ s}^{-1} \text{ cm}^3$, (5) $4 \times 10^{-12} \text{ s}^{-1} \text{ cm}^3$, (6) $5 \times 10^{-12} \text{ s}^{-1} \text{ cm}^3$.

(b) Solvent dichloromethane. Curves are calculated for $k_1 = 5 \times 10^4 \text{ s}^{-1}$ ($\phi_{D,0} = 2.2 \times 10^{-4}$), and (1) $k_2 = 0$, (2) $2 \times 10^{-12} \text{ s}^{-1} \text{ cm}^3$, (3) $4 \times 10^{-12} \text{ s}^{-1} \text{ cm}^3$, (4) $6 \times 10^{-12} \text{ s}^{-1} \text{ cm}^3$, (5) $8 \times 10^{-12} \text{ s}^{-1} \text{ cm}^3$, (6) $1 \times 10^{-11} \text{ s}^{-1} \text{ cm}^3$.

(c) Solvent methanol. Curves are calculated for $k_1 = 3.5 \times 10^6 \text{ s}^{-1}$ ($\phi_{D,0} = 7.7 \times 10^{-3}$), and (1) $k_2 = 0$, (2) $1 \times 10^{-11} \text{ s}^{-1} \text{ cm}^3$, (3) $2 \times 10^{-11} \text{ s}^{-1} \text{ cm}^3$, (4) $3 \times 10^{-11} \text{ s}^{-1} \text{ cm}^3$, (5) $5 \times 10^{-11} \text{ s}^{-1} \text{ cm}^3$.

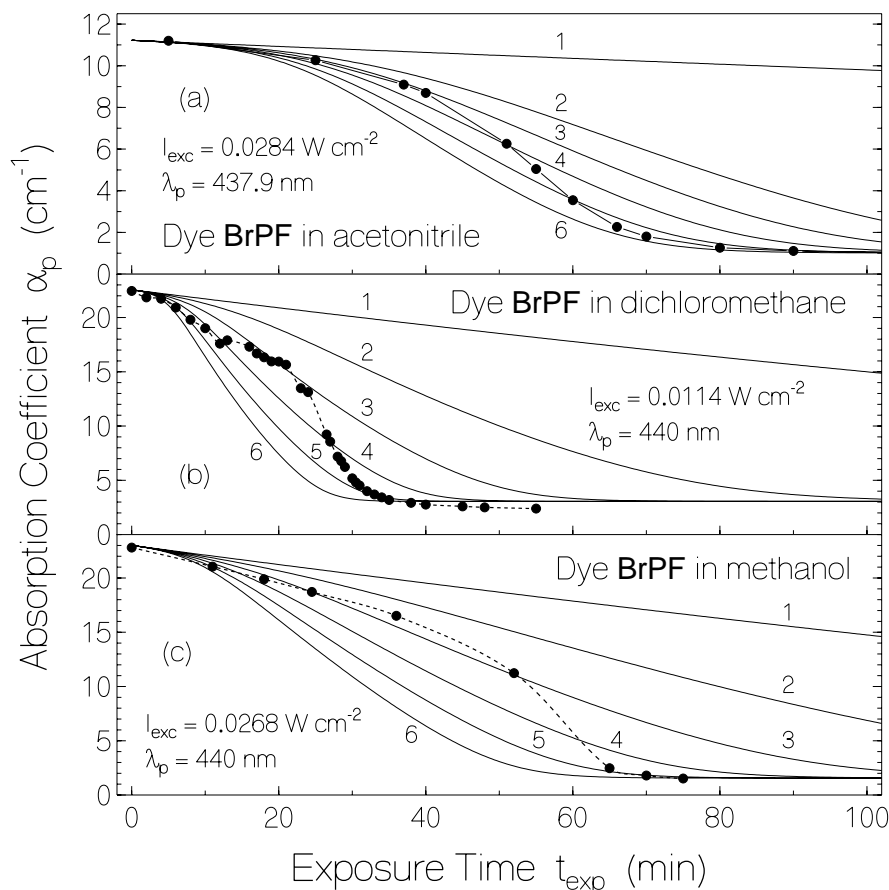


Figure 4.11: Dependence of peak S_0 - S_1 absorption coefficient, α_p , of dye BrPF on exposure time at fixed excitation intensity. Excitation wavelength $\lambda_{exc} = 428$ nm. Data are taken from Figure 4.9.

(a) Solvent acetonitrile. Curves are calculated (Equations 14-16) for $k_1 = 4 \times 10^3 \text{ s}^{-1}$ ($\phi_{D,0} = 2.2 \times 10^{-5}$), and (1) $k_2 = 0$, (2) $4 \times 10^{-13} \text{ s}^{-1} \text{ cm}^3$, (3) $5 \times 10^{-13} \text{ s}^{-1} \text{ cm}^3$, (4) $6 \times 10^{-13} \text{ s}^{-1} \text{ cm}^3$, (5) $7 \times 10^{-13} \text{ s}^{-1} \text{ cm}^3$, (6) $8 \times 10^{-13} \text{ s}^{-1} \text{ cm}^3$.

(b) Solvent dichloromethane. Curves are calculated for $k_1 = 5 \times 10^4 \text{ s}^{-1}$ ($\phi_{D,0} = 2.7 \times 10^{-4}$), and (1) $k_2 = 0$, (2) $1 \times 10^{-12} \text{ s}^{-1} \text{ cm}^3$, (3) $2 \times 10^{-12} \text{ s}^{-1} \text{ cm}^3$, (4) $3 \times 10^{-12} \text{ s}^{-1} \text{ cm}^3$, (5) $4 \times 10^{-12} \text{ s}^{-1} \text{ cm}^3$, (6) $5 \times 10^{-12} \text{ s}^{-1} \text{ cm}^3$.

(c) Solvent methanol. Curves are calculated for for $k_1 = 2.5 \times 10^4 \text{ s}^{-1}$ ($\phi_{D,0} = 9.5 \times 10^{-5}$), and (1) $k_2 = 0$, (2) $2 \times 10^{-13} \text{ s}^{-1} \text{ cm}^3$, (3) $4 \times 10^{-13} \text{ s}^{-1} \text{ cm}^3$, (4) $6 \times 10^{-13} \text{ s}^{-1} \text{ cm}^3$, (5) $8 \times 10^{-13} \text{ s}^{-1} \text{ cm}^3$, (6) $1 \times 10^{-12} \text{ s}^{-1} \text{ cm}^3$.

The changes in the fluorescence quantum distributions due to light exposure are shown in Figure 4.12a and 4.12b for the samples IAE in acetonitrile and BrPF in methanol, respectively. The samples were degraded by light exposure at $\lambda_{exc} = 428$ nm. The fluorescence spectra were taken after certain times of light exposure and the fluorescence quantum distributions are calculated. The fluorescence quantum yields, $\phi_F = \int E_F(\lambda) d\lambda$, decrease with exposure time to a certain limit. At the longest times of applied exposure the

4. Results and discussion: Phenyl-isoalloxazines dye IAE and BrPF

fluorescence quantum yields are $\phi_F(\text{IAE}_{\text{degraded}}, \text{acetonitrile}) \approx 0.03$ and $\phi_F(\text{BrPF}_{\text{degraded}}, \text{methanol}) \approx 0.05$. The fluorescence quantum distributions broadened due to fluorescence contributions from several photoproducts.

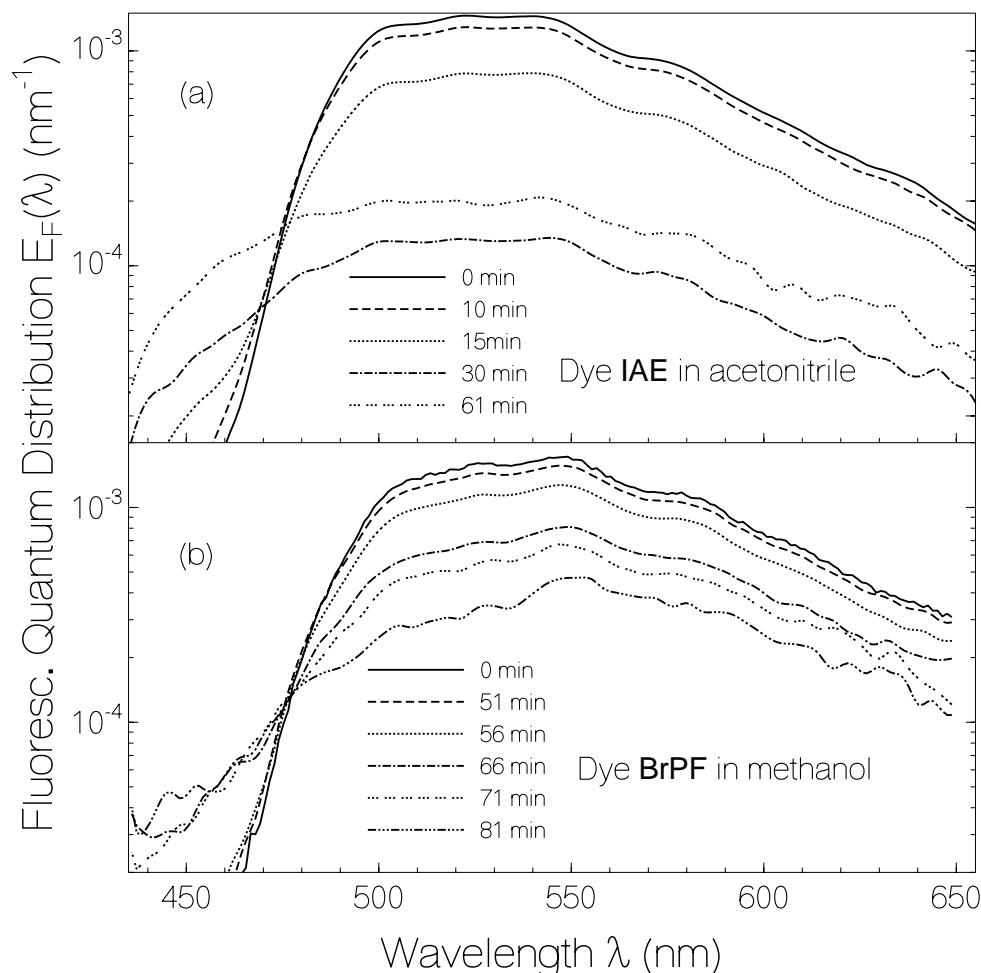


Figure 4.12: Fluorescence quantum distributions after several durations of light exposure at $\lambda_{\text{exc}} = 428$ nm.

(a) Dye IAE in acetonitrile. Excitation intensity $I_{\text{exc}} = 0.029 \text{ W cm}^{-2}$.

(b) Dye BrPF in methanol. $I_{\text{exc}} = 0.027 \text{ W cm}^{-2}$.

The temporal fluorescence traces of the photo-degraded dye IAE in acetonitrile and the photo-degraded dye BrPF in methanol show single-exponential fluorescence decays with lifetimes $\tau_F(\text{IAE}_{\text{degraded}}, \text{acetonitrile}) = 8.6 \text{ ns}$ and $\tau_F(\text{BrPF}_{\text{degraded}}, \text{methanol}) = 3.4 \text{ ns}$ (curves not depicted). The fluorescence traces were obtained by excitation of the light-exposed samples with picosecond light pulses of duration $\Delta t_L \approx 35 \text{ ps}$ and of wavelength $\lambda_L = 347.15 \text{ nm}$

4. Results and discussion: Phenyl-isoalloxazines dye IAE and BrPF

(second harmonic of mode-locked ruby laser) and collecting the fluorescence in the wavelength region from 500 nm to 610 nm. The effective radiative lifetimes, $\tau_{\text{rad}} = \tau_{\text{F}}/\phi_{\text{F}}$, of the emitting photoproducts are $\tau_{\text{rad}}(\text{IAE}_{\text{degraded,acetonitrile}}) \approx 290$ ns and $\tau_{\text{rad}}(\text{BrPF}_{\text{degraded,methanol}}) \approx 70$ ns. The radiative lifetimes of the photoproducts are longer than the radiative lifetimes of the original dyes. This finding is in agreement with the small long-wavelength absorption strength of the products seen in Figures 4.8 and 4.9.

The mass spectra of the dyes IAE and BrPF in the different solvents after light exposure are shown by the second rows in Figures 4.6 and 4.7. The analysis reveals the presence of several photoproducts. From their m/z values they may be attributed to phenyl-benzoperidine (isoalloxazine) derivatives (abbreviation I), tetraaza-benzo-aceanthrylene derivatives (abbreviation A), dihydro-quinooxaline derivatives (Q), and pyrazino-carbazole derivatives (C). The structural formulae of these compounds are shown in Figure 4.15. The supposed photoproduct compositions fitting to the m/z peaks are listed in the captions of Figures 4.6 and 4.7. The photoproduct classes (I, A, Q, C) are indicated in the mass spectra. The mass spectra of the dyes IAE and BrPF in the different solvents before and after light exposure in the range from 490 to 800 g mol^{-1} could be shown in Figures 4.13 and 4.14. The peaks are not further identified because of the complexity of possible combination.

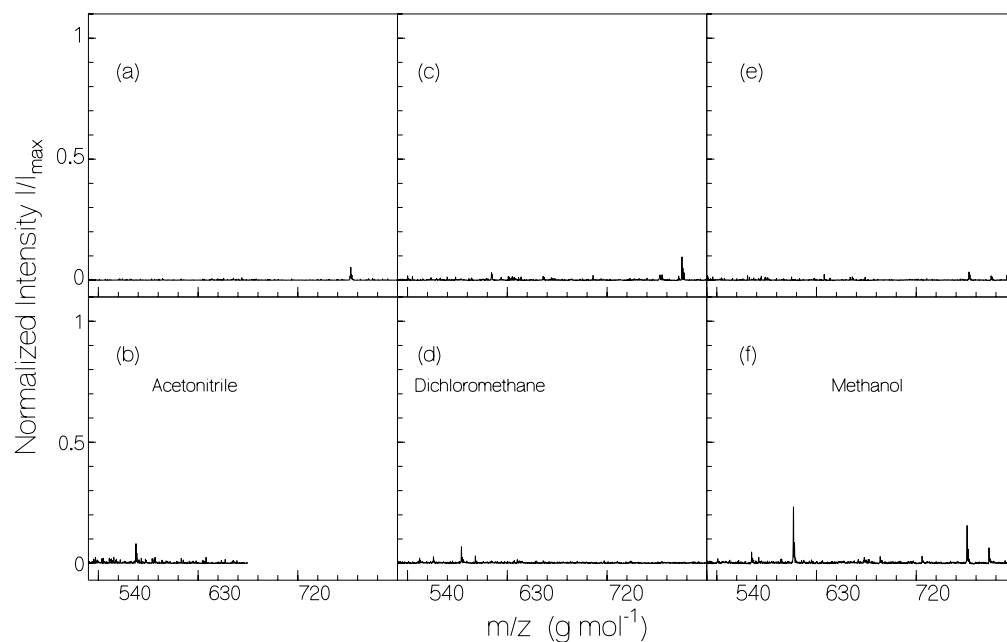


Figure 4.13: Mass spectra of dye IAE in the solvents acetonitrile, dichloromethane, and methanol before (top row) and after light exposure (bottom row) in the range from 490 to 800 g mol^{-1} . Excitation occurred at 428 nm. The excitation intensities, I_{exc} , and the periods of exposure, t_{exp} , are 0.0175 W cm^{-2} and 50 min for acetonitrile (b), 0.0175 W cm^{-2} and 79 min for dichloromethane (d), 0.0182 W cm^{-2} and 7 min for methanol (f).

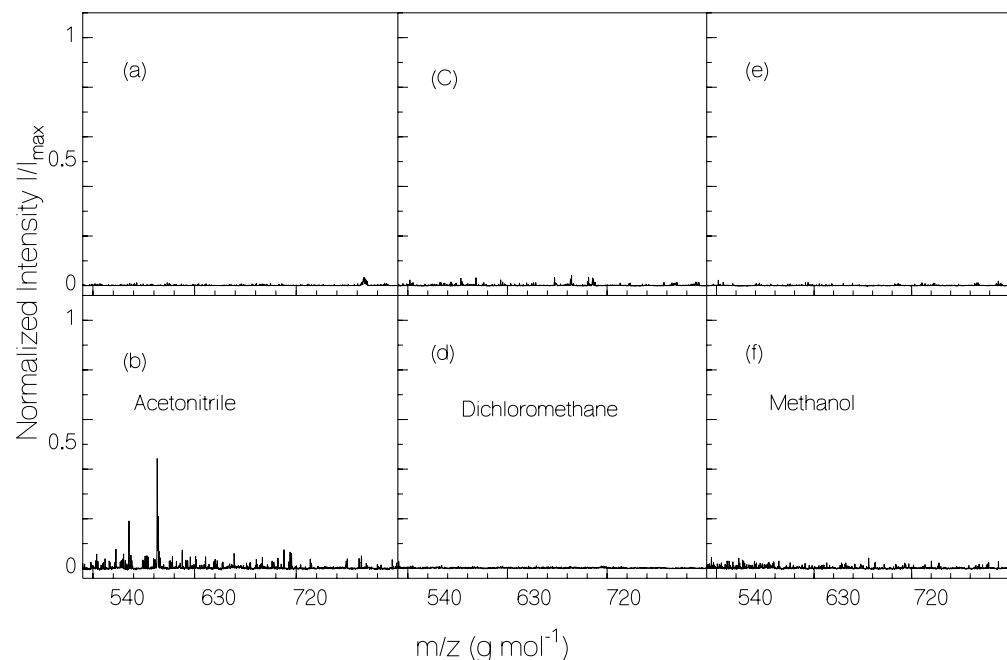


Figure 4.14: Mass spectra of dye BrPF in the solvents acetonitrile, dichloromethane, and methanol before (top row) and after light exposure (bottom row) in the range from 490 to 800 g mol^{-1} . Excitation occurred at 428 nm. The excitation intensities, I_{exc} , and the periods of exposure, t_{exp} , are 0.0155 W cm^{-2} and 167 min for acetonitrile (b), 0.0175 W cm^{-2} and 54 min for dichloromethane (d), 0.0182 W cm^{-2} and BrPF 70 min for methanol (f).

4. Results and discussion: Phenyl-isoalloxazines dye IAE and BrPF

Table 4.1: Parameters of investigated dyes. Excitation wavelength $\lambda_{\text{exc}} = 428$ nm.

Dye	IAE	IAE	IAE	BrPF	BrPF	BrPF
Solvent	CH ₂ Cl ₂	CH ₃ CN	CH ₃ OH	CH ₂ Cl ₂	CH ₃ CN	CH ₃ OH
n_F	1.4271	1.3481	1.3290	1.4271	1.3481	1.3290
n_A	1.4340	1.3528	1.3364	1.4340	1.3528	1.3364
ϕ_F	0.223±0.0	0.154±0.0	0.09±0.01	0.282±0.0	0.246±0.0	0.17±0.01
	2	2		2	2	
P_F	0.05±0.01	0.05±0.01	0.05±0.01	0.039±0.0	0.038±0.0	0.038±0.0
				1	1	1
τ_F (ns)	4.4±0.2	3.3±0.2	2.1±0.2	5.3±0.2	5.5±0.2	3.8±0.2
τ_{rad} (ns)	19.7±1	21.4±1.5	23.3±2.5	18.8±1	22.4±1.5	22.3±1.5
$\tau_{\text{or},\mu}$ (ps)	407±30	306±30	195±30	370±30	375±30	260±30
$\sigma_{\text{a,FI}}$ (cm ²)	3.60×10 ⁻¹⁷	3.73×10 ⁻¹⁷	3.99×10 ⁻¹⁷	3.38×10 ⁻¹⁷	3.54×10 ⁻¹⁷	4.28×10 ⁻¹⁷
$\sigma_{\text{a,FIPr}}$ (cm ²)	6.83×10 ⁻¹⁸	5.25×10 ⁻¹⁸	6.91×10 ⁻¹⁸	3.4×10 ⁻¹⁸	3.6×10 ⁻¹⁸	4.13×10 ⁻¹⁸
λ_p (nm)	444	440.6	443	440	437.9	440
$\sigma_{\text{a,p,FI}}$ (cm ²)	3.97×10 ⁻¹⁷	3.79×10 ⁻¹⁷	4.50×10 ⁻¹⁷	4.20×10 ⁻¹⁷	4.0×10 ⁻¹⁷	4.14×10 ⁻¹⁷
$\sigma_{\text{a,p,FIPr}}$ (cm ²)	5.40×10 ⁻¹⁸	3.42×10 ⁻¹⁸	3.07×10 ⁻¹⁸	4.06×10 ⁻¹⁸	4.53×10 ⁻¹⁸	3.97×10 ⁻¹⁸
k_1 (s ⁻¹)	≈5×10 ⁴	≈5×10 ⁴	≈3.5×10 ⁶	≈5×10 ⁴	≈4×10 ³	≈2.5×10 ⁴
k'_2 (s ⁻¹ mol ⁻¹ dm ³)	≈3.6×10 ⁹	≈2.4×10 ⁹	2.4×10 ¹⁰	≈1.2×10 ⁹	≈3×10 ⁸	≈1.8×10 ⁸
$\phi_{D,0}$	≈2.2×10 ⁻⁴	≈1.7×10 ⁻⁴	≈7.7×10 ⁻³	≈2.7×10 ⁻⁴	≈2.2×10 ⁻⁵	≈9.5×10 ⁻⁵

Abbreviations: n_F , average refractive index in fluorescence region; n_A , average refractive index in S₀-S₁ absorption region; ϕ_F , fluorescence quantum yield; P_F , degree of fluorescence polarisation; τ_F , fluorescence lifetime; $\tau_{\text{or},\mu}$, reorientation time of transition dipole moment; $\sigma_{\text{a,FI}}$, absorption cross-section of initial dye at λ_{exc} ; $\sigma_{\text{a,FIPr}}$, absorption cross-section of photoproducts at λ_{exc} ; λ_p , wavelength of peak S₀-S₁ absorption; $\sigma_{\text{a,p,FI}}$, absorption cross-section of initial dye at λ_p ; $\sigma_{\text{a,p,FIPr}}$, absorption cross-section of photoproducts at λ_p ; k_1 , unimolecular rate constant of photo-degradation; k'_2 , initial bimolecular rate constant of photo-degradation. $\phi_{D,0}$, initial quantum yield of photo-degradation.

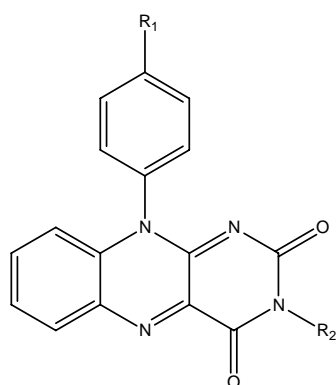
4.1.2 Discussion

The absorption behaviour of dye IAE and dye BrPF in acetonitrile, dichloromethane, and methanol is somehow similar. The fluorescence quantum yields are limited between 9 % (dye IAE in methanol) and 28 % (dye BrPF in dichloromethane) indicating that the dominant excited state deactivation is due to non-radiative decay (singlet-triplet intersystem crossing [Ghi89, Isl03] and internal conversion). The radiative lifetime, τ_{rad} , determined by fluorescence lifetime and fluorescence quantum yield measurements (Equation 2.13) is in reasonable agreement with the Strickler-Berg radiative lifetime, $\tau_{\text{rad,SB}}$ (Equation 2.14), indicating simple single-component exponential S_1 -state relaxation (exact absorption cross-sections somewhat uncertain because of experimental difficulty of exact dye concentration determination). The changes of the fluorescence quantum yields with solvent indicate solvent dependences of the efficiency of intersystem crossing, ϕ_{ISC} , and internal conversion, ϕ_{IC} . The efficiency of intersystem-crossing is expected to be in the range of $\phi_{\text{ISC}} \approx 0.4$ to 0.6 [Cha88, Isl03]. The quantum efficiency of internal conversion is given by $\phi_{\text{IC}} = 1 - \phi_{\text{F}} - \phi_{\text{ISC}}$.

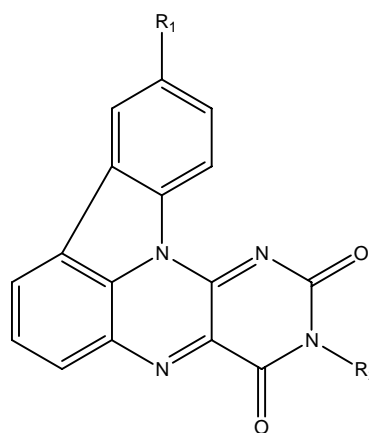
The photo-stability of the dyes IAE and BrPF is limited by excited-state reaction towards the formation of a series of photoproducts as is manifested by the mass spectra in Figures 4.6 and 4.7. The not extra excited dyes (top rows in Figures 4.6 and 4.7) already show the presence of some photoproducts, since they were exposed to some room light during preparation and analysis. Only dye IAE and dye BrPF in dichloromethane have about the same moderate photo-stability (initial quantum yield of photo-degradation $\phi_{\text{D},0} \approx 2.5 \times 10^{-4}$). For the other solvents the photo-stability of dye IAE and dye BrPF differs strongly ($\phi_{\text{D},0}(\text{IAE,acetonitrile}) \approx 1.7 \times 10^{-4}$, $\phi_{\text{D},0}(\text{BrPF,acetonitrile}) \approx 2.2 \times 10^{-5}$, and $\phi_{\text{D},0}(\text{IAE,methanol}) \approx 7.7 \times 10^{-3}$, $\phi_{\text{D},0}(\text{BrPF,methanol}) \approx 9.5 \times 10^{-5}$).

Four groups of compounds are attributed to the mass spectra peaks. They are phenyl-isoalloxazine derivatives (I), tetraaza-benzo-aceanthrylene derivatives (A), dihydro-

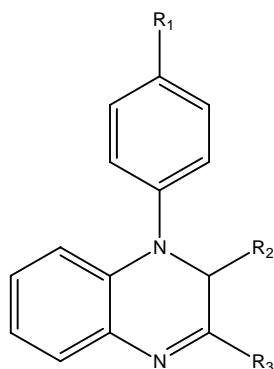
quinoxaline derivatives (Q), and pyrazino-carbazole derivatives (C). The dyes IAE and BrPF in acetonitrile and dichloromethane primarily seem to degrade in tetraaza-benzo-aceanthrylene derivatives (A) by ring closure between C9 of the isoalloxazine part and C6 of the phenyl ring. This reaction is less pronounced for dye IAE and dye BrPF in methanol. The tetraaza-benzo-aceanthrylene derivatives A with their carbazole-like structure are thought to be responsible for the long-wavelength photoproduct absorption seen in Figures 4.8 and 4.9.



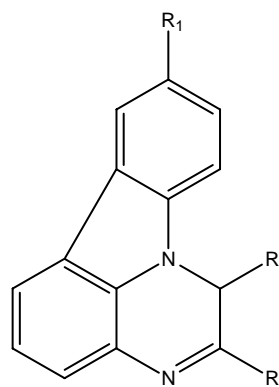
Phenyl-benzo-pteridine derivatives (I)



Tetraaza-benzo-aceanthrylene derivatives (A)



Dihydro-quinoxaline derivatives (Q)

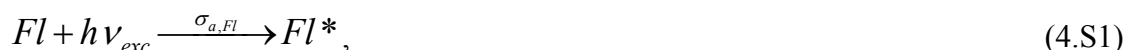


Pyrazino-carbazole derivatives (C)

Figure 4.15: The structural formulae of the supposed photoproduct classes. They are abbreviated by I for phenyl-isoalloxazine derivatives, A for tetraaza-benzo-aceanthrylene derivatives, Q for dihydro-quinoxaline derivatives, and C for pyrazino-carbazole derivatives.

In [Kna76, Kna74] the photo-induced N1, N10 benzo-bridged isoalloxazine formation out of N10-phenyl-substituted isoalloxazine derivatives was observed in the presence of weak organic acids in organic solvents (no change of mass by benzo-bridge formation). The formation of N1, N10 benzo-bridged isoalloxazine derivatives is not observed here for dye IAE and dye BrPF in acetonitrile and dichloromethane (original mass peaks are no longer present after degradation). The formation is likely for dye BrPF in methanol where the m/z of dye BrPF (383.0 and 385.0) is still strongly present after light exposure.

The changes of the absorption coefficient spectra due to photoproduct formation are displayed in Figures 4.8 and 4.9. The temporal absorption decrease at the S_0 - S_1 absorption peak wavelength, λ_p , caused by light exposure is seen in Figures 4.10 and 4.11. The observed absorption changes with exposure time cannot be fitted by a simple unimolecular reaction of the photo-excited molecules. The photo-degradation speeds up with the amount of photoproducts formed. The generated photoproducts (one or some of them) seem to catalyse the photo-degradation. This dynamics may be described in its simplest form by the scheme (4.S1-S3), where Fl stands for dye IAE or BrPF, Fl^* is the photo-excited flavin, and $FlPr$ represents the photoproducts.



The photo-reaction dynamics for this scheme is given by

$$\frac{\partial N_{Fl}}{\partial t} = -\frac{\sigma_{a,Fl}}{h\nu_{exc}} I_{exc} N_{Fl} + \frac{N_{Fl^*}}{\tau_F}, \quad (4.2)$$

$$\frac{\partial N_{Fl^*}}{\partial t} = \frac{\sigma_{a,Fl}}{h\nu_{exc}} I_{exc} N_{Fl} - \frac{N_{Fl^*}}{\tau_F} - k_1 N_{Fl^*} - k_2 N_{FlPr} N_{Fl^*}, \quad (4.3)$$

4. Results and discussion: Phenyl-isoalloxazines dye IAE and BrPF

$$\frac{\partial N_{FlPr}}{\partial t} = k_1 N_{Fl*} + k_2 N_{FlPr} N_{Fl*}, \quad (4.4)$$

$$N_0 = N_{Fl} + N_{Fl*} + N_{FlPr}, \quad (4.5)$$

$$\frac{\partial I_{exc}}{\partial z} = -(\sigma_{a,Fl} N_{Fl} + \sigma_{a,FlPr} N_{FlPr}) I_{exc}, \quad (4.6)$$

where $\sigma_{a,Fl}$ is the absorption cross-section of the educts (dye IAE or BrPF), and $\sigma_{a,FlPr}$ is the absorption cross-section of the photoproducts. I_{exc} is the intensity of the excitation light. N_{Fl} , N_{Fl*} , and N_{FlPr} are the number densities of the initial dye, the photo-excited dye, and the photoproducts, respectively. N_0 is the initial number density of dye molecules before light exposure. k_1 is the unimolecular rate constant of photo-degradation (k_1 in s^{-1}), and k_2 is the photoproduct-averaged bimolecular rate constant of catalysed photo-degradation (k_2 in $s^{-1}cm^3$, or $k'_2 = k_2 N_A / 1000$ in $s^{-1}mol^{-1}dm^3$).

Under steady-state conditions, $\tau_F \ll t$ (t is time duration of light exposure), the number density of photo-excited molecules, N_{Fl*} , is given by (the time derivatives can be set to zero)

$$N_{Fl*} = \frac{\sigma_{a,Fl}}{h\nu_{exc}} \frac{N_{Fl} I_{exc}}{\tau_F^{-1} + k_1 + k_2 N_{FlPr}} \approx \frac{\sigma_{a,Fl} \tau_F}{h\nu_{exc}} N_{Fl} I_{exc} \approx \frac{\sigma_{a,Fl} \tau_F}{h\nu_{exc}} (N_0 - N_{FlPr}) I_{exc}. \quad (4.7)$$

Under our experimental conditions of $I_{exc} \ll I_{sat} = h\nu_{exc} / (\sigma_{a,Fl} \tau_F)$, where I_{sat} is the saturation intensity of ground-state depletion [Her67], it is $N_{Fl*} \ll N_{Fl}$, and the equation system (4.3-7) reduces to

$$\frac{\partial N_{FlPr}}{\partial t} = (k_1 + k_2 N_{FlPr}) \frac{\sigma_{a,Fl} \tau_F}{h\nu_{exc}} (N_0 - N_{FlPr}) I_{exc}. \quad (4.8)$$

$$\frac{\partial I_{exc}}{\partial z} = -[\sigma_{a,Fl} (N_0 - N_{FlPr}) + \sigma_{a,FlPr} N_{FlPr}] I_{exc}. \quad (4.9)$$

The light intensity attenuation at the probe wavelength, λ_p , is given by

$$\frac{\partial I_p}{\partial z} = -[\sigma_{a,p,Fl} (N_0 - N_{FlPr}) + \sigma_{a,p,FlPr} N_{FlPr}] I_p. \quad (4.10)$$

The equation system (4.8-4.10) is solved numerically.

4. Results and discussion: Phenyl-isoalloxazines dye IAE and BrPF

The transmission, T_{exc} , of the excitation light at wavelength λ_{exc} , and the transmission, T_p , of the probe light at the probe wavelength, λ_p , are given by $T_{\text{exc}} = I_{\text{exc}}(\ell)/I_{\text{exc}}(0)$, and $T_p = I_p(\ell)/I_p(0)$, where ℓ is the sample length. The absorption coefficient at the probe wavelength, λ_p , is given by $\alpha_p = -\ln(T_p)/\ell$. Some calculated curves of $\alpha_p(t)$ are shown in Figures 4.10 and 4.11, where the rate constants k_1 and k_2 are varied. The best fitting parameters are listed in Table 4.1.

The quantum yield of photo-degradation, ϕ_D , is given by the relation

$$\phi_D = \frac{k_1 + k_2 N_{\text{FlPr}}}{\tau_F^{-1} + k_1 + k_2 N_{\text{FlPr}}} \approx (k_1 + k_2 N_{\text{FlPr}})\tau_F = (k_1 + k_2 \chi_{\text{FlPr}} N_0)\tau_F, \quad (4.11)$$

where $\chi_{\text{FlPr}} = N_{\text{FlPr}}/N_0$ is the mole-fraction of photoproducts. The approximation at the second express is valid for $\phi_D \ll 1$.

The initial quantum yield of photo-degradation of dye IAE or BrPF is given by (N_{FlPr} still zero)

$$\phi_{D,0} = k_1 \tau_F, \quad (4.12)$$

and the final quantum yield of photo-degradation of dye IAE or BrPF is given by ($N_{\text{FlPr}} = N_0$)

$$\phi_{D,1} = (k_1 + k_2 N_0)\tau_F. \quad (4.13)$$

The initial quantum yields of photo-degradation of dye IAE and dye BrPF in the applied solvents are listed in Table 4.1. They range from $\phi_{D,0}(\text{BrPF, acetonitrile}) \approx 2.2 \times 10^{-5}$ to $\phi_{D,0}(\text{IAE, methanol}) \approx 7.7 \times 10^{-3}$.

The photo-degradation dynamics of dye IAE in acetonitrile fits reasonably well to the applied unimolecular and bimolecular relaxation scheme. For dye IAE in dichloromethane the degradation follows the described scheme during the first 40 min of light exposure, then a degradation with faster (bimolecular) rate sets in. For dye IAE in methanol the described

4. Results and discussion: Phenyl-isalloxazines dye IAE and BrPF

scheme was followed over the first 5 min, and then the rate of degradation slowed down. For dye BrPF in all applied solvents the initial degradation can be fitted by the described unimolecular and bimolecular degradation scheme, but at longer times the decay rates become faster (stronger catalytic degradation action of one or several photoproducts).

4.2 Pyrene and 1-methylpyrene

4.2.1 Results

Pyrene and 1-methylpyrene are constituents of the investigated pyrene-isoalloxazine dyad (PFD) and the pyrene-isoalloxazine-phenothiazine triad (PYFPT). To understand the behaviour of the investigated PFD dyad, and PYFPT triad, a detailed knowledge of the photo-physical behaviour of the pyrene and 1-methylpyrene constituents is helpful [Ber71, Mur93, Win93, Bir70, Har80, Kar95, Nak73, Van98]. Some absorption and emission spectroscopic characterisation of pyrene and 1-methylpyrene is given in this section [Shi07a].

The absorption cross-section spectra of pyrene and 1-methylpyrene in dichloromethane and acetonitrile are shown in Figure 4.16. The weak S_0 - S_1 absorption band of pyrene and 1-methylpyrene in the absorption tail of the strong S_0 - S_2 band is seen. The pyrene and 1-methylpyrene electronic transitions have a well resolved vibronic structure. The 1-methylpyrene absorption spectrum is slightly red-shifted compared to the pyrene absorption spectrum, and the S_0 - S_1 absorption of 1-methylpyrene is approximately a factor of 3.7 (dichloromethane) to 5.3 (acetonitrile) stronger than the corresponding absorption of pyrene.

The stimulated emission cross-section spectra of pyrene and 1-methylpyrene are included in Figure 4.16. The pyrene stimulated emission cross-section spectrum is very small because of the forbidden S_1 - S_0 transition [Win93, Kar95, Kal77]. The stimulated emission cross-section spectrum of 1-methylpyrene is somewhat larger since the methyl group reduces somewhat the molecular symmetry and the strength of the forbidden S_1 - S_0 transition.

There is practically no Stokes shift (wavenumber difference between S_0 - S_1 absorption peak and S_1 - S_0 emission peak) between the zero-vibration S_1 - S_0 emission peak and the zero-vibration S_0 - S_1 absorption peak, as is expected from the high symmetry of pyrene.

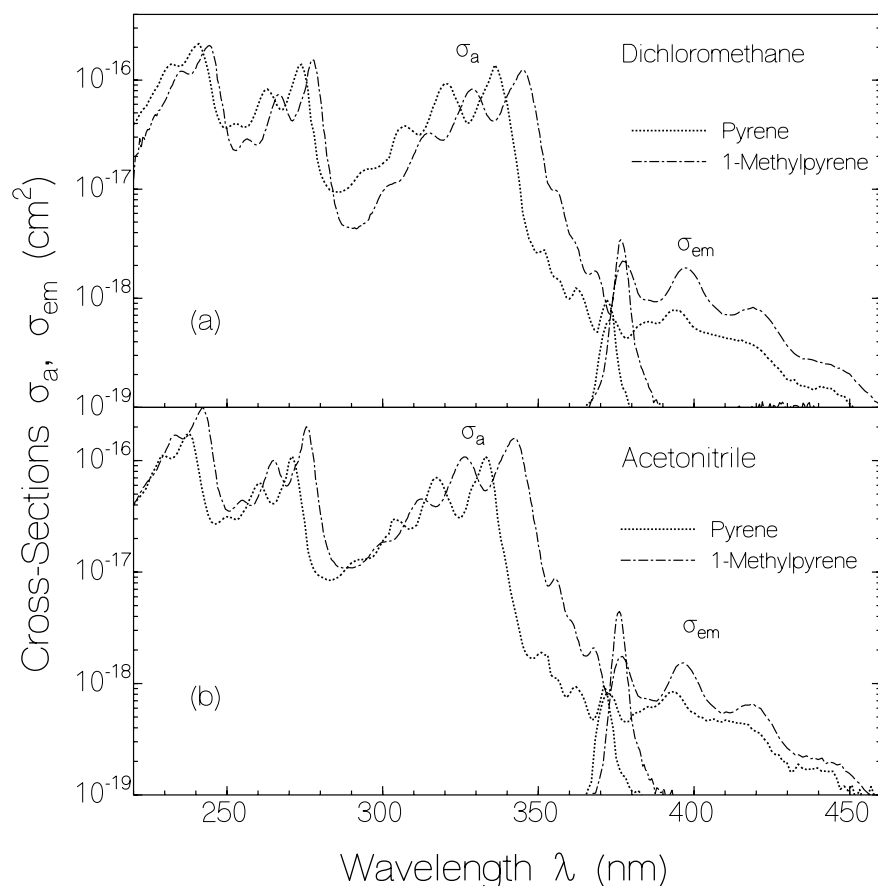


Figure 4.16: Absorption and stimulated emission cross-section spectra of pyrene and 1-methylpyrene in dichloromethane and acetonitrile. The applied dye concentrations in the measurements were: C (pyrene, dichloromethane) = 3.5×10^{-4} mol dm $^{-3}$, C (pyrene, acetonitrile) = 3.9×10^{-4} mol dm $^{-3}$, C (1-methylpyrene, dichloromethane) = 5.2×10^{-5} mol dm $^{-3}$, and C (1-methylpyrene, acetonitrile) = 6×10^{-5} mol dm $^{-3}$.

The fluorescence quantum distributions, $E_F(\lambda)$, of the pyrene and 1-methylpyrene in as-delivered dichloromethane and acetonitrile are shown in the top parts of Figure 4.17 and Figure 4.18, respectively. The corresponding fluorescence quantum yields, $\phi_F = \int E_F(\lambda) d\lambda$, are listed in Table 4.2. The fluorescence quantum yields of pyrene are $\phi_F(\text{dichloromethane}, \lambda_{\text{exc}} = 311 \text{ nm}) \approx 0.068$ and $\phi_F(\text{acetonitrile}, \lambda_{\text{exc}} = 311 \text{ nm}) \approx 0.031$. The results for 1-methylpyrene are $\phi_F(\text{dichloromethane}, \lambda_{\text{exc}} = 311 \text{ nm}) \approx 0.125$ and $\phi_F(\text{acetonitrile}, \lambda_{\text{exc}} = 311 \text{ nm}) \approx 0.049$.

4. Results and discussion: Pyrene and 1-methylpyrene

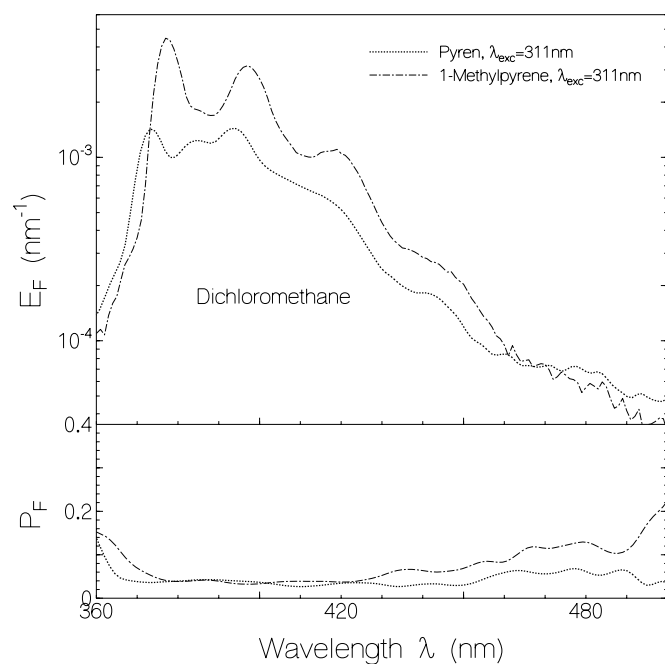


Figure 4.17: Fluorescence quantum distribution (top part) and degree of fluorescence polarization (lower part) of pyrene and 1-methylpyrene in dichloromethane. Excitation wavelengths, λ_{exc} , are indicated in the figures. Concentrations are $C = 1.4 \times 10^{-4} \text{ mol dm}^{-3}$ for pyrene, and 5.1×10^{-5} for 1-methylpyrene.

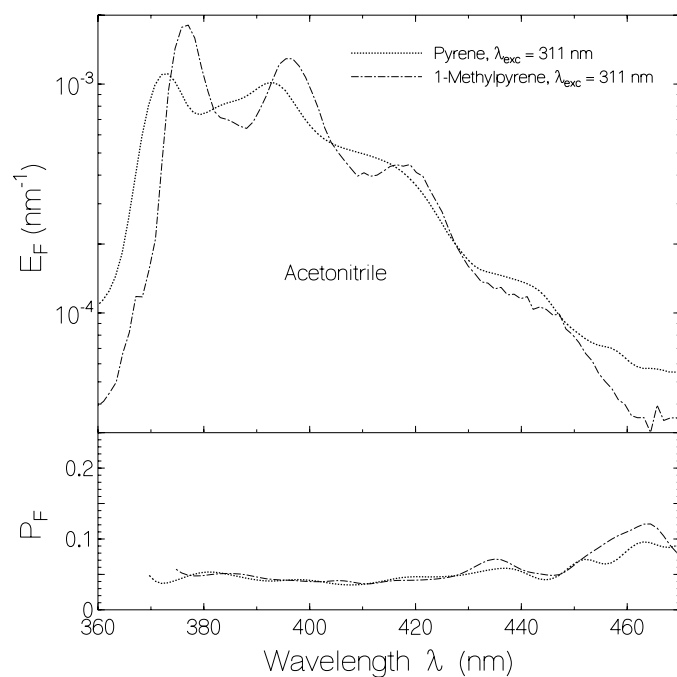


Figure 4.18: Fluorescence quantum distribution (top part) and degree of fluorescence polarization (lower part) of pyrene and 1-methylpyrene in acetonitrile. Excitation wavelengths, λ_{exc} , are indicated in the figures. Concentrations are $C = 1.5 \times 10^{-4} \text{ mol dm}^{-3}$ for pyrene, and 6.3×10^{-5} for 1-methylpyrene.

The fluorescence polarisation spectra, $P_F(\lambda)$, of pyrene and 1-methylpyrene are plotted in the lower parts of Figures 4.17 and Figure 4.18, and the average degrees of fluorescence polarization are listed in Table 4.2. For pyrene and 1-methylpyrene the degree of fluorescence polarisation is low indicating a short molecular reorientation time compared to the fluorescence lifetime.

Temporal fluorescence traces of pyrene and 1-methylpyrene are shown in Figure 4.19. The excitation wavelength was 347.15 nm (duration $\Delta t_L \approx 30$ ps). The fluorescence signals of pyrene and 1-methylpyrene in the two solvents, dichloromethane and acetonitrile, decay single-exponentially within our experimental accuracy.

The fluorescence lifetimes of pyrene and 1-methylpyrene in as-delivered solvents (no de-aerating) are in the few tens of ns range. The determined lifetimes are listed in Table 4.2.

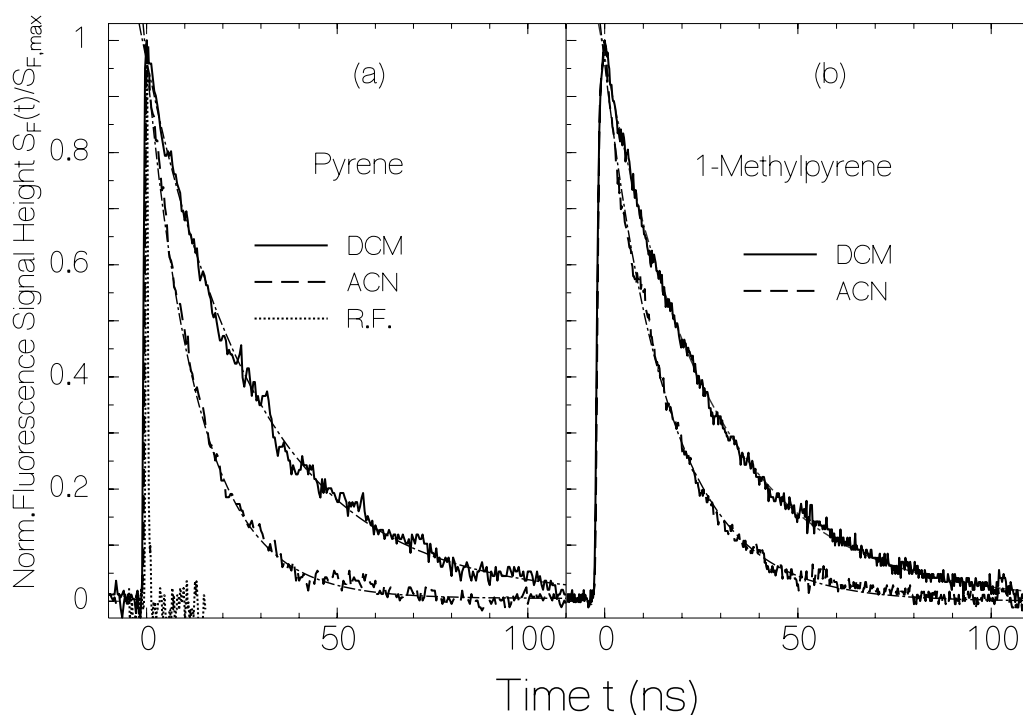


Figure 4.19: Temporal fluorescence traces. Dotted curve is response functions. Dash-dotted curves are single-exponential fits (Equation 2.4)

(a) Pyrene in dichloromethane (solid curve, $\tau_F = 29.3$ ns) and acetonitrile (dashed curve, $\tau_F = 13.5$ ns). $\lambda_{exc} = 347.15$ nm, $\Delta t_{exc} = 30$ ps.

(b) 1-methylpyrene in dichloromethane (solid curve, $\tau_F = 27.4$ ns) and acetonitrile (dashed curve, $\tau_F = 16.3$ ns). $\lambda_{exc} = 347.15$ nm, $\Delta t_{exc} = 30$ ps.

In Figure 4.20 the absorption changes due to long-time blue-light excitation of pyrene in dichloromethane (part a, excitation at $\lambda_{\text{exc}} = 311\text{ nm}$, excitation intensity $I_{\text{exc}} = 0.001\text{ W cm}^{-2}$), and acetonitrile (part b, excitation at 311 nm , $I_{\text{exc}} = 0.047\text{ W cm}^{-2}$) are shown. Absorption coefficient spectra are depicted for different times of light exposure. The photo-degradation is more severe in dichloromethane than in acetonitrile. Within the displayed wavelength range no build-up of a photoproduct absorption band is observed.

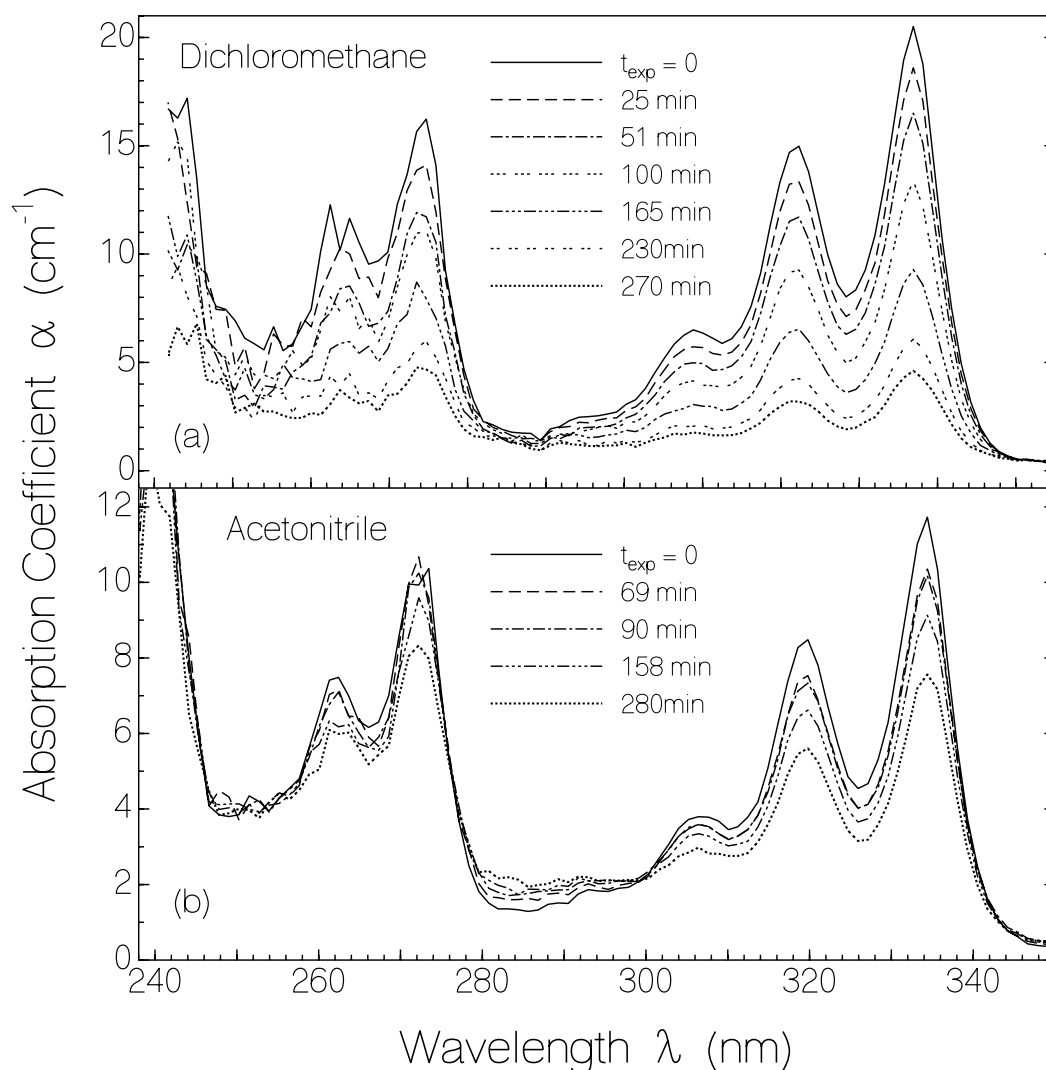


Figure 4.20: Absorption coefficient spectra of pyrene after several durations of light exposure. Exposure times, t_{exp} , are listed in figure.

(a) Solvent dichloromethane. Excitation intensity, $I_{\text{exc}} = 1 \times 10^{-3}\text{ W cm}^{-2}$, Excitation wavelength, $\lambda_{\text{exc}} = 311\text{ nm}$.

(b) Solvent acetonitrile. $I_{\text{exc}} = 4.7 \times 10^{-3}\text{ W cm}^{-2}$, $\lambda_{\text{exc}} = 311\text{ nm}$.

The transmission rise of pyrene at wavelength position, λ_{pr} , (at peak absorption of pyrene around 335 nm) with exposed energy density at the excitation wavelength, $\lambda_{exc} = 311$ nm for acetonitrile and dichloromethane, are displayed in Figure 4.21 (data extracted from Figure 4.20). The transmission change versus light exposure will be used below to calculate the quantum yield of photo-degradation as a function of the exposed energy density.

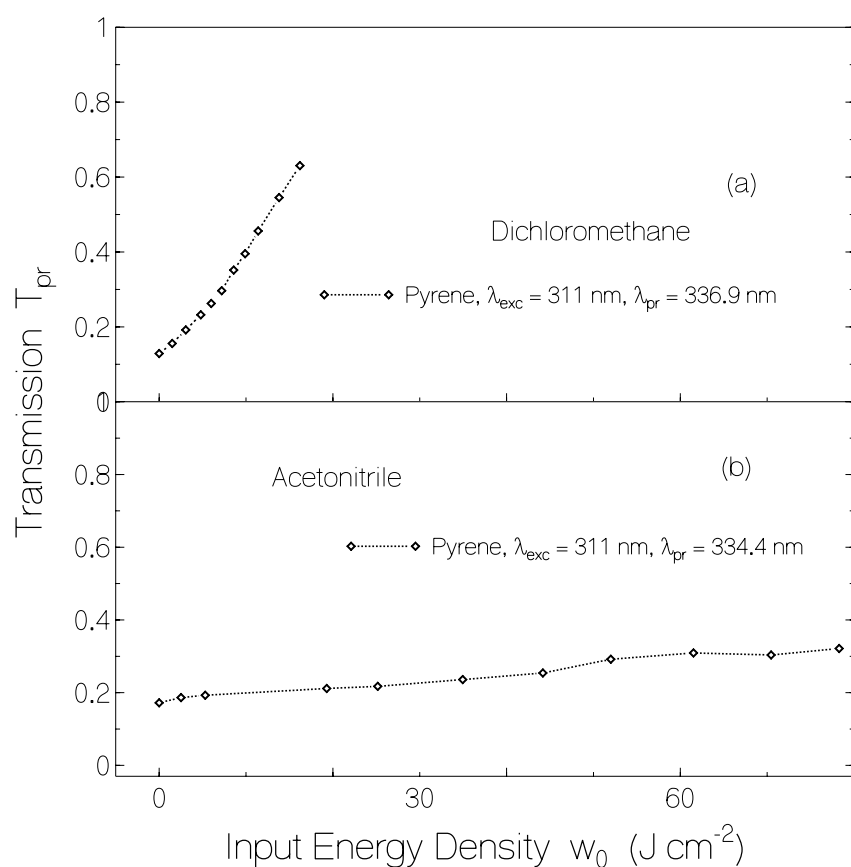


Figure 4.21: Transmission, $T_{pr}(w_0)$, at probe wavelength, λ_{pr} , versus exposed input energy density, w_0 , at excitation wavelength, $\lambda_{exc}=311$, for pyrene. Data are extracted from Figure 4.20.

(a) Dichloromethane. Excitation intensity, $I_{exc}(\text{pyrene}) = 0.001 \text{ W cm}^{-2}$.
(b) Acetonitrile. Excitation intensity, and $I_{exc}(\text{pyrene}) = 0.0047 \text{ W cm}^{-2}$.

4.2.2 Discussion

The fluorescence quantum yield of pyrene in as-delivered solvents was measured to be $\phi_F(\text{dichloromethane}) \approx 0.068$ and $\phi_F(\text{acetonitrile}) \approx 0.031$. The small fluorescence quantum yields are thought to be caused by molecular oxygen quenching. In degassed solvents fluorescence quantum yields of $\phi_F(\text{pyrene in dichloromethane}) \approx 0.38$ and $\phi_F(\text{pyrene in acetonitrile}) \approx 0.62$ were determined [Kar95]. The fluorescence quantum yield of 1-methylpyrene in the as-delivered solvents dichloromethane and acetonitrile were measured to be $\phi_F \approx 0.124$ and $\phi_F \approx 0.049$, respectively. The fluorescence quantum yields of 1-methylpyrene are higher than those of pyrene because of shorter radiative lifetime (stronger S_0 - S_1 absorption). For deoxygenated solutions of 1-methylpyrene in cyclohexane, dioxane, and water fluorescence quantum yields of 0.48, 0.46, and 0.34, respectively, were determined in [Lia80]. Their radiative lifetimes $\tau_{rad} = \tau_F / \phi_F$ (Equation 2.13) are also listed in Table 4.2. The 1-methylpyrene has shorter radiative lifetime because it has stronger S_0 - S_1 absorption band respect to pyrene.

The photo-degradation of pyrene was studied in Figures 4.20 and 4.21. Calculation of the quantum yields of photo-degradation as a function of the exposed energy density was done according to Equations 3.2-3.4 with using data in Figure 4.21.

The obtained quantum yields of photo-degradation, ϕ_D , as a function of the exposed energy density are shown in Figure 4.22.

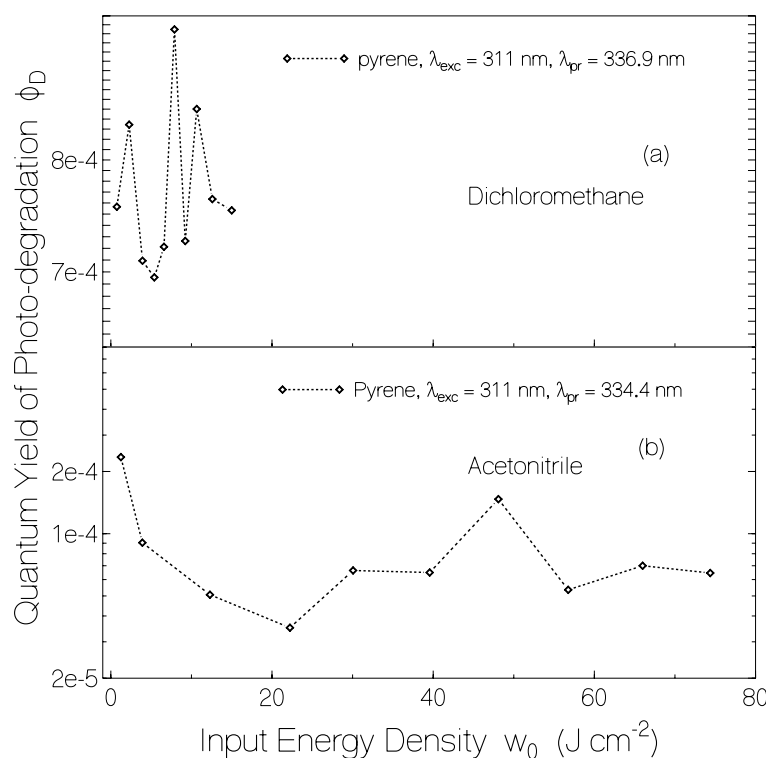


Figure 4.22: Quantum yields of photo-degradation, ϕ_D , at probe wavelength, λ_{pr} , versus exposed input energy density, w_0 , at excitation wavelength, $\lambda_{\text{exc}}=311$, for pyrene. Data are calculated from Figure 4.21.

(a) Dichloromethane. Excitation intensity, $I_{\text{exc}}(\text{pyrene}) = 0.001 \text{ W cm}^{-2}$.
 (b) Acetonitrile. Excitation intensity, and $I_{\text{exc}}(\text{pyrene}) = 0.0047 \text{ W cm}^{-2}$.

The obtained initial quantum yields of photo-degradation, $\phi_{D,0}$, are listed in Table 4.2. The photo-degradation of pyrene in dichloromethane and in acetonitrile is independent of the already deposited energy. The photo-stability of pyrene (Figure 4.20, $\lambda_{\text{exc}} = 311 \text{ nm}$) is rather low in dichloromethane ($\phi_{D,0} \approx 1.8 \times 10^{-3}$) and moderate in acetonitrile ($\phi_{D,0} \approx 1.5 \times 10^{-4}$). No photoproduct absorption shows up in the displayed wavelength range of Figure 4.20 ($\lambda > 240 \text{ nm}$). This leads to the suggestion that the π -electron conjugation is lost and 4,5,9,10-tetrahydro-pyrene derivatives are formed (Figure 4.23).

4. Results and discussion: Pyrene and 1-methylpyrene

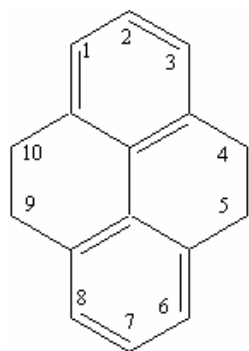


Figure 4.23: Structural formulae of 4,5,9,10-tetrahydro-pyrene. Formula: $C_{16}H_{14}$, Molar mass: $206.25 \text{ g mol}^{-1}$

Table 4.2 Spectroscopic parameters of pyrene and 1-methylpyrene at room temperature

Dye	Pyrene		1-Methylpyrene	
	dichloromethane	acetonitrile	dichloromethane	Acetonitrile
$\lambda_{\text{abs,max}}(\text{nm})$	320nm, 336nm, 372nm	317nm, 333nm, 371nm	328nm, 345nm, 376nm	326nm, 343nm, 376nm
$\lambda_{\text{F,max}}(\text{nm})$	373nm, 394nm	372nm, 392nm	377nm, 397nm	375nm, 396nm
n_{F}	1.4390	1.3581	1.4390	1.3581
n_{A}	1.4559	1.3713	1.4559	1.3713
ϕ_{F}	0.068 ± 0.005	0.031 ± 0.003	0.124 ± 0.01	0.049 ± 0.005
P_{F}	≈ 0.03	≈ 0.04	≈ 0.04	≈ 0.04
$\tau_{\text{F}} (\text{ns})$	29.2 ± 1	14 ± 0.5	27.4 ± 1	16 ± 1
$\tau_{\text{rad}} (\text{ns})$	429.4 ± 20	451.6 ± 20	221 ± 10	327 ± 20
$\phi_{\text{D},0}$	≈ 0.0018	$\approx 1.5 \times 10^{-4}$		

4.3 Heptyl-phenothiazine and heptyl-phenyl-phenothiazine

4.3.1 Results

Heptyl-phenothiazine (abbreviated by HPT) and heptyl-phenyl-phenothiazine (abbreviated by HPPT) are constituents of the investigated phenothiazine-flavin dyad (PTFD), and pyrene-flavin-phenothiazine triad (PYFPT). In order to understand the electron transfer and energy transfer processes in the PTFD dyad and the PYFPT triad a detailed knowledge of the photo-physical behaviour of the phenothiazine derivatives is necessary. Optical spectroscopic data on phenothiazine are found in [Rag64, Dom77, Kaw86, Kaw86b, Bau01]. Some absorption and emission spectroscopic characterisation of HPT and HPPT is given in this section [Shi07b].

The absorption cross-section spectra of HPT and HPPT in dichloromethane and HPT in acetonitrile are shown in Figure 4.24. The absorption cross-section spectrum of HPPT in dichloromethane is taken from [Pro04, She03]. The HPPT absorption is 10 nm to 15 nm red-shifted and strongly enhanced. This indicates that the phenyl ring of HPPT is in the plane of phenothiazine ring structure.

The stimulated emission cross-section spectra of the HPT in dichloromethane and acetonitrile, and HPPT in dichloromethane are shown in Figure 4.24. The stimulated emission cross-section spectra of HPT are very small indicating the emission from a state in the tail of the absorption band. The stimulated emission cross-section spectrum of HPPT is considerably larger than the stimulated emission cross-section spectrum of HPT as is also the case for the absorption cross-section spectrum. The shapes of the S_1 - S_0 emission spectra and of the first absorption bands of HPT and HPPT are not mirror images since within the first absorption band the S_0 - S_1 and S_0 - S_2 absorption is overlapping.

4. Results and discussion: Heptyl-phenothiazine and Heptyl-phenyl-phenothiazine

The fluorescence quantum distributions, $E_F(\lambda)$, of the investigated dyes in dichloromethane and acetonitrile are shown in the top parts of Figures 4.25a and 4.25b, respectively. The corresponding fluorescence quantum yields, $\phi_F = \int E_F(\lambda)d\lambda$, are listed in Table 4.3. The fluorescence quantum yields of HPT are $\phi_F(\text{dichloromethane}) \approx 0.0085$ and $\phi_F(\text{acetonitrile}) \approx 0.00785$, while the fluorescence quantum yield of HPPT in dichloromethane is $\phi_F \approx 0.26$ [Pro04, She03].

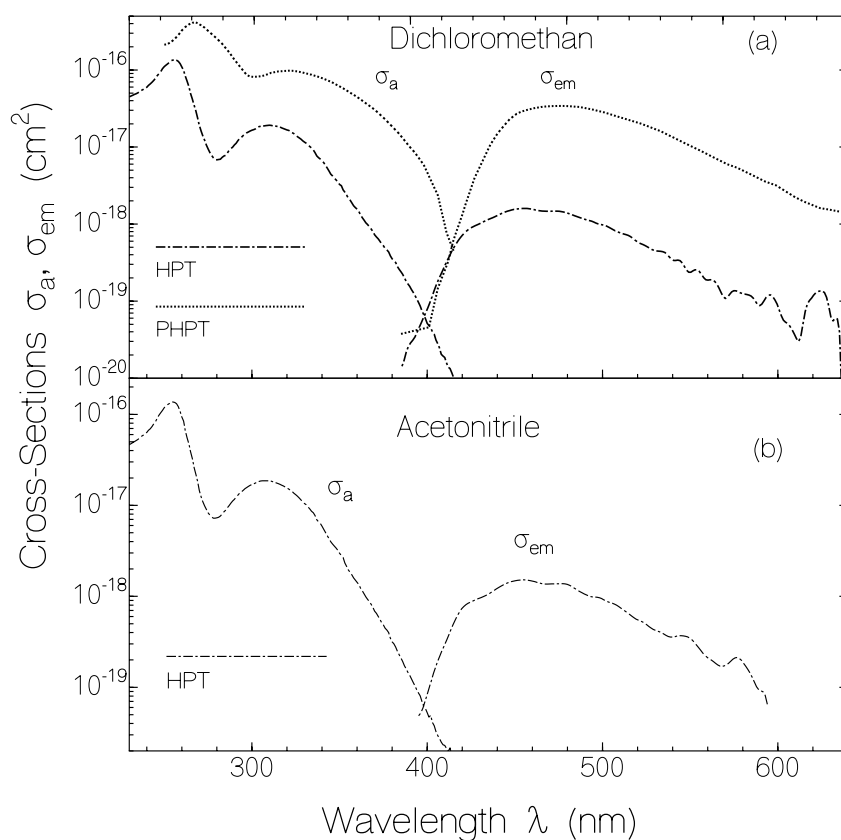
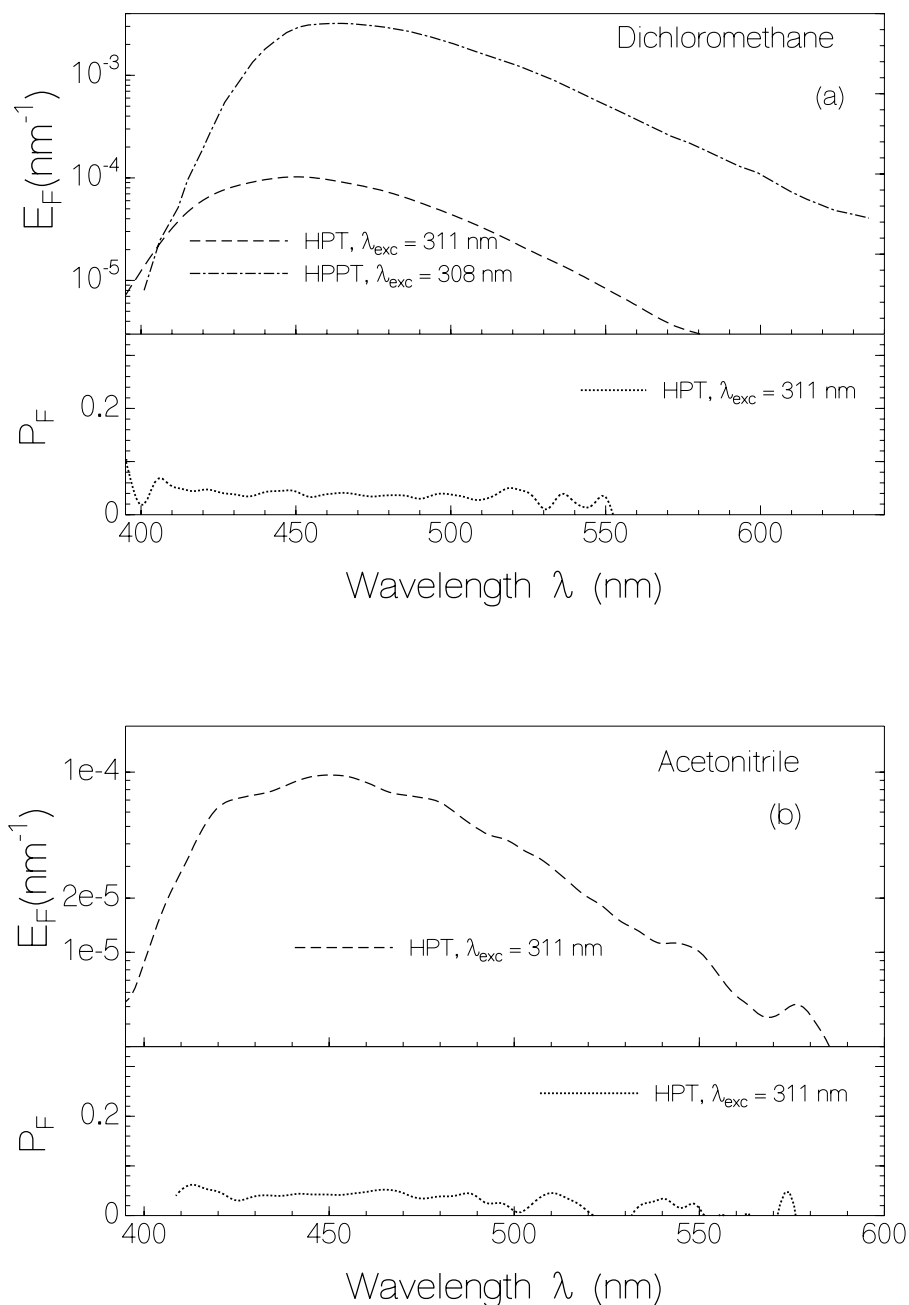


Figure 4.24: Absorption and stimulated emission cross-section spectra of investigated dyes in dichloromethane (a) and acetonitrile (b). The applied dye concentrations in the measurements were: $C(\text{HPT, dichloromethane}) = 2.38 \times 10^{-4} \text{ mol dm}^{-3}$, and $C(\text{HPT, acetonitrile}) = 4.46 \times 10^{-4} \text{ mol dm}^{-3}$. Spectra for 10-heptyl-3-phenyl-phenothiazine (HPPT) are taken from [Pro04, She03].

The fluorescence polarisation spectra, $P_F(\lambda)$, of HPT is plotted in lower part of Figures 4.25a and 4.25b, respectively, for the solvents dichloromethane and acetonitrile. The degree

of fluorescence polarisation is low indicating a short molecular reorientation time compared to the fluorescence lifetime.



Figures 4.25: Fluorescence quantum distributions (top part) and degrees of fluorescence polarization (lower part) of dyes in dichloromethane (a) and acetonitrile (b). Dyes and excitation wavelengths, λ_{exc} , are indicated in the figures. Concentrations are $C(\text{dichloromethane, HPT})=1.36 \times 10^{-4} \text{ mol dm}^{-3}$, and $C(\text{acetonitrile, HPT})=1.2 \times 10^{-4} \text{ mol dm}^{-3}$. Curve for HPPT in dichloromethane is taken from [Pro04, She03].

Temporal fluorescence traces of the HPT in dichloromethane and acetonitrile are shown in Figure 4.26. A fluorescence lifetime of $\tau_F = 5.86$ ns is reported for HPPT in dichloroethane [Pro04, She03]. The fluorescence signals of the HPT or HPPT decay single-exponentially within our experimental accuracy according to Equation 2.4. The obtained fluorescence lifetimes, τ_F , in the ns range are listed in Figure 4.26 and Table 4.3. Their radiative lifetimes $\tau_{rad} = \tau_F / \phi_F$ (Equation 2.13) are also listed in Table 4.3.

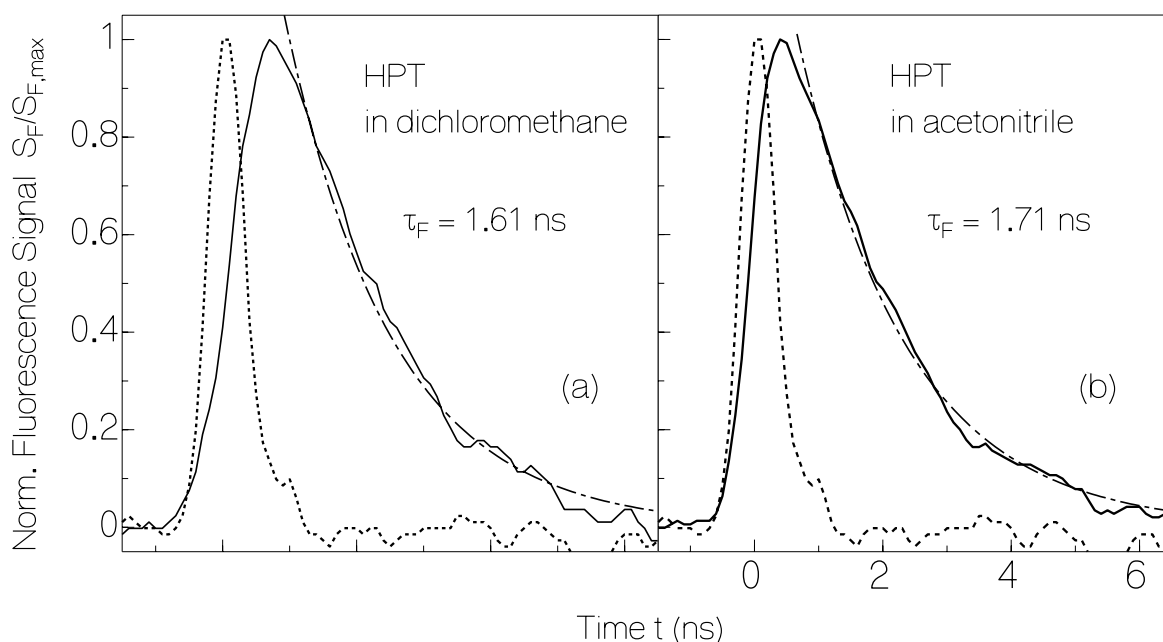


Figure 4.26: Temporal fluorescence (oscilloscope) traces of component HPT. Solid curves: samples. Dash-dotted lines: single-exponential fits (Equation 2.4). Dotted lines: response functions. (a) HPT in dichloromethane. (b) HPT in acetonitrile.

Absorption changes due to long-time blue-light excitation of HPT in dichloromethane (part a, excitation in range of 260 nm - 380 nm, excitation intensity $I_{exc} = 0.015$ W cm⁻²), and acetonitrile (part b, $\lambda_{exc}=260$ nm - 380 nm., excitation intensity $I_{exc} = 0.015$ W cm⁻²) are shown in Figure 4.27. Absorption coefficient spectra are depicted for different times of light

exposure at fixed excitation intensities, I_{exc} . In both solvent new absorption bands of photoproduct are build up by photo-degradation.

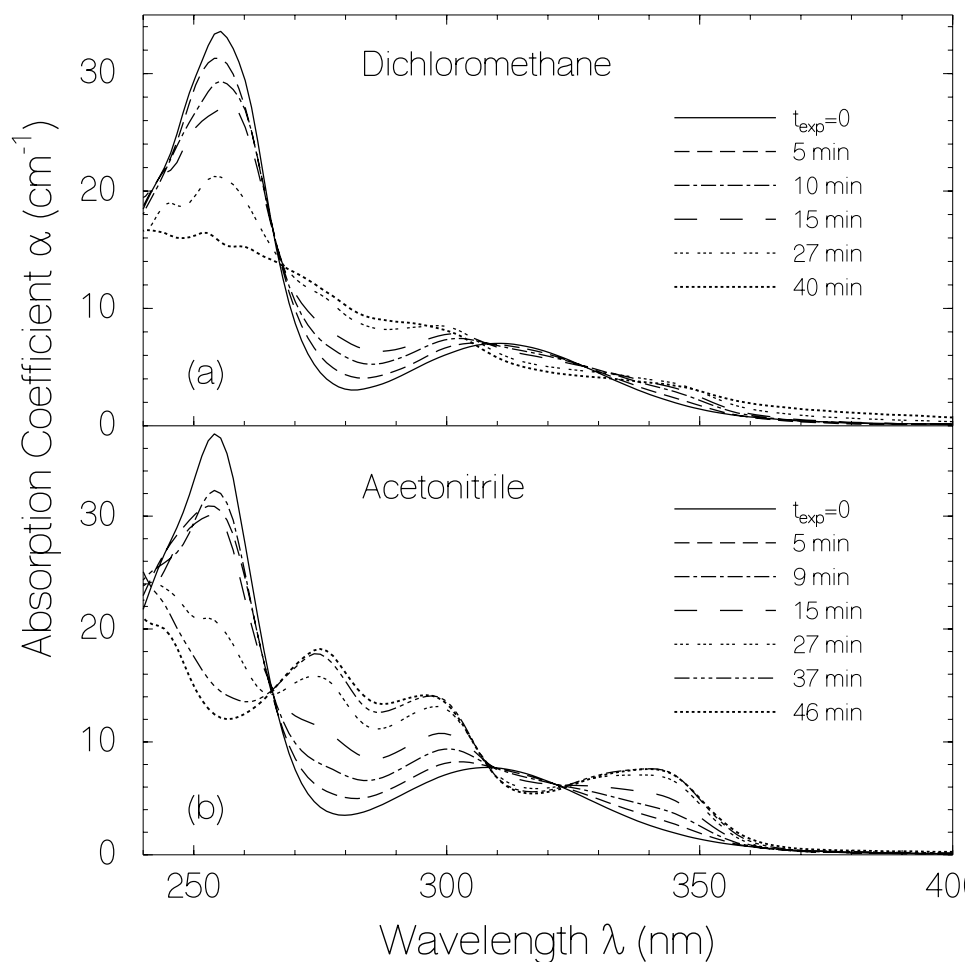


Figure 4.27: Absorption coefficient spectra of HPT after several durations of light exposure. Exposure times, t_{exp} , are listed in figure.

(a) Solvent dichloromethane, excitation intensity, $I_{\text{exc}} = 0.015 \text{Wcm}^{-2}$, excitation wavelength, $\lambda_{\text{exc}} = 260\text{nm}-380\text{nm}$

(b) Solvent acetonitrile, $I_{\text{exc}} = 0.015 \text{Wcm}^{-2}$, $\lambda_{\text{exc}} = 260\text{nm}-380\text{nm}$.

The transmission changes of HPT at wavelength position, λ_{pr} , versus exposed energy density (excitation wavelength, $\lambda_{\text{exc}} = 260\text{nm}-380\text{nm}$) for acetonitrile and dichloromethane, are displayed in Figure 4.28 (data extracted from Figure 4.27). The transmission change versus light exposure will be used below (in section 4.3.1) to calculate the quantum yield of photo-degradation as a function of the exposed energy density.

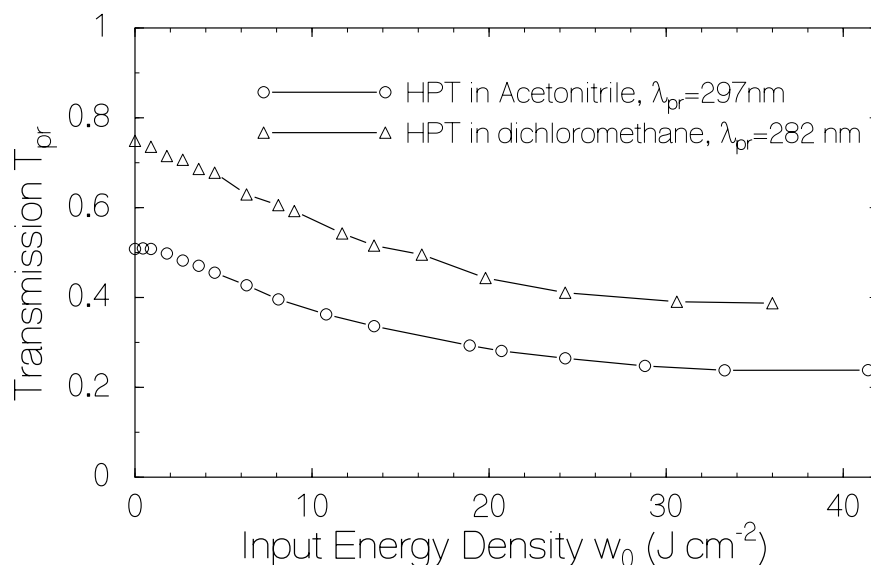


Figure 4.28: Transmission, $T_{pr}(w_0)$, at probe wavelength, λ_{pr} , versus exposed input energy density, w_0 , at excitation wavelength, $\lambda_{exc}=260\text{nm}-380\text{nm}$, excitation intensity, $I_{exc} = 0.015 \text{ W cm}^{-2}$, for HPT in dichloromethane and acetonitrile. Data are extracted from Figure 4.27.

4.3.2 Discussion

The fluorescence quantum yield of HPT in as-delivered solvents (no de-aeration) was measured to be $\phi_F(\text{dichloromethane}) \approx 0.0085$ and $\phi_F(\text{acetonitrile}) \approx 0.00785$. The small fluorescence quantum yields are thought to be caused by intersystem-crossing, internal conversion and by the weak S_1 - S_0 absorption and emission strength (long radiative lifetime of $\tau_{rad} \approx 200 \text{ ns}$). In degassed solvents the same fluorescence quantum yields as in air-saturated solutions of HPT was measured. The fluorescence quantum yield of HPPT in dichloromethane was reported to be $\phi_F = 0.26$ with a fluorescence lifetime of $\tau_F = 5.86 \text{ ns}$. This dye has a stronger S_0 - S_1 absorption strength and S_1 - S_0 emission strength. A radiative lifetime of $\tau_{rad} \approx 22.5 \text{ ns}$ is determined.

The photo-degradation of HPT was studied in Figures 4.27 and 4.28. From the absorption change at probe wavelength, $\lambda_{pr}=297\text{nm}$ for acetonitrile and $\lambda_{pr}=282\text{nm}$ for dichloromethane

4. Results and discussion: Heptyl-phenothiazine and Heptyl-phenyl-phenothiazine

with exposure time, t , the quantum yield of photo-degradation was calculated according to Equations 3.2-3.4.

The obtained initial quantum yields of photo-degradation, $\phi_{F,0}$, are listed in Table 4.3. The photo-stability of HPT (Figure. 4.27, $\lambda_{exc} = 260\text{nm}-380\text{nm}$) is rather low in dichloromethane ($\phi_{D,0} \approx 6.1 \times 10^{-3}$) and moderate in acetonitrile ($\phi_{D,0} \approx 4.5 \times 10^{-4}$).

Table 4.3: Spectroscopic parameters of HPT and HPPT at room temperature

Dye	HPT	HPT	HPPT
Solvent	dichloromethane	acetonitrile	dichloromethane
n_F	1.4320	1.3503	1.4306
n_A	1.4559	1.3713	1.4504
$\phi_F(428 \text{ nm})$			
$\phi_F(311 \text{ nm})$	0.0085	0.00785	0.26 [Pro04, She03]
$P_F(428 \text{ nm})$			
$P_F(311 \text{ nm})$	0.04	0.04	
τ_F (ns)	1.61	1.71	5.86 [Pro04, She03]
τ_{rad} (ns)	190	218	22.5
$\phi_{D,0}$	0.0061	4.5×10^{-4}	

4.4 Pyrene–flavin dyad (PFD)

4.4.1 Results

The pyrene – flavin (isoalloxazine) dyad (abbreviated by PFD) is made up of a phenyl-isoalloxazine derivative and of 1-methylpyrene, in which both chromophores are linked via an enantiomerically pure dipeptide bridge of R-configuration (Section 3.1.1). Detailed studies have been carried out in [Shi06]. The absorption cross-section spectra of the investigated PFD dyad in dichloromethane and acetonitrile are shown in Figure 4.29. The absorption cross-section spectra of the structural subunits of the dyad, (i) pyrene and 1-methylpyrene, and (ii) isoalloxazine acetic acid ethyl ester (abbreviated by IAE) are also included in Figure 4.29.

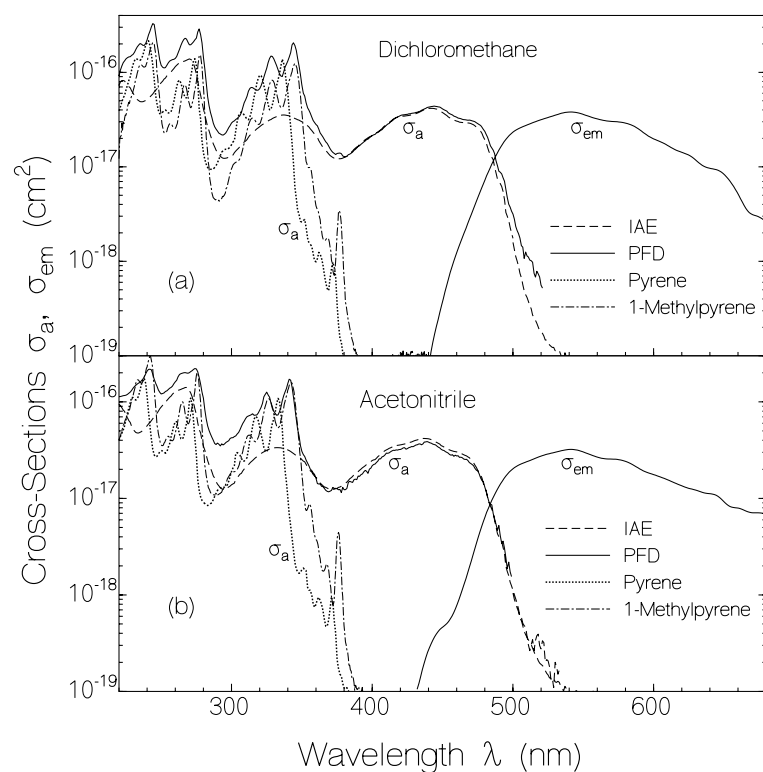


Figure 4.29: Absorption and stimulated emission cross-section spectra of investigated compounds in dichloromethane and acetonitrile. The applied dye concentrations in the measurements were: $C(\text{PFD, dichloromethane}) = 3.1 \times 10^{-4} \text{ mol dm}^{-3}$, $C(\text{PFD, acetonitrile}) = 4.5 \times 10^{-5} \text{ mol dm}^{-3}$, $C(\text{IAE, dichloromethane}) = 1.17 \times 10^{-3} \text{ mol dm}^{-3}$, $C(\text{IAE, acetonitrile}) = 5.6 \times 10^{-4} \text{ mol dm}^{-3}$, $C(\text{pyrene, dichloromethane}) = 3.5 \times 10^{-4} \text{ mol dm}^{-3}$, $C(\text{pyrene, acetonitrile}) = 3.9 \times 10^{-4} \text{ mol dm}^{-3}$, $C(\text{1-methylpyrene, dichloromethane}) = 5.2 \times 10^{-5} \text{ mol dm}^{-3}$, and $C(\text{1-methylpyrene, acetonitrile}) = 6 \times 10^{-5} \text{ mol dm}^{-3}$.

4. Results and discussion: Pyrene-flavin dyad (PFD)

The absorption spectrum of the dyad PFD is roughly the sum of the absorption spectra of the components, IAE and 1-methylpyrene, indicating that both components retain their electronic structures and transition dipoles.

The stimulated emission cross-section spectrum of PFD, is also included in Figure 4.29. The stimulated emission cross-section spectrum of PFD is roughly the mirror image of the S_0 - S_1 absorption spectrum with a spectral Stokes shift of about $\delta\tilde{\nu}_{St} \approx 4100 \text{ cm}^{-1}$.

The fluorescence quantum distributions, $E_F(\lambda)$, of PFD in as-delivered dichloromethane and acetonitrile are shown in the top parts of Figures 4.30a and 4.30b, respectively. The corresponding fluorescence quantum yields, $\phi_F = \int E_F(\lambda)d\lambda$, are listed in table 4.4. The fluorescence quantum yield of PFD is very low, i.e. $\phi_F(\text{dichloromethane}, \lambda_{exc} = 428 \text{ nm}) \approx 0.0031$ and $\phi_F(\text{acetonitrile}, \lambda_{exc} = 428 \text{ nm}) \approx 0.011$. In the case of excitation at 428 nm only the isoalloxazine (flavin) part of the dyad is excited and the typical isoalloxazine fluorescence spectrum is observed. In the case of excitation at 311 nm the light is absorbed by the 1-methylpyrene moiety (fraction of $\chi_{Py} \approx 0.44$ for solvent dichloromethane, and $\chi_{Py} \approx 0.60$ for acetonitrile) and the isoalloxazine moiety (fraction of $\chi_{Fl} \approx 0.56$ for dichloromethane, and $\chi_{Fl} \approx 0.40$ for acetonitrile). The fluorescence emission from the isoalloxazine part is reduced to $\phi_F(311\text{nm}) \approx 0.47 \times \phi_F(428\text{nm})$ in the case of solvent dichloromethane, and to $\phi_F(311\text{nm}) \approx 0.4 \times \phi_F(428\text{nm})$ in the case of solvent acetonitrile. The observed fluorescence approximately agrees with the emission of the directly excited isoalloxazine part. A weak emission from the pyrene part is observed.

The fluorescence polarisation spectra, $P_F(\lambda)$, of PFD in dichloromethane and acetonitrile are plotted in the lower parts of Figures 4.30a and 4.30b, and the average degrees of fluorescence polarization are listed in Table 4.4.

4. Results and discussion: Pyrene-flavin dyad (PFD)

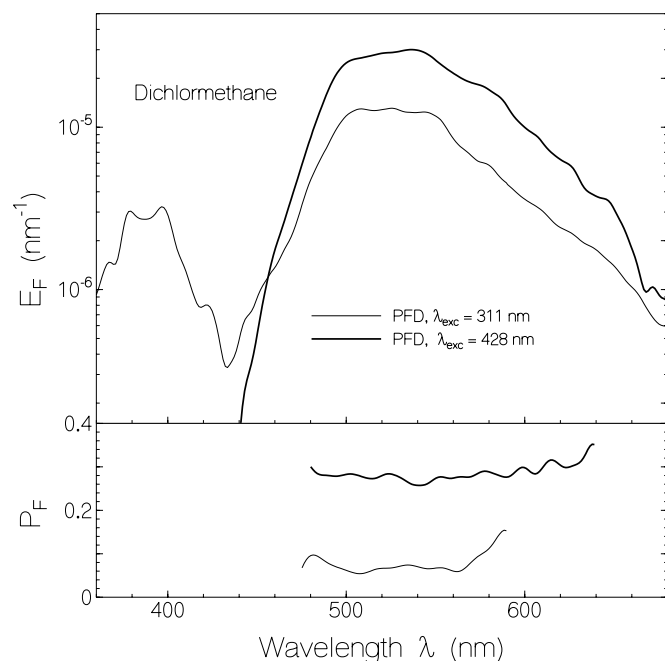


Figure 4.30a: Fluorescence quantum distribution (top part) and degree of fluorescence polarization (lower part) of PFD in dichloromethane. Excitation wavelengths, λ_{exc} , are indicated in the figure. Concentration is $C = 3.3 \times 10^{-5}$ mol dm⁻³.

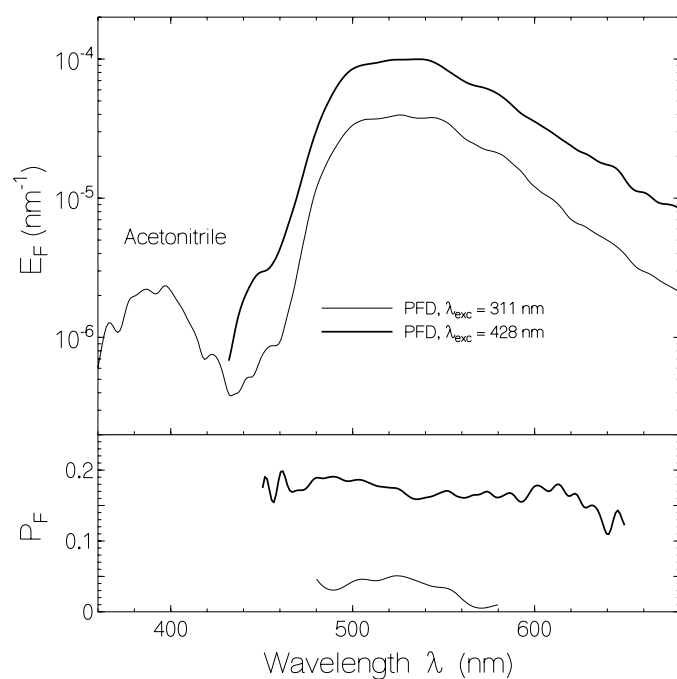


Figure 4.30b: Fluorescence quantum distribution (top part) and degree of fluorescence polarization (lower part) of PFD in acetonitrile. Excitation wavelengths, λ_{exc} , are indicated in the figure. Concentration is $C = 2.4 \times 10^{-5}$ mol dm⁻³.

In the case of excitation at 428 nm the degree of fluorescence polarisation is reasonably high because the fluorescence lifetime is short (small fluorescence quantum yield). In the case of 311 nm excitation the degree of fluorescence polarization is low indicating a different orientation of the transition dipole moments of 311 nm excitation and of S_1 - S_0 emission. Also reorientation in the energy transfer from pyrene to isoalloxazine (see section 4.4.2) may contribute to the reduction of the degree of fluorescence polarisation.

Temporal fluorescence traces of the PFD dye are shown in Figure 4.31. The excitation wavelength was $\lambda_{\text{exc}} = 400$ nm (excitation of flavin part of PFD only).

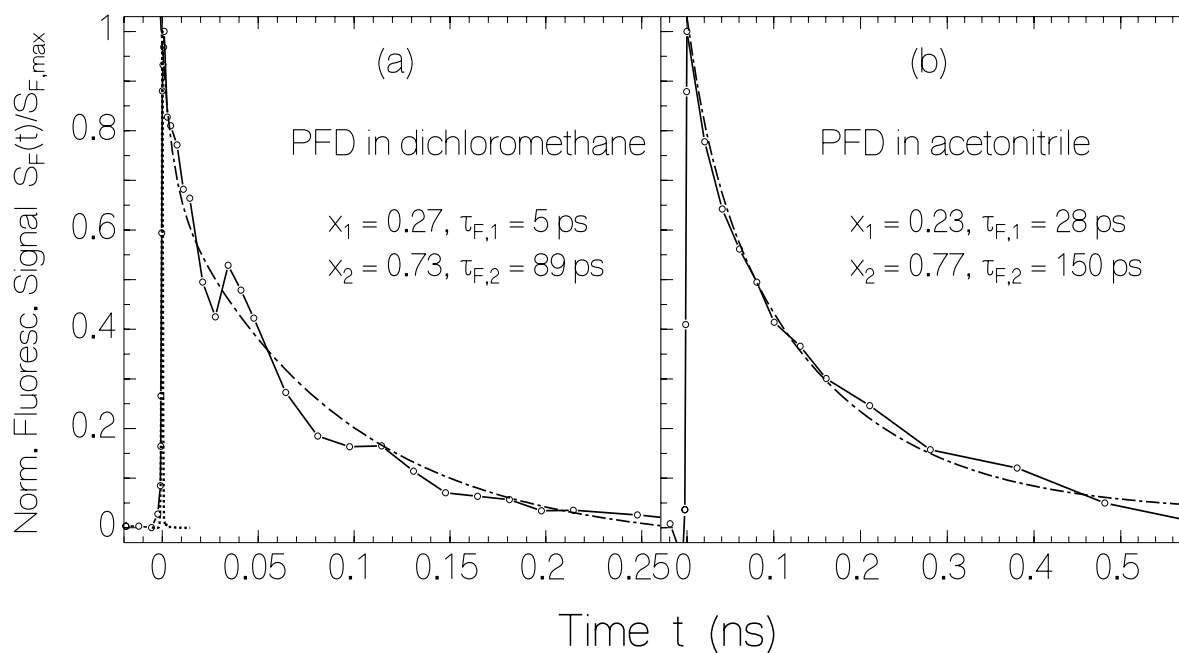


Figure 4.31: Temporal fluorescence traces. Dotted curve is response function. Dash-dotted curves are double-exponential fits (Equation 4.14).

(a) PFD in dichloromethane (up-converted fluorescence signal). Excitation wavelength $\lambda_{\text{exc}} = 400$ nm, excitation pulse duration $\Delta t_{\text{exc}} = 150$ fs.

(b) PFD in acetonitrile (up-converted fluorescence signal). $\lambda_{\text{exc}} = 400$ nm, $\Delta t_{\text{exc}} = 150$ fs.

The fluorescence up-conversion traces of PFD in dichloromethane and acetonitrile are well fitted by a two-component single-exponential decay according to

$$S_F(t) = S_{F,0} [x_1 \exp(-t/\tau_{F,1}) + x_2 \exp(-t/\tau_{F,2})], \quad (4.14)$$

where x_1 and x_2 are the weight-factors, while $\tau_{F,1}$ and $\tau_{F,2}$ are the fluorescence decay times. The obtained fluorescence lifetimes are in the several ps up to 150 ps range. In the case of double-exponential decay we define an average fluorescence lifetime by $\tau_F = x_1\tau_{F,1} + x_2\tau_{F,2}$. The determined fluorescence lifetimes and average fluorescence lifetimes are listed in Table 4.4.

The results of the picoseconds pump-probe measurements are shown in Figure 4.32. For both, PFD in dichloromethane (a) and PFD in acetonitrile (b), the probe pulse transmission is reduced after the pump pulse passage through the sample indicating that the excited-state absorption at the excitation wavelength ($\lambda_{exc} = 400$ nm) is slightly higher than the ground-state absorption. The transmission recovery is fitted in the figure by the following single-exponential function

$$T(t) = T_{ini} - \Delta T_{jump} \exp(-t / \tau_{a,rec}), \quad (4.15)$$

where T_{ini} is the initial transmission before excitation, ΔT_{jump} is the pump pulse induced transmission jump, and $\tau_{a,rec}$ is the ground-state absorption recovery time. In the case of PFD in dichloromethane the ground-state absorption recovers with a time constant of $\tau_{a,rec} \approx 100$ ps, while a bi-exponential fluorescence decay with the time constants $\tau_{F,1} \approx 5$ ps and $\tau_{F,2} \approx 89$ ps was observed (Figure 4.31a). This indicates that after excitation a non-fluorescing intermediate state is formed (charge-transfer state) with a time constant of $\tau_{F,1} \approx 5$ ps which relaxes slower than it is formed with a time constant of $\tau_{a,rec} \approx \tau_{F,2} \approx 100$ ps. For PFD in acetonitrile the probe pulse transmission is only very weakly reduced by the pump pulse excitation, the absorption recovery time of $\tau_{a,rec} \approx 150$ ps agrees within the experimental accuracy with the fluorescence signal decay of $\tau_{F,2} \approx 150$ ps. This indicates that the expected non-fluorescent intermediate state (charge-transfer state, see section 4.4.2) is formed with a time constant of $\tau_{F,1} \approx 28$ ps and has an approximate lifetime of $\tau_{a,rec} \approx \tau_{F,2} \approx 150$ ps.

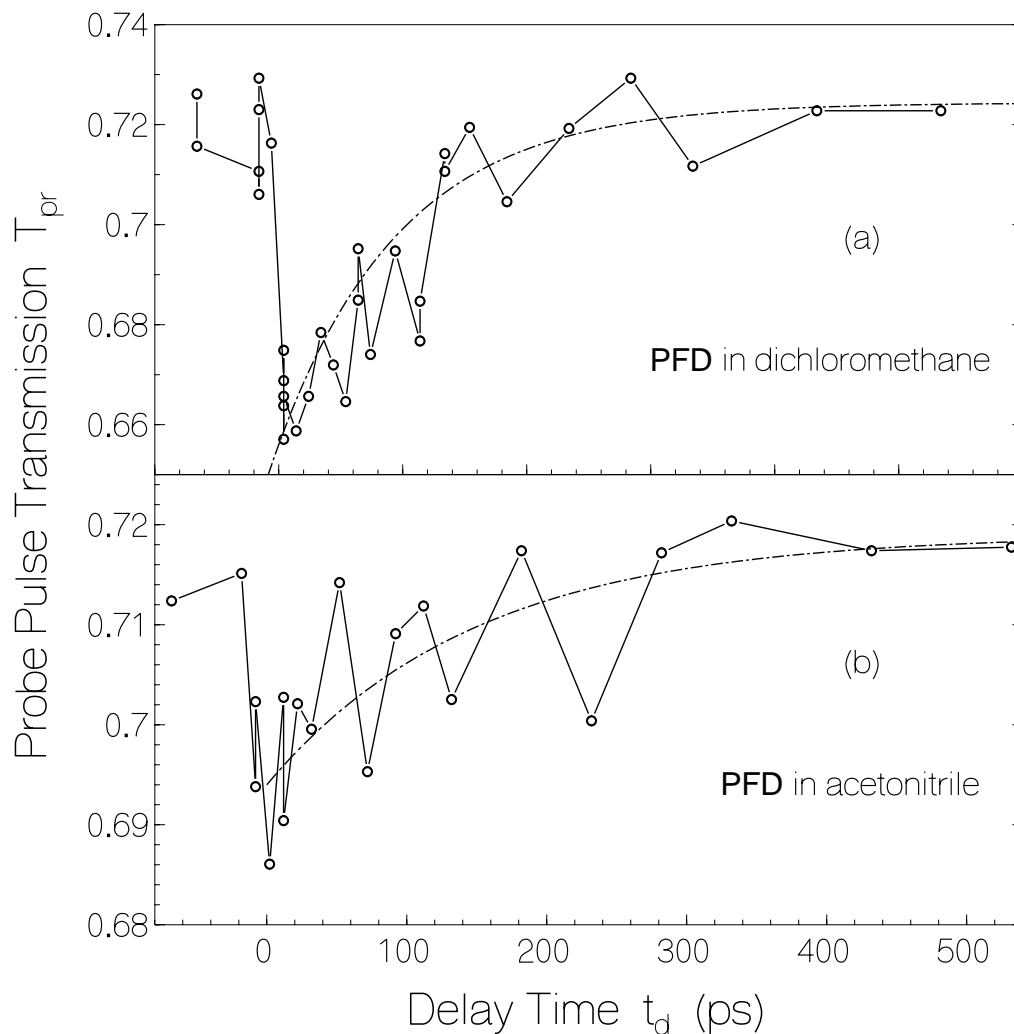


Figure 4.32: Probe pulse transmission through PFD in dichloromethane (a) and acetonitrile (b) as a function the delay time between probe pulse passage and pump pulse passage through the sample. Cell length 1 mm. Pulse duration 1.4 ps, laser wavelength 400 nm, pump pulse energy ca. 200 μJ , probe pulse energy ca. 20 μJ . Pulse focusing with 50 cm lenses in 46 cm distance from sample. Dash-dotted curves are fits of Equation 4.15 to the data points with $\tau_{a,rec} = 100$ ps (a) and 150 ps (b).

In Figure 4.33 the absorption changes due to long-time blue-light excitation of PFD in dichloromethane (part a, excitation in range of 400 nm - 440 nm, excitation intensity $I_{exc} = 0.02 \text{ W cm}^{-2}$), and acetonitrile (part b, excitation at 428 nm, $I_{exc} = 0.029 \text{ W cm}^{-2}$) are shown. Absorption coefficient spectra are depicted for different times of light exposure. In both solvents the S_0 - S_1 absorption of the isoalloxazine part decreased with exposure time. The pyrene part was not directly excited, but the pyrene absorption reduced strongly in dichloromethane.

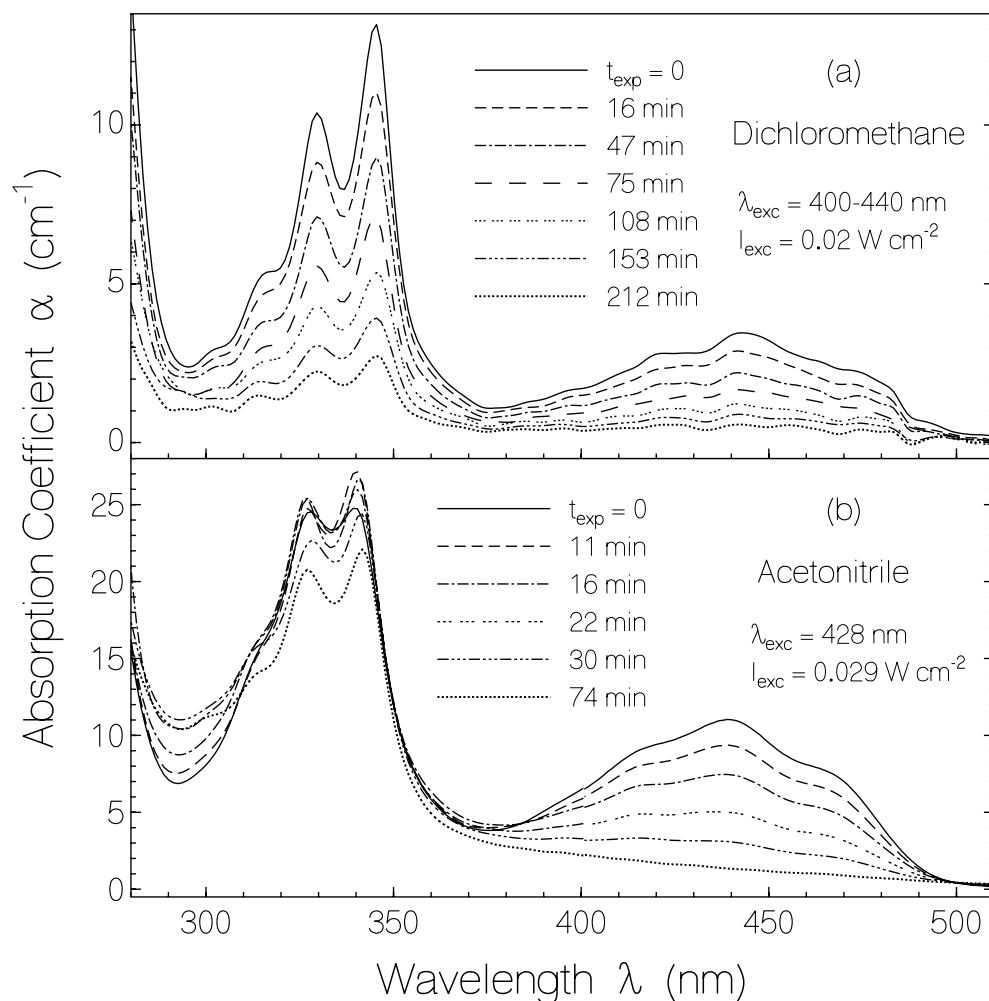


Figure 4.33: Absorption coefficient spectra of PFD after several durations of light exposure. Excitation wavelengths, λ_{exc} , excitation intensities, I_{exc} , and exposure times, t_{exp} , are listed in figure.

(a) Solvent dichloromethane.

(b) Solvent acetonitrile.

The transmission rise of PFD at two wavelength positions, λ_{pr} , (one at peak absorption of isoalloxazine part around 440 nm, and one at peak absorption of 1-methylpyrene part around 340 nm) with exposed energy density at the excitation wavelengths, $\lambda_{\text{exc}} = 428 \text{ nm}$ (acetonitrile) or 400-440 nm (dichloromethane), are displayed in Figure 4.34 (data extracted from Figure 4.33). The transmission change versus light exposure will be used (section 4.4.2) to calculate the quantum yield of photo-degradation as a function of the exposed energy density.

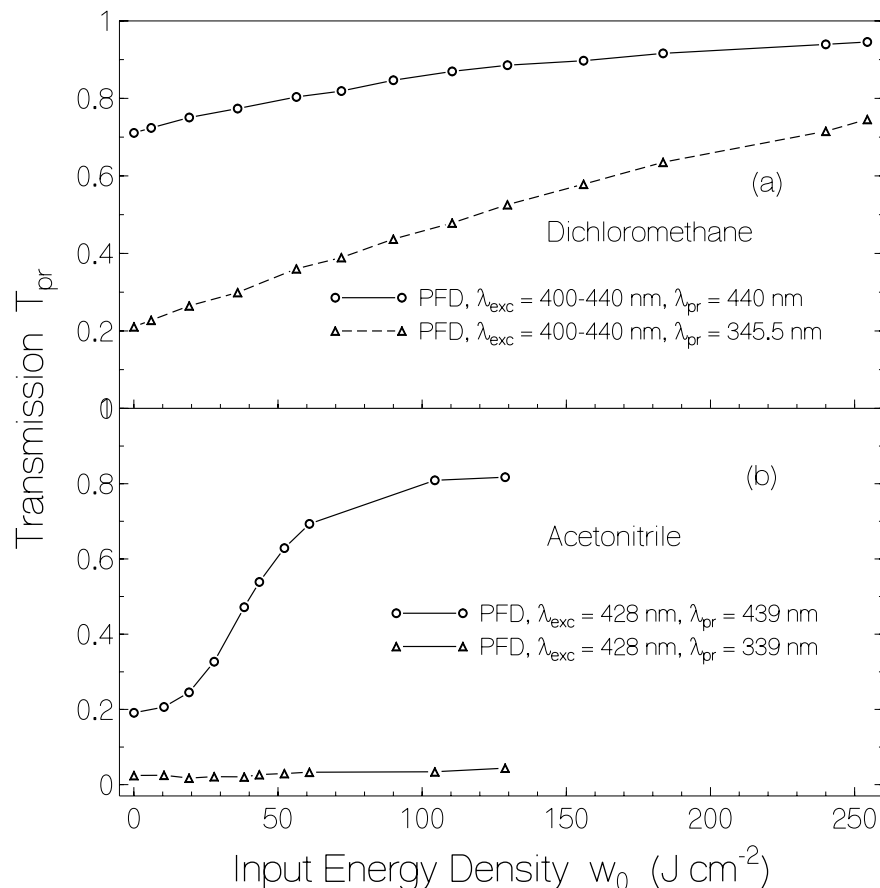
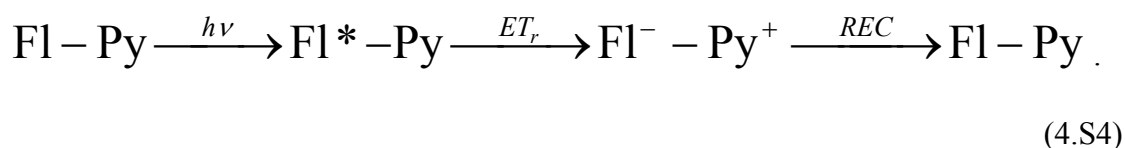


Figure 4.34: Transmission, $T_{pr}(w_0)$, at probe wavelengths, λ_{pr} , versus exposed input energy density, w_0 , at excitation wavelength, λ_{exc} , for PFD. Data are extracted from Figure 4.33. (a) Dichloromethane. Excitation intensities, $I_{exc}(PFD) = 0.02\ W\ cm^{-2}$. (b) Acetonitrile. Excitation intensities, $I_{exc}(PFD) = 0.029\ W\ cm^{-2}$.

4.4.2 Discussion

The fluorescence efficiency in the PFD is strongly reduced compared to the constituents, IAE and 1-methyl-pyrene. The weak fluorescence efficiency of PFD in the case of excitation at $\lambda_{exc} = 428\ nm$ is thought to be caused by photo-induced reductive electron transfer [Val02] from the ground-state pyrene moiety to the flavin chromophore according to the reaction scheme



The photon absorption excites the isoalloxazine (flavin) part Fl, reductive electron transfer (ET_r) forms the ion pair Fl^-Py^+ , which finally recovers (REC) to the original compound. The processes are illustrated in Figure 4.35. The measured fluorescence lifetimes $\tau_{F,1}$ ($\lambda_{exc} = 400$ nm) give excited-state lifetimes of Fl^*-Py . The rate of reductive electron transfer, k_{ET_r} , is approximately given by $k_{ET_r} \approx \tau_{F,1}^{-1}(\text{PFD}) - \tau_F^{-1}(\text{IAE})$. The measured ground-state absorption recovery times $\tau_{a,rec}$ ($\lambda_{exc} = 400$ nm) are determined by the relaxation channels of the PFD molecules (radiative relaxation, internal conversion, triplet-singlet relaxation, charge-transfer complex recombination). The recombination rate is approximately given by $k_{REC} \approx \tau_{a,rec}^{-1}(\text{PFD}) \approx \tau_{F,2}$. Values of k_{ET_r} and k_{REC} are included in Table 4.4.

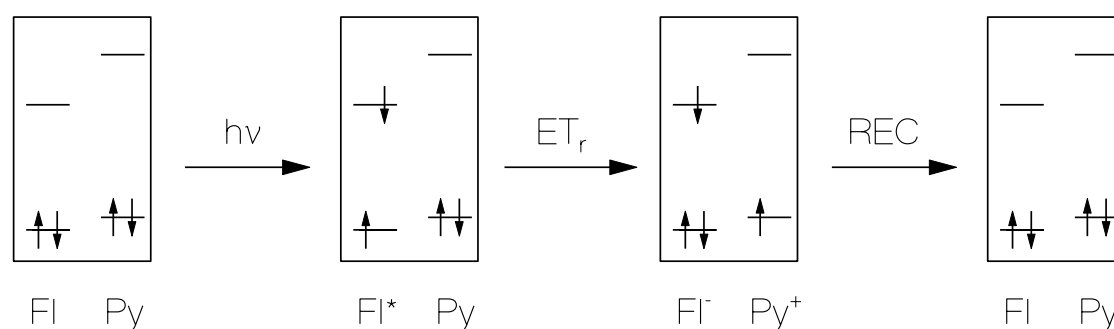
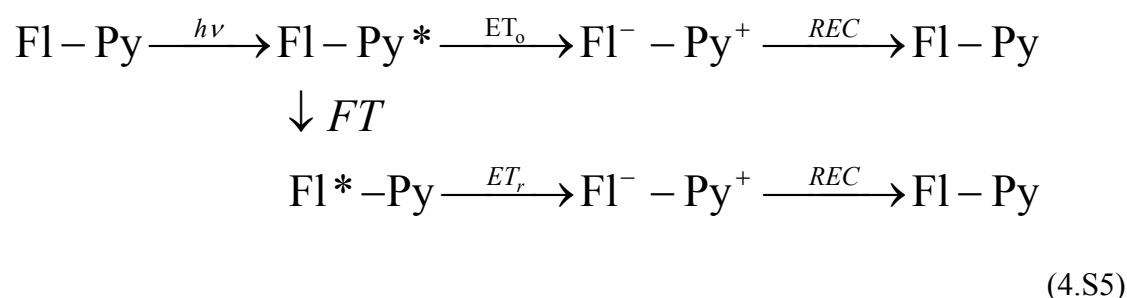


Figure 4.35: Illustration of photo-induced reductive electron transfer from ground-state pyrene part to isoalloxazine part in the case of excitation of the S_1 state of the isoalloxazine moiety of the dyad PFD

In the case of excitation at 311 nm both the pyrene and the flavin moieties are excited. Weak emission from the 1-methylpyrene part and from the flavin part is observed. The 1-methylpyrene fluorescence is reduced by i) Förster-type energy transfer (rate constant k_{FT}), and ii) photo-induced oxidative electron transfer [Val02] (rate constant k_{ET_o}) from excited 1-methylpyrene to isoalloxazine. The fluorescence emission from the flavin part is slightly more than a factor of two reduced compared to the long-wavelength excitation. The fluorescence reduction roughly agrees with the fraction of excitation light absorbed by the 1-methylpyrene moiety. In the case of efficient excitation energy transfer from the 1-methylpyrene part to the

flavin part there should be no reduction of the fluorescence emission from flavin part. Oxidative electron transfer from excited 1-methylpyrene to flavin does not contribute to flavin emission. Since we observe fluorescence reduction, we think that the photo-induced oxidative excited-state electron transfer from excited 1-methylpyrene to flavin dominates over the Förster-type energy transfer from excited 1-methylpyrene to flavin. The processes are illustrated in Figure 4.36. The following reaction scheme is thought to apply:



with dominance of the oxidative electron transfer. *FT* indicates the Förster-type energy transfer, and *ET_o* indicates the photo-induced excited-state oxidative electron transfer from *Py** to *Fl*.

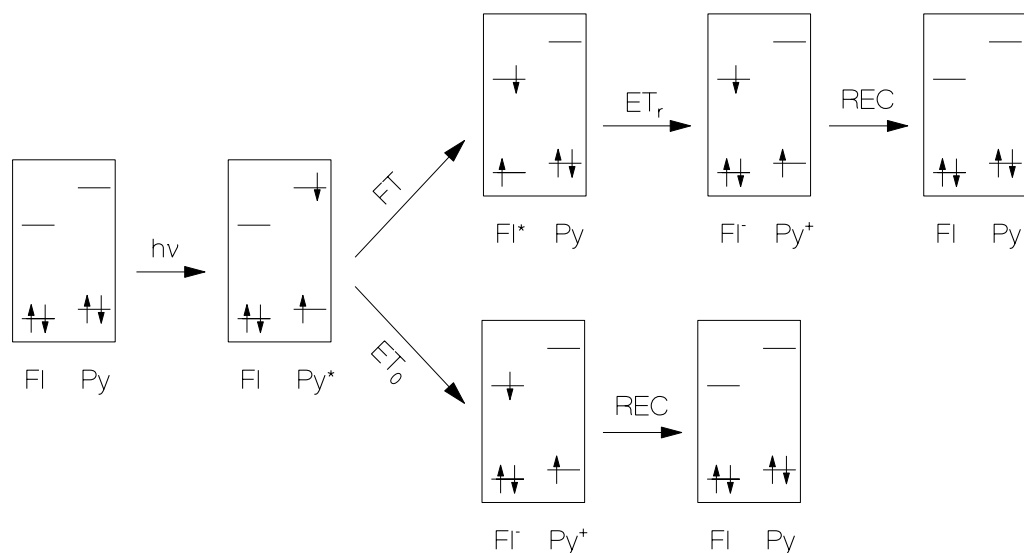


Figure 4.36: Illustration of photo-induced excited-state electron transfer and Förster-type energy transfer from pyrene part to isoalloxazine part in the case of excitation to the *S₂* state of the pyrene moiety.

4. Results and discussion: Pyrene-flavin dyad (PFD)

The rate of Förster-type energy transfer, k_{FT} , from the 1-methylpyrene moiety (energy donor) to the flavin moiety (energy acceptor) was determined by use of Equation 2.17-20 (Section 2.6).

For the considered situation of energy transfer from the 1-methylpyrene part to the flavin part in PFD the distance between donor and acceptor is approximately 1.26 nm [She03], and statistical isotropic orientation of the transition dipoles is assumed ($\overline{\kappa^2} = 2/3$). The calculated critical Förster distances are $R_0(\text{Py-FI, dichloromethane}) = 2.5$ nm, and $R_0(\text{Py-FI, acetonitrile}) = 2.26$ nm. The energy transfer rate constants are calculated to be $k_{FT}(\text{Py-FI, dichloromethane}) \approx 2.22 \times 10^9 \text{ s}^{-1}$ ($k_{F,0,d} = (27.4 \text{ ns})^{-1}$), and $k_{FT}(\text{Py-FI, acetonitrile}) \approx 2.08 \times 10^9 \text{ s}^{-1}$ ($k_{F,0,d} = (16 \text{ ns})^{-1}$) by using the fluorescence lifetimes of 1-methylpyrene in the solvents.

The rate of excitation transfer from the 1-methylpyrene moiety to the flavin moiety, $k_{ex} = k_{FT} + k_{ET_o}$ is approximately given by $k_{ex} \approx \tau_F^{-1}(\text{Py}^*-\text{Fl}) - \tau_F^{-1}(\text{Py})$, where $\tau_F(\text{Py}^*-\text{Fl}) \approx \tau_F(\text{Py}) \phi_F(\text{Py}^*-\text{Fl})/[x_{\text{Py}} \phi_F(\text{Py})]$. Thereby $\tau_F(\text{Py})$ is the fluorescence lifetime of 1-methylpyrene, $\phi_F(\text{Py})$ is the fluorescence quantum yield of 1-methylpyrene, $\phi_F(\text{Py}^*-\text{Fl})$ is fluorescence quantum yield contribution of the 1-methylpyrene part in PFD, and x_{Py} is the fraction of excitation light absorbed by the 1-methylpyrene part. The estimated values of k_{ex} and k_{FT} ($\lambda_{exc} = 311$ nm) are included in Table 4.4. It is found that $k_{ET_o} \gg k_{FT}$.

The relevant photodynamics of the pyrene-flavin dyad is determined by the occurring three photo-induced electron transfer reactions, the reductive electron transfer ET_r from HOMO-Py to HOMO-Fl* when the flavin part is excited, the oxidative electron transfer ET_o from LUMO-Py* to LUMO-Fl when the pyrene part is excited, and electron recombination LUMO-Fl⁻ to HOMO-Py⁺ after electron transfer.

The electron transfer processes may be analysed by the Marcus theory of electron transfer and illustrated by Marcus-type potential parabolae in reaction coordinate diagrams as described in chapter 2.7 and as it will be illustrated for the phenothiazine-flavin dyad in the next section.

4. Results and discussion: Pyrene-flavin dyad (PFD)

The rate of the reductive electron transfer was found to be $k_{ET_r}^{-1} \approx 5$ ps for PFD in dichloromethane. It indicates an electron transfer in the normal Marcus region (donor slightly above acceptor level) with a typical rate. The rate of oxidative electron transfer for PFD in dichloromethane was found to be $k_{ET_o}^{-1} \approx 77$ ps. It indicates an electron transfer in the normal Marcus region (donor slightly above acceptor level). The electron recombination occurs from a high lying donor state (LUMO-FI⁻) to a low lying acceptor state (HOMO-Py⁺). Therefore this transition is likely in the inverted Marcus region. A recombination speed of $k_{REC}^{-1} \approx 100$ ps was found. This indicates a not too high lying crossing point of the Marcus potential parabola above the donor electron energy level.

The photo-degradation of PFD was studied in Figures. 4.33 and 4.34. From the data in Figure 4.34 the quantum yields of photo-degradation were calculated as a function of the exposed energy density to the samples using Equations 3.2-3.4.

The obtained initial quantum yields of photo-degradation, $\phi_{F,0}$, are listed in Table 4.4. PFD dyad was excited in the flavin absorption part ($\lambda_{exc} = 400-440$ nm for dichloromethane, and $\lambda_{exc} = 428$ nm for acetonitrile). This long-wavelength excitation in the flavin part of the dyad causes also degradation of the pyrene part. The quantum yield of photo-degradation of the pyrene part is lower compared to pure pyrene in solution ($\phi_{D,0} \approx 1.5 \times 10^{-4}$ in dichloromethane, and $\phi_{D,0} \approx 2 \times 10^{-5}$ in acetonitrile). The energy inputted to the dyads causes some disruptive action on the not electronically excited pyrene part. The photo-induced degradation of the flavin part of PFD in dichloromethane is ($\phi_D \approx 1.5 \times 10^{-4}$) independent of the already inputted energy. In the solvent acetonitrile the quantum yield of photo-degradation of the flavin part rises from initially $\phi_{D,0} \approx 1 \times 10^{-4}$ to $\phi_D \approx 7 \times 10^{-4}$ at exposed energy density of $w_0 = 30$ J cm⁻² and remains then approximately constant. The formed photo-fragments seem to speed-up the photo-degradation.

4. Results and discussion: Pyrene-flavin dyad (PFD)

Table 4.4: Spectroscopic parameters of investigated dyes at room temperature

Dye	PFD		IAE	
Solvent	dichloromethane	acetonitrile	dichloromethane	Acetonitrile
ϕ_F				
428 nm	0.0031±0.0003	0.011±0.001	0.223±0.02	0.154±0.02
311 nm	0.0016±0.0002	0.0044±0.0004		
P_F				
428 nm	≈ 0.28	≈ 0.18	≈ 0.05	≈ 0.05
311 nm	≈ 0.07	≈ 0.03		
$\tau_{F,1}$ (ps)	≈ 5	≈ 28		
$\tau_{F,2}$ (ps)	≈ 89	≈ 150		
τ_F (ns)	≈ 0.062	≈ 0.121	4.4±0.2	3.3±0.2
τ_{rad} (ns)	≈ 19.5	≈ 19.5	≈ 19.5	≈ 19.5 [Drö03]
$\tau_{a,rec}$ (ps)	≈ 100	≈ 150		
k_{REC} (s ⁻¹)	≈ 9.9×10 ⁹	≈ 9.9×10 ⁹		
k_{ET_r} (s ⁻¹)	≈ 1.99×10 ¹¹	≈ 3.54×10 ¹⁰		
k_{ex} (s ⁻¹)	≈ 1.5×10 ¹⁰	≈ 1.7×10 ¹⁰		
k_{FT} (s ⁻¹)	≈ 2.2×10 ⁹	2.1×10 ⁹		
k_{ET_o} (s ⁻¹)	≈ 1.3×10 ¹⁰	≈ 1.5×10 ¹⁰		
$\phi_{D,0}$	≈ 1.5×10 ⁻⁴ a) ≈ 1.5×10 ⁻⁴ c)	≈ 1×10 ⁻⁴ b) ≈ 2×10 ⁻⁵ d)	≈ 5×10 ⁻⁴	≈ 6×10 ⁻⁴

a: $\lambda_{exc} = 400-440$ nm and $\lambda_{pr} = 440$ nm. b: $\lambda_{exc} = 428$ nm and $\lambda_{pr} = 439$ nm. c: $\lambda_{exc} = 400-440$ nm and $\lambda_{pr} = 345.5$ nm. d: $\lambda_{exc} = 428$ nm and $\lambda_{pr} = 339$ nm.

4.5 Phenothiazine–flavin dyad (PTFD)

4.5.1 Results

The phenothiazine-phenyl-isoalloxazine dyad, (called PTFD) is made up of the approximate constituents of the, HPT, or HPPT (phenothiazine moiety), and BrPF (isoalloxazine moiety) (Section 3.1.3). Detailed studies have been carried out in [Shi07b]. The absorption cross-section spectra of the investigated dyad PTFD in dichloromethane and acetonitrile are shown in Figures 4.37a and 4.37b, respectively. The absorption cross-section spectra of BrPF and of HPT are also included. In Figure 4.37a also the absorption cross-section spectrum of HPPT in dichloromethane is shown (taken from [Pro04, She03]). The PTFD absorption cross-section spectrum is roughly given by the sum of the full absorption of BrPF and of about 60 % of the absorption of HPPT. This indicates that in the dyad the isoalloxazine moiety and the phenothiazine moiety retain their electronic structure and transition dipoles (separate chromophores, local excitations), and that the phenyl group is not fully in the plane of the phenothiazine ring structure (less absorption strength).

The stimulated emission cross-section spectra of PTFD are included in Figures 4.37a and 4.37b. The stimulated emission spectra of PTFD are roughly the mirror image of the S_0 - S_1 absorption spectra. The spectral Stokes shifts are about $\delta\tilde{\nu}_{st} \approx 4300 \text{ cm}^{-1}$.

The fluorescence quantum distributions, $E_F(\lambda)$, of PTFD in dichloromethane and acetonitrile are shown in the top parts of Figures 4.38a and 4.38b, respectively. The corresponding fluorescence quantum yields, $\phi_F = \int E_F(\lambda)d\lambda$, are listed in Table 4.5.

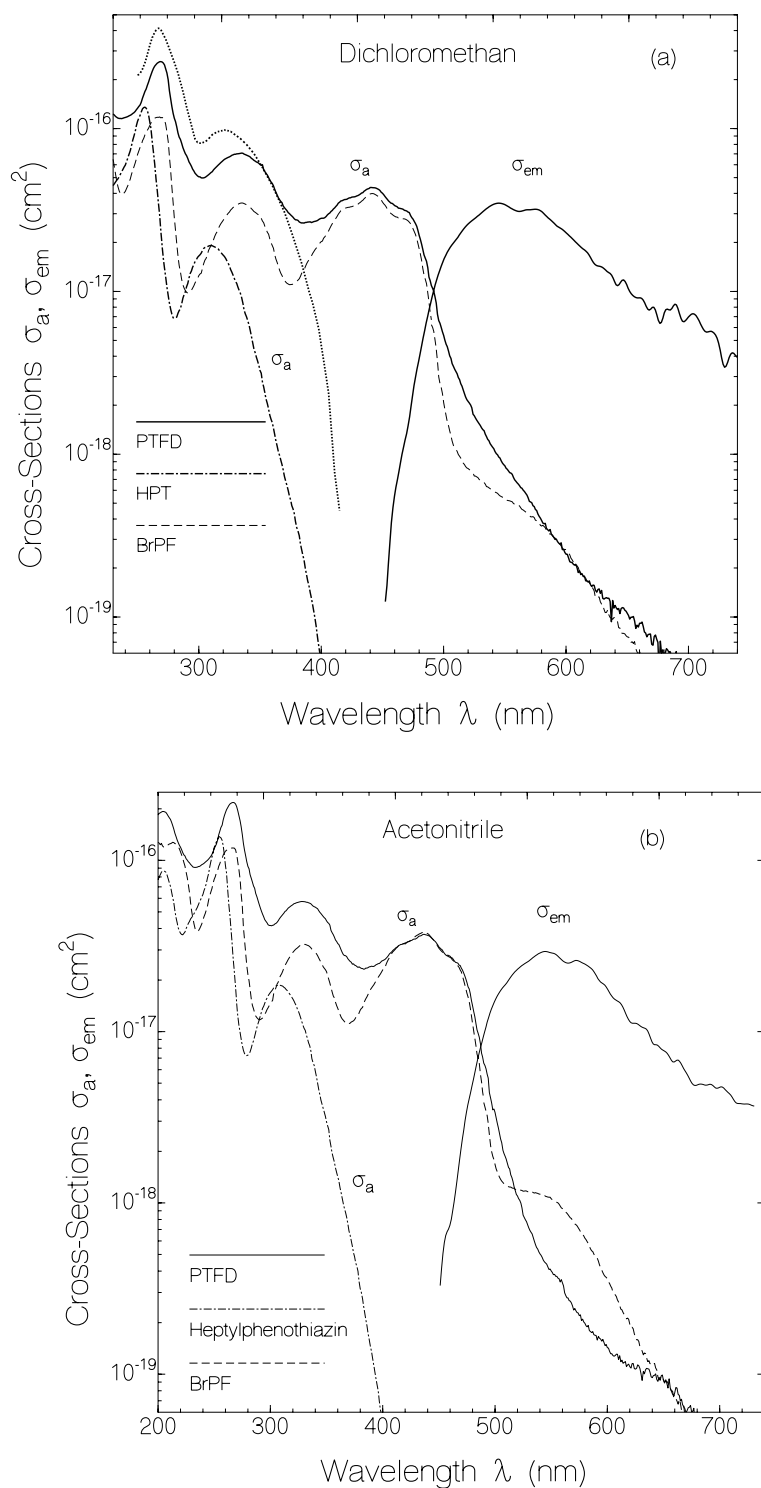


Figure 4.37: Absorption and stimulated emission cross-section spectra of investigated dyes in dichloromethane (a) and acetonitrile (b). The applied dye concentrations in the measurements were: $C(\text{PTFD, dichloromethane}) = 1.34 \times 10^{-4} \text{ mol dm}^{-3}$, $C(\text{PTFD, acetonitrile}) = 1.14 \times 10^{-5} \text{ mol dm}^{-3}$, $C(\text{BrPF, dichloromethane}) = 6.1 \times 10^{-4} \text{ mol dm}^{-3}$, $C(\text{BrPF, acetonitrile}) = 4.5 \times 10^{-4} \text{ mol dm}^{-3}$, $C(\text{heptylphenothiazine, dichloromethane}) = 2.38 \times 10^{-4} \text{ mol dm}^{-3}$, and $C(\text{heptylphenothiazine, acetonitrile}) = 4.46 \times 10^{-4} \text{ mol dm}^{-3}$. Spectra for 10-heptyl-3-phenylphenothiazine (HPPT) are taken from [Pro04, She03].

The fluorescence quantum yield of PTFD is low. In the case of excitation at 428 nm only the isoalloxazine (flavin) part of the dyad is excited and the typical isoalloxazine fluorescence spectrum is observed. The fluorescence quantum yields are $\phi_F(\text{PTFD, dichloromethane}) \approx 4.8 \times 10^{-4}$ and $\phi_F(\text{PTFD, acetonitrile}) \approx 4.9 \times 10^{-4}$. The fluorescence of the isoalloxazine moiety is reduced approximately a factor of 500 compared to the BrPF fluorescence efficiency. This fluorescence reduction will be interpreted below to be caused by reductive electron transfer from the HPPT moiety to the isoalloxazine moiety (see section 2.7). In the case of excitation at 311 nm the light is absorbed by the HPPT moiety (approximately $\chi_{\text{HPPT}} \approx 0.64$ for solvent dichloromethane, and $\chi_{\text{HPPT}} \approx 0.53$ for acetonitrile) and the isoalloxazine moiety (approximately $\chi_{\text{FI}} \approx 0.36$ for dichloromethane, and $\chi_{\text{FI}} \approx 0.47$ for acetonitrile). The fluorescence quantum yields are $\phi_F(\text{PTFD, dichloromethane}) \approx 0.0026$ and $\phi_F(\text{PTFD, acetonitrile}) \approx 0.0029$. The fluorescence originates dominantly from the HPPT moiety. The fluorescence efficiency is reduced approximately a factor of 100 compared to the HPPT fluorescence efficiency. This fluorescence reduction will be interpreted below to be caused by oxidative electron transfer from the phenothiazine moiety to the isoalloxazine moiety (see section 2.7).

The fluorescence polarisation spectra, $P_F(\lambda)$, of PTFD are plotted in the lower parts of Figures 4.38a and 4.38b, respectively for the solvents dichloromethane and acetonitrile. In the case of excitation at 428 nm the degree of fluorescence polarisation is low in the range of 0.04 (acetonitrile) to 0.1 (dichloromethane). This indicates that the PTFD fluorescence spectra are dominated by emission from a slowly relaxing excited state (formed charge-transfer state, see below) when the isoalloxazine moiety is excited.

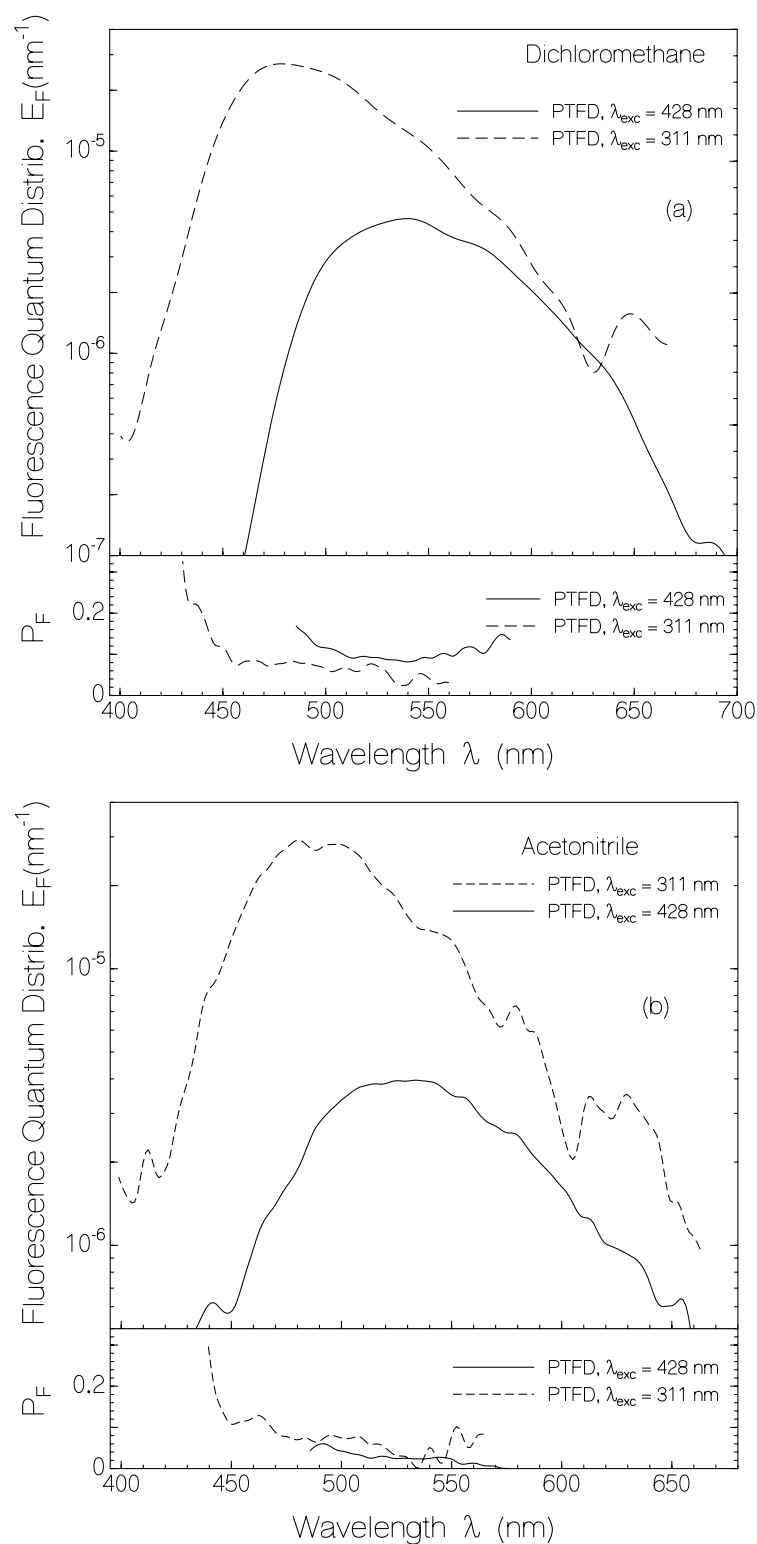


Figure 4.38: Fluorescence quantum distributions (top part) and degrees of fluorescence polarization (lower part) of PTFD in dichloromethane (a) and acetonitrile (b). Excitation wavelengths, λ_{exc} , are indicated in the figures. Applied dye concentrations are C (PTFD, dichloromethane) = 3.91×10^{-4} mol dm $^{-3}$ and C (PTFD, acetonitrile) = 3.11×10^{-4} mol dm $^{-3}$.

In the case of excitation at 311 nm the fluorescence comes mainly from the HPPT moiety. The degree of fluorescence polarisation is small despite the short fluorescence lifetime. It is thought that mainly the S₂ state of HPPT is excited and that emission occurs from the S₁ state with different transition dipole moment orientation resulting in a small degree of fluorescence polarisation.

Temporal fluorescence traces of the dyad PTFD are shown in Figure 4.39. The excitation wavelength was $\lambda_{\text{exc}} = 400$ nm (excitation of flavin part of PTFD only). The fluorescence up-conversion measurements revealed a fast lifetime component ($\tau_{\text{F},1}$) of sub-picosecond duration (Figures 4.39a and 4.39c), and real time fluorescence oscilloscope measurement revealed a slow lifetime component ($\tau_{\text{F},2}$) of about 5 ns duration (Figures 4.39b and 4.39d). The fast component is thought to originate from the isoalloxazine part with radiative lifetime of $\tau_{\text{rad},1} \approx 19.5$ ns [Shi06]. The fluorescence quantum yield of this contribution is $\phi_{\text{F},1} \approx \tau_{\text{F},1}/\tau_{\text{rad},1}$ ($\approx 3.5 \times 10^{-5}$). The slow component is thought to originate from the formed charge-transfer state (see below). Its fluorescence quantum yield is given by $\phi_{\text{F},2} \approx \phi_{\text{F}} - \phi_{\text{F},1}$ ($\approx 4.5 \times 10^{-4}$). The radiative lifetime of the charge-transfer state is $\tau_{\text{rad},2} \approx \tau_{\text{F},2}/\phi_{\text{F},2}$ (≈ 10 μs). The parameters are collected in Table 4.5.

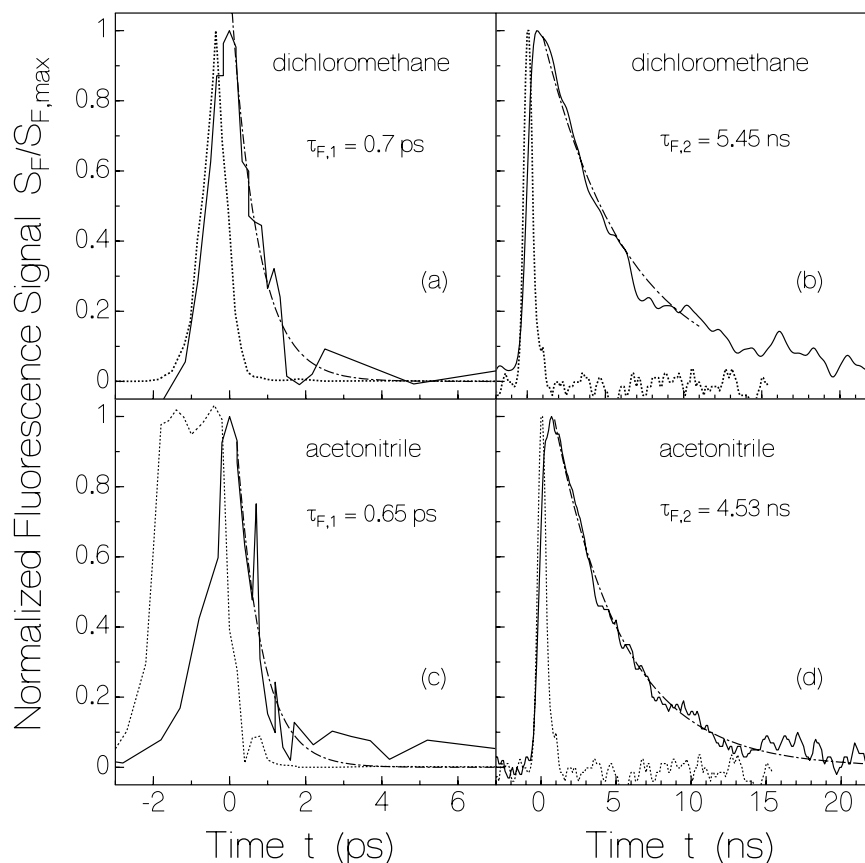


Figure 4.39: Temporal fluorescence traces of dyad PTFD. Solid curves: samples. Dash-dotted lines: single-exponential fits (Equation 4.2). Dotted lines: response functions.

- (a) Solvent dichloromethane (up-converted fluorescence signal)
- (b) Solvent dichloromethane (oscilloscope trace).
- (c) Solvent acetonitrile (up-converted fluorescence signal)
- (d) Solvent acetonitrile (oscilloscope trace).

Absorption changes due to long-time blue-light excitation of dyad PTFD in dichloromethane (part a, excitation in range of 400 nm - 440 nm, excitation intensity $I_{\text{exc}} = 0.02 \text{ W cm}^{-2}$), and acetonitrile (part b, excitation at 428 nm, $I_{\text{exc}} = 0.0356 \text{ W cm}^{-2}$) are shown in Figure 4.40. Absorption coefficient spectra are depicted for two different times of light exposure at fixed excitation intensities, I_{exc} . In the solvent dichloromethane the absorption reduced only slightly. In the solvent acetonitrile no absorption change by the applied light exposure is observed. The transmission changes will be used in the next section 4.5.2 to calculate the quantum yield of photo-degradation.

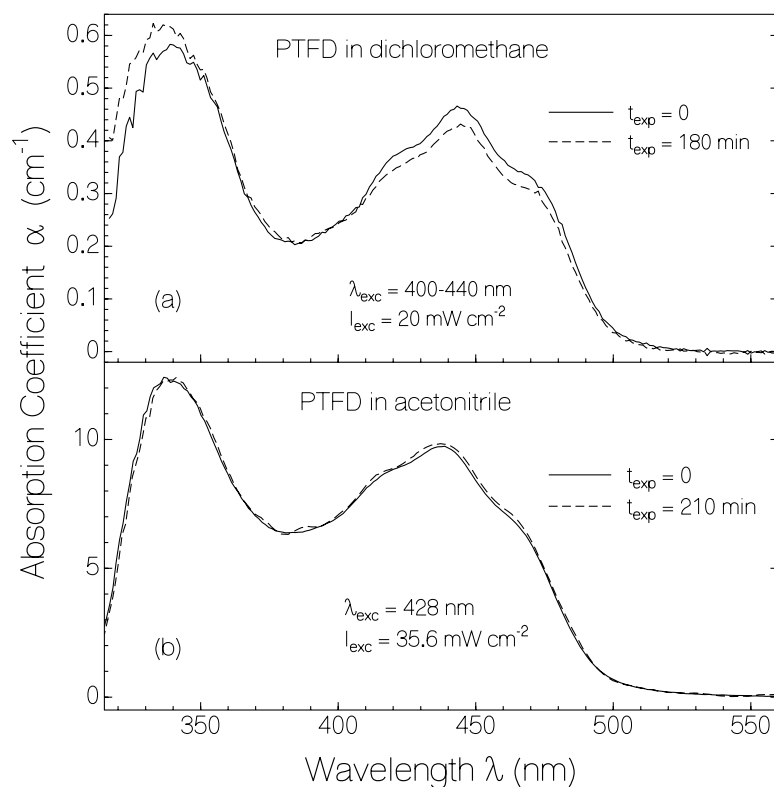


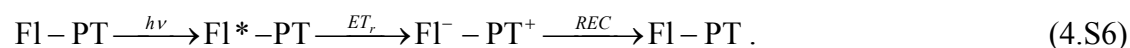
Figure 4.40: Absorption coefficient spectra of dyad PTFD after several durations of light exposure. Excitation wavelengths, λ_{exc} , excitation intensities, I_{exc} , and exposure times, t_{exp} , are listed in figure.

(a) Solvent dichloromethane. Sample length $\ell = 5$ mm.

(b) Solvent acetonitrile. Sample length $\ell = 1.5$ mm.

4.5.2 Discussion

The fluorescence efficiency in the dyad PTFD is strongly reduced compared to the constituents, HPPF and BrPF. The weak fluorescence efficiency of the dyad PTFD in the case of excitation at $\lambda_{\text{exc}} = 428$ nm is thought to be caused by photo-induced reductive electron transfer from the ground-state HPPT moiety to the flavin moiety according to the reaction scheme



The photon absorption excites the isoalloxazine (flavin) part Fl, reductive electron transfer forms the ion pair (intramolecular charge-transfer state) Fl^-PT^+ , and finally charge

recombination (REC) forms the original compound. The reductive electron transfer from PT to Fl* requires that the HOMO level of PT is higher than the HOMO level of Fl. The processes are illustrated in Figure 4.41.

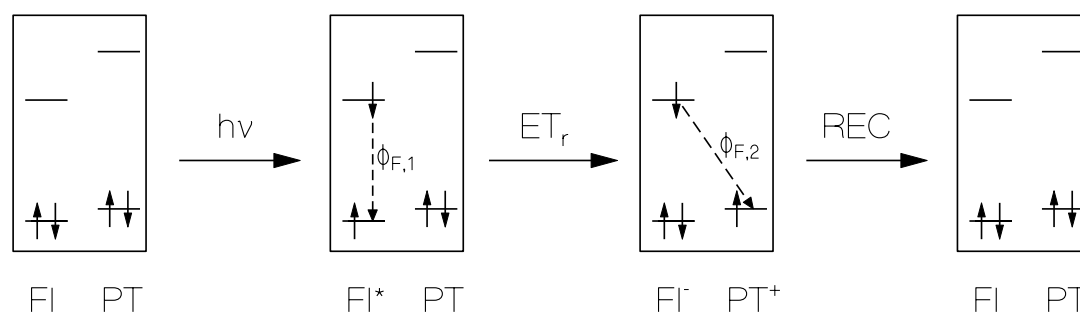
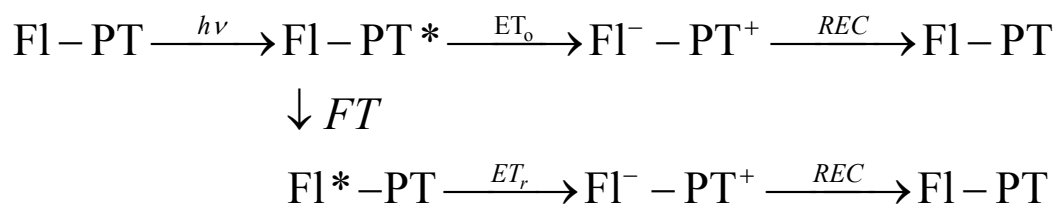


Figure 4.41: Illustration of photo-induced reductive electron transfer from ground-state phenyl-phenothiazine part to isoalloxazine part in the case of excitation of the S_1 state of the isoalloxazine moiety.

In the case of excitation at 311 nm both the phenothiazine moiety and the flavin moiety are excited. Approximately 60 % of the absorbed incident light is used to excite the phenothiazine part and about 40 % is used to excite the flavin part. Emission from the phenothiazine part together with weak emission from the flavin part (hidden in the stronger phenothiazine emission) is observed. Without phenothiazine–flavin excitation transfer a fluorescence quantum yield of $\phi_{F,PTFD}(311nm) = x_{HPPT}\phi_{F,HPPT} + x_{BrPF}\phi_{F,PTFD}(428nm) \approx 0.156$ is expected [$x_{HPPT} = 0.6$, $x_{BrPF} = 0.4$, $\phi_{F,HPPT} = 0.26$, $\phi_{F,PTFD}(428\text{ nm}) = 4.8 \times 10^{-4}$]. The experimental fluorescence quantum yield is only $\phi_{F,PTFD}(331\text{ nm}) = 0.0026$. This indicates efficient excitation transfer by oxidative electron transfer from the excited phenothiazine moiety to the flavin moiety and Förster-type energy transfer from the excited phenothiazine part to the ground-state flavin part. It turns out that the dominant excitation transfer is due to oxidative photo-induced electron-transfer from the excited phenothiazine part to the LUMO level of the unexcited flavin part. After electron transfer the system recovers dominantly by charge

recombination. The following excitation transfer and relaxation scheme is thought to be relevant:



(4.S7)

FT indicates the Förster-type energy transfer, *ET_o* indicates the photo-induced excited-state oxidative electron transfer from PT* to Fl, and *ET_r* denote the ground-state reductive electron transfer form PT to FL. *REC* indicates the charge recombination. The expected processes are illustrated in Figure 4.42.

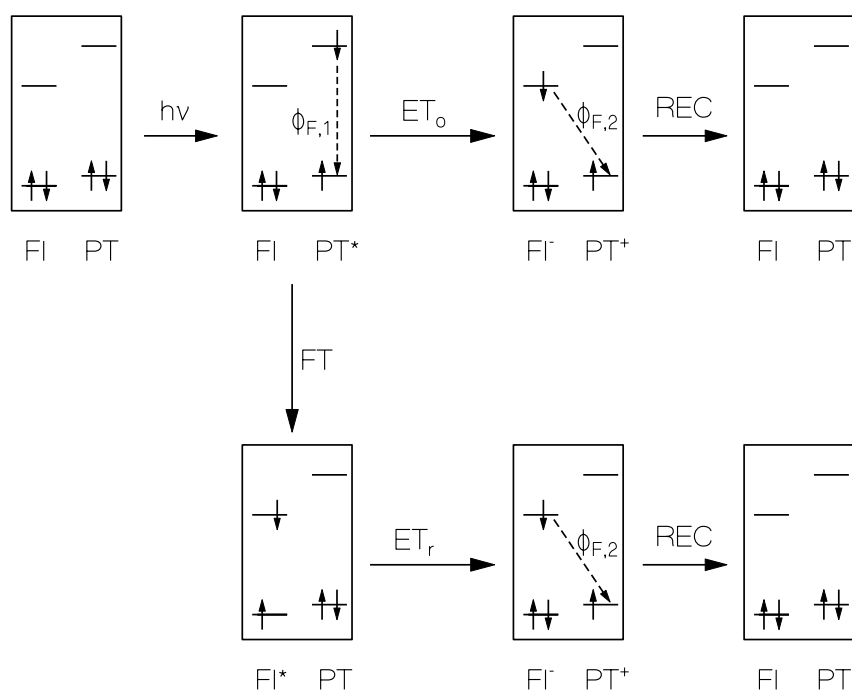


Figure 4.42: Illustration of photo-induced oxidative electron transfer from phenyl-phenothiazine part to isoalloxazine part and of Förster-type energy transfer in the case of excitation to the S_2 state of the phenyl-phenothiazine moiety.

The quantum efficiency of Förster-type energy transfer, ϕ_{FT} , between the HPPT moiety (energy donor) and the flavin moiety (energy acceptor) are calculated by use of Equations 2.17-20.

For the considered situation of energy transfer from the phenothiazine part to the flavin part in dyad PTFD the distance between donor and acceptor is $R_d \approx 1.18$ nm [She03], and the angles are estimated to be $\varphi_d \approx 12^\circ$, $\varphi_a \approx 83^\circ$, and $\varphi_{da} \approx 72^\circ$ (see structural formula of PTFD in Figure 3.1) giving $\kappa^2 \approx 0.0024$ (see Equation 2.19). The calculated critical Förster distance (see Equation 2.18) is $R_0(\text{Py-Fl, dichloromethane}) \approx 1.18$ nm. The energy transfer rate constant (see Equation 2.17) is calculated to be $k_{FT}(\text{PT-Fl, dichloromethane}) \approx 1.7 \times 10^8 \text{ s}^{-1}$ ($k_{F,0,d} = (5.86 \text{ ns})^{-1}$) by using the fluorescence lifetime of HPPT (donor) in the dichloromethane.

The rate of excitation transfer from the HPPT moiety to the flavin moiety, $k_{ex} = k_{FT} + k_{ET,o}$, is approximately given by $k_{ex} \approx \tau_F^{-1}(\text{PT}^*-\text{Fl}) - \tau_F^{-1}(\text{HPPT})$, where $\tau_F(\text{PT}^*-\text{Fl}) \approx \tau_{rad}(\text{HPPT}) \phi_F(\text{PTFD}, 311 \text{ nm})/x_{HPPT}$. Thereby $\tau_{rad}(\text{HPPT}) = \tau_F(\text{HPPT})/\phi_F(\text{HPPT})$ is the radiative lifetime of HPPT (section 4.3), $\phi_F(\text{HPPT})$ is the fluorescence quantum yield of HPPT, and x_{HPPT} is the fraction of excitation light absorbed by the HPPT part. The estimated value is $k_{ex} \approx 1 \times 10^{10} \text{ s}^{-1}$. It is found that $k_{ET,o} \gg k_{FT}$ (see obtained $k_{FT} \approx 1.7 \times 10^8 \text{ s}^{-1}$). Roughly it is $k_{ET,o} \approx k_{ex}$.

The time-resolved fluorescence studies (excitation at 400 nm in absorption region of flavin part) revealed an initial fast fluorescence decay ($\tau_{F,1} = 650$ to 700 fs) followed by a slow fluorescence decay ($\tau_{F,2} = 4.5$ to 5.5 ns). It is thought that during and after femtosecond pulse excitation reductive electron transfer (from phenothiazine HOMO donor to half-occupied flavin HOMO acceptor) takes place which quenches the locally excited state fluorescence. The fast fluorescence decay is determined by the rate of reductive electron transfer, i.e. $k_{ET,r} \approx \tau_{F,1}^{-1}$. The formed charge-transfer state has low oscillator strength (long radiative

lifetime $\tau_{\text{rad},2}$). The charge-separated state recombines on a nanosecond time-scale, and during this time weak fluorescence light is emitted. The charge recombination time is given by the slow fluorescence time constant, i.e. $\tau_{\text{rec}} = \tau_{\text{F},2}$.

A level scheme of the proposed dynamics in the case of flavin part excitation at 400 nm is shown in Figure 4.43. ν_L and σ_L denote the excitation laser frequency and the absorption cross-section at the laser frequency. k_{ex} denotes the rate of excitation transfer. $k_{\text{nr},1}$ and $k_{\text{rad},1}$ are the non-radiative and radiative relaxation rates of the initial locally excited flavin state, respectively, while $k_{\text{nr},2}$ and $k_{\text{rad},2}$ are the non-radiative and radiative relaxation rates of the final charge-transfer state. The proposed model is supported by a recent *ab-initio* quantum chemical study of the PTFD dyad at the level of coupled cluster response theory [Sad07].

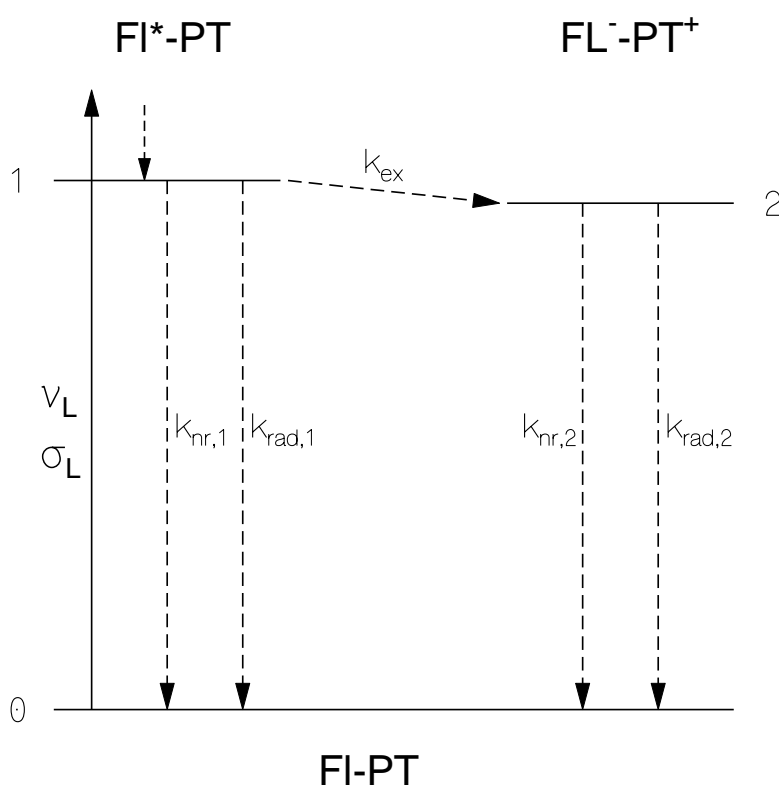


Figure 4.43: Level scheme of dyad local state excitation (flavin moiety), charge-transfer state formation (electron transfer from phenothiazine part to flavin part), and radiative and non-radiative relaxation.

4. Results and discussion: Phenothiazine-flavin dyad (PTFD)

The relaxation of the population number density, N_1 , of the locally excited state 1 (excitation at time $t = 0$) is given by

$$\frac{\partial N_1}{\partial t} = -(k_{rad,1} + k_{nr,1} + k_{ex})N_1 = -N_1 / \tau_{F,1}. \quad (4.16)$$

The build-up and decay of the population number density, N_2 , of the charge-transfer state 2 is given by

$$\frac{\partial N_2}{\partial t} = k_{ex}N_1 - (k_{nr,2} + k_{rad,2})N_2 = k_{ex}N_1 - N_2 / \tau_{F,2} \approx N_1 / \tau_{F,1} - N_2 / \tau_{F,2}. \quad (4.17)$$

The fluorescence signal, $S_F(t)$, is given by

$$S_F(t) = \kappa(k_{rad,1}N_1 + k_{rad,2}N_2), \quad (4.18)$$

where κ is a proportionality constant.

The solution of Equation 4.16 is

$$N_1(t) = N_{1,0} \exp(-t / \tau_{F,1}). \quad (4.19)$$

Insertion of Equation 4.19 into Equation 4.17 leads to an ordinary linear differential equation with the solution

$$N_2(t) = \frac{k_{ex}N_{1,0}\tau_{F,1}\tau_{F,2}}{\tau_{F,2} - \tau_{F,1}} \left[\exp\left(-\frac{t}{\tau_{F,2}}\right) - \exp\left(-\frac{t}{\tau_{F,1}}\right) \right]. \quad (4.20)$$

Insertion of Equations 4.19 and 4.20 into Equation 4.18 leads to

$$\begin{aligned} S_F(t) &= \kappa N_{1,0} \left[\left(\frac{1}{\tau_{rad,1}} - \frac{k_{ex}\tau_{F,1}\tau_{F,2}}{\tau_{rad,2}(\tau_{F,2} - \tau_{F,1})} \right) \exp\left(-\frac{t}{\tau_{F,1}}\right) + \frac{k_{ex}\tau_{F,1}\tau_{F,2}}{\tau_{rad,2}(\tau_{F,2} - \tau_{F,1})} \exp\left(-\frac{t}{\tau_{F,2}}\right) \right] \\ &\approx \frac{\kappa N_{1,0}}{\tau_{rad,1}} \left[\exp\left(-\frac{t}{\tau_{F,1}}\right) + \frac{\tau_{rad,1}}{\tau_{rad,2}} \exp\left(-\frac{t}{\tau_{F,2}}\right) \right] \end{aligned} \quad (4.21)$$

In the last approximation the relations $\tau_{F,1} \ll \tau_{F,2}$, $\tau_{rad,1} \ll \tau_{rad,2}$, and $k_{ex}\tau_{F,1} \approx 1$ have been used. The bi-exponential fluorescence of Equation 4.21 agrees with the experimental observations of Figure 4.39.

Photo-excitation of the PTFD dyad cause non-adiabatic (diabatic) electron transfer (section 2.7), since coupling between electron donor (phenothiazine) and electron acceptor (flavin) is

weak. This is seen from the dyad ground-state absorption spectra which show up as the sum of the constituent absorption spectra.

The studied PTFD photo-dynamics involves three Marcus-type electron transfers: the HOMO-PT \rightarrow HOMO-FI* reductive electron transfer (ET_r , called hole transfer in polymeric systems with band structure –valence band- description) in the case of FI excitation, the LUMO-PT* \rightarrow LUMO-FI oxidative electron transfer (ET_o , called electron transfer in polymeric systems with band structure –conduction band- description) in the case of PT excitation, and the LUMO-FL $^- \rightarrow$ HOMO-PT $^+$ charge recombination (REC). The Marcus-type potential energy parabola reaction coordinate diagrams for these three processes are illustrated in Figures 4.44-46. The available experimental data do not allow us to extract the Marcus theory parameters, V_0^2 , ΔG^0 , and λ of the occurring electron transfer processes. But the Marcus theory illustration gives a qualitative understanding of the dynamics. The ground-state reductive electron transfer rate is fast ($k_{ET,r}^{-1} \approx 700$ fs) indicating reasonable large coupling V_0^2 . The level position of the phenothiazine HOMO higher than the flavin HOMO leads to electron transfer in the normal Marcus region (Figure 4.44).

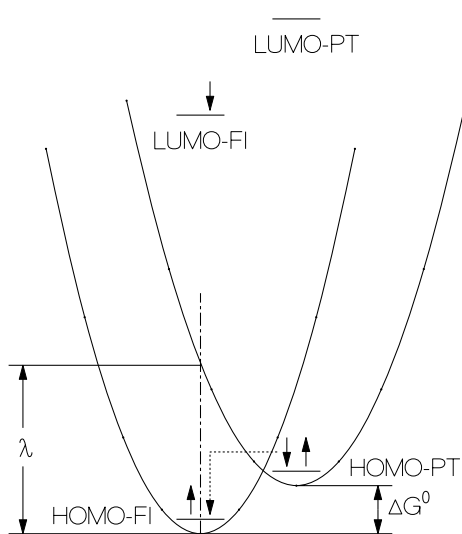


Figure 4.44: Potential energy Marcus-parabola reaction coordinate diagram for reactive electron transfer from HOMO-phenothiazine to HOMO flavin.

4. Results and discussion: Phenothiazine-flavin dyad (PTFD)

The excited-state oxidative electron transfer rate ($k_{\text{ET},o}^{-1} \approx 100$ ps) is slower than the transfer rate in the ground-state indicating smaller coupling V_0^2 and higher energy barrier, $\lambda - |\Delta G^0|$ in the normal Marcus region. The charge recombination rate ($k_{\text{REC}}^{-1} \approx 5.5$ ns) is the slowest electron transfer process in the PTFD dyad which may be attributed to the coupling constant and/or the energy barrier. The recombination process is expected to be in the inverted Marcus region (Figure 4.46). Dexter-type excitation transfer [Dex53, Spe96] (concerted two-electron transfer, combined reductive and oxidative electron transfer) is not expected to occur since for FI*PT (Fig 4.41) the oxidative electron transfer from LUMO-FI to LUMO-PT is energetically forbidden, and for FI PT* (Figure 4.42) the reductive electron transfer from HOMO-FI to HOMO-PT is energetically forbidden.

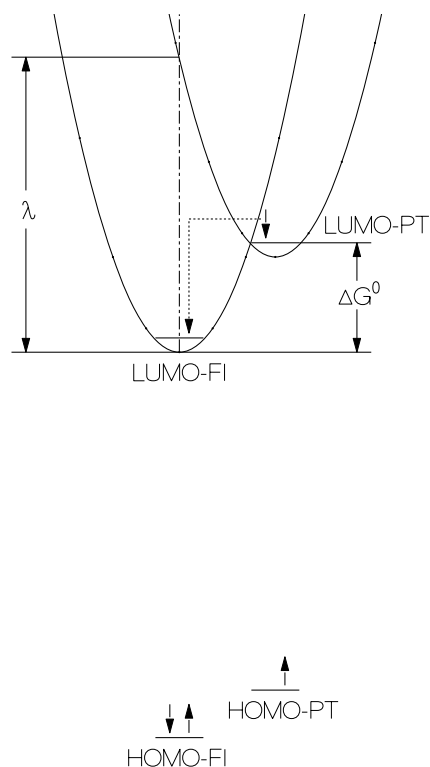


Figure 4.45: Potential energy Marcus-parabola reaction coordinate diagram for oxidative electron transfer from LUMO phenothiazine to LUMO flavin.

Table 4.5: Spectroscopic parameters of investigated PTFD dyad at room temperature

Dye	PTFD	PTFD	Comments
Solvent	dichloromethane	acetonitrile	
n_F	1.4271	1.3481	
n_A	1.4340	1.3528	
$\phi_F(428 \text{ nm})$	4.8×10^{-4}	4.9×10^{-4}	Figure 4.38
$\phi_F(311 \text{ nm})$	0.0026	0.0029	Figure 4.38
$P_F(428 \text{ nm})$	≈ 0.1	≈ 0.04	Figure 4.38
$P_F(311 \text{ nm})$	≈ 0.07	≈ 0.07	Figure 4.38
$\tau_{F,1} \text{ (fs)}$	700	650	Figure 4.39
$\tau_{F,2} \text{ (ns)}$	5.45	4.53	Figure 4.39
$\tau_{\text{rad},1} \text{ (ns)}$	≈ 19.5	≈ 19.5	[Drö03]
$\tau_{\text{rad},2} \text{ (}\mu\text{s)}$	12.2	9.9	Figure 4.38
$\phi_{F,1}$	$\approx 3.6 \times 10^{-5}$	$\approx 3.3 \times 10^{-5}$	Figure 4.38
$\phi_{F,2}$	4.44×10^{-4}	4.57×10^{-4}	$\phi_F(488 \text{ nm})-$ $\phi_{F,1}$
ϕ_D	1.6×10^{-5}	$< 4 \times 10^{-6}$	Figure 4.40
$k_{\text{ET},r} \text{ (s}^{-1}\text{)}$	1.4×10^{12}	1.5×10^{12}	$k_{\text{ET},r} \approx \tau_{F,1}^{-1}$
$k_{\text{ET},o} \text{ (s}^{-1}\text{)}$	1.0×10^{10}	9.2×10^9	
$\tau_{\text{REC}} \text{ (ns)}$	5.45	4.53	$\tau_{\text{REC}} = \tau_{F,2}$

4.6 Pyrene-flavin-phenothiazine triad

4.6.1 Results

The pyrene-flavin-phenothiazine triad, (abbreviated by PYFPT) is made up of the approximate constituents 1-methylpyrene (pyrene moiety, section 4.2), BrPF (isoalloxazine moiety, section 4.1), and HPPT (phenothiazine moiety, section 4.3). Its photodynamic has been studied in [Shi07c].

The absorption cross-section spectra of the investigated triad PYFPT in dichloromethane and acetonitrile are shown in Figure 4.47a and 4.47b, respectively. The absorption cross-section spectra of the approximate constituents, BrPF, HPPT (phenyl-phenothiazine moiety, 60 % of absorption strength compared to planar free molecule (section 4.3)), and 1-methylpyrene are included in Figure 4.47a. In Figure 4.47b the absorption cross-section spectra of BrPF, HPT, and 1-methylpyrene are included. Absorption cross-section spectra of HPPT in acetonitrile cannot be shown since HPPT is not available for measurement. The PYFPT absorption is roughly given by the sum of the absorptions of the constituents. This indicates that in the triad the isoalloxazine moiety, the pyrene moiety, and the phenothiazine moiety remain their electronic structure and transition dipole moments (separate chromophores, local excitations, weakly coupled system).

4. Results and discussion: Pyrene-flavin-phenothiazine triad (PYFPT)

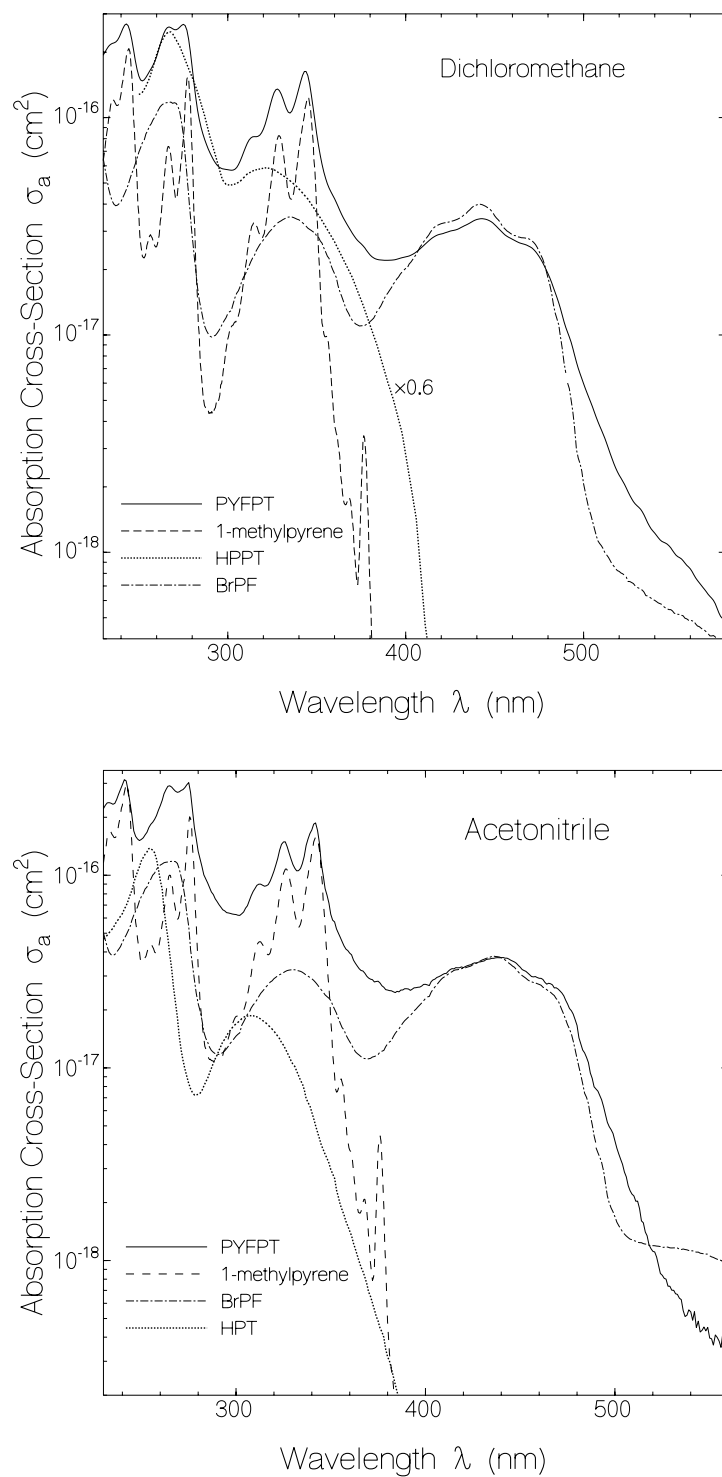


Figure 4.47: Absorption cross-section spectra of investigated dyes in dichloromethane (a) and acetonitrile (b). The applied dye concentrations in the measurements were: $C(\text{PYFPT, dichloromethane}) = 1.11 \times 10^{-4} \text{ mol dm}^{-3}$, $C(\text{PYFPT, acetonitrile}) = 7.11 \times 10^{-5} \text{ mol dm}^{-3}$, $C(\text{1-methylpyrene, dichloromethane}) = 5.2 \times 10^{-5} \text{ mol dm}^{-3}$, and $C(\text{1-methylpyrene, acetonitrile}) = 6 \times 10^{-5} \text{ mol dm}^{-3}$, $C(\text{BrPF, dichloromethane}) = 6.1 \times 10^{-4} \text{ mol dm}^{-3}$, $C(\text{BrPF, acetonitrile}) = 4.5 \times 10^{-4} \text{ mol dm}^{-3}$, $C(\text{HPT, acetonitrile}) = 4.46 \times 10^{-4} \text{ mol dm}^{-3}$. Spectra for 10-heptyl-3-phenyl-phenothiazine (HPPT) are taken from [Pro04,She03].

4. Results and discussion: Pyrene-flavin-phenothiazine triad (PYFPT)

The fluorescence quantum distributions, $E_F(\lambda)$, of triad PYFPT in dichloromethane and acetonitrile are shown in the top parts of Figures 4.48a and 4.48b, respectively. The corresponding fluorescence quantum yields, $\phi_F = \int E_F(\lambda)d\lambda$, are listed in Table 4.6. The fluorescence quantum yields depend on the excitation wavelength. In the case of excitation at 428 nm only the isoalloxazine (flavin) part of the triad is excited and the typical isoalloxazine fluorescence spectrum is observed. The fluorescence quantum yields are $\phi_F(\text{PYFPT, dichloromethane}) \approx 3 \times 10^{-4}$ and $\phi_F(\text{PYFPT, acetonitrile}) \approx 2.4 \times 10^{-4}$. The fluorescence of the isoalloxazine moiety is reduced approximately a factor of 500 compared to the BrPF fluorescence efficiency (section 4.1). This fluorescence reduction will be interpreted below (section 4.6.2) to be caused by reductive electron transfer (section 2.7) from the phenothiazine moiety to the isoalloxazine moiety (section 4.5).

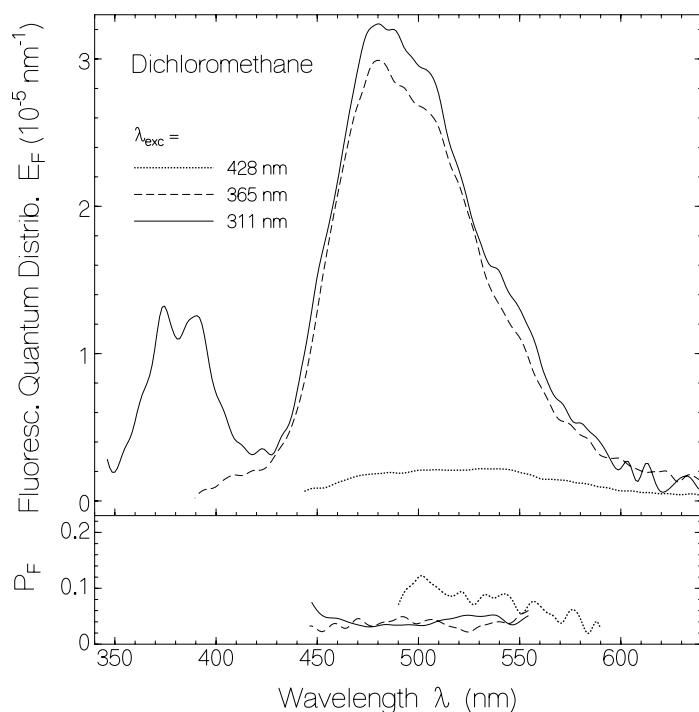


Figure 4.48a: Fluorescence quantum distributions (top part) and degrees of fluorescence polarization (lower part) of triad PYFPT in dichloromethane. Excitation wavelengths, λ_{exc} , are indicated in the figure. Applied dye concentrations are $C = 2 \times 10^{-5} \text{ mol dm}^{-3}$ in dichloromethane, and $4 \times 10^{-5} \text{ mol dm}^{-3}$ in acetonitrile.

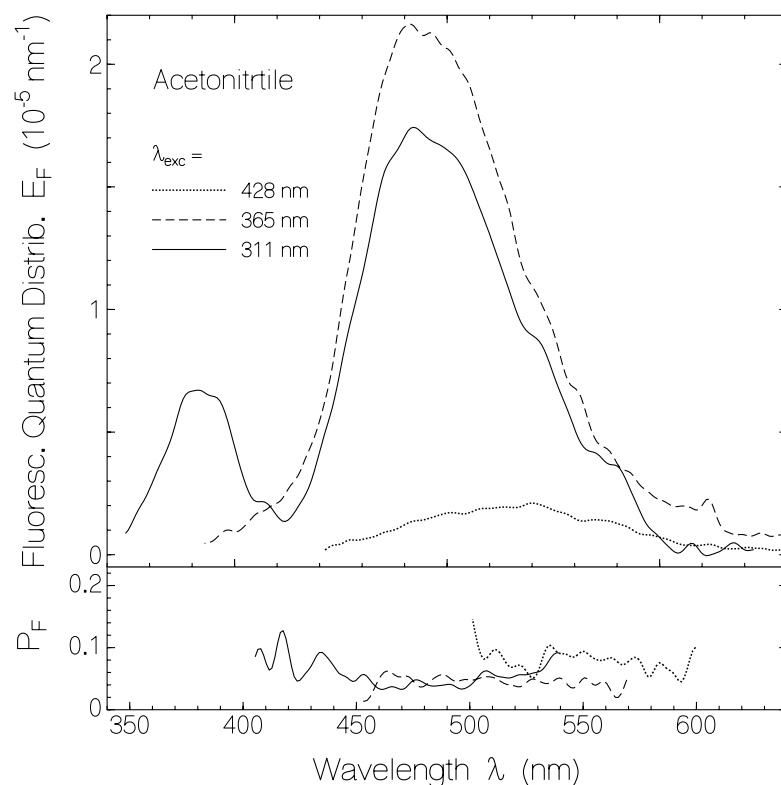


Figure 4.48b: Fluorescence quantum distributions (top part) and degrees of fluorescence polarization (lower part) of triad PYFPT in acetonitrile (b). Excitation wavelengths, λ_{exc} , are indicated in the figure. Applied dye concentrations are $C = 2 \times 10^{-5} \text{ mol dm}^{-3}$ in dichloromethane, and $4 \times 10^{-5} \text{ mol dm}^{-3}$ in acetonitrile.

In the case of excitation at 365 nm the light is dominantly absorbed by the HPPT moiety (approximately $\chi_{\text{PT}} \approx 0.58$) and the isoalloxazine moiety (approximately $\chi_{\text{FI}} \approx 0.365$, see Figure 4.47a). Only a small part ($\chi_{\text{PY}} \approx 0.055$) is absorbed by the pyrene moiety. The fluorescence quantum yields are $\phi_{\text{F}}(\text{PYFPT, dichloromethane}) \approx 0.0028$ and $\phi_{\text{F}}(\text{PYFPT, acetonitrile}) \approx 0.0022$. The fluorescence originates dominantly from the HPPT moiety. The fluorescence efficiency is reduced approximately a factor of 100 compared to the HPPT fluorescence efficiency (section 4.3). This fluorescence reduction will be interpreted below to be caused by oxidative electron transfer (section 2.7) from the phenothiazine moiety to the isoalloxazine moiety (section 4.5). In the case of excitation at 311 nm the light is absorbed by the HPPT moiety (approximately $\chi_{\text{PT}} \approx 0.54$), the 1-methylpyrene moiety (approximately $\chi_{\text{PY}} \approx 0.26$), and the isoalloxazine moiety (approximately $\chi_{\text{FI}} \approx 0.20$, see Figure 4.47a). The

4. Results and discussion: Pyrene-flavin-phenothiazine triad (PYFPT)

fluorescence quantum yields are $\phi_F(\text{PYFPT, dichloromethane}) \approx 0.0035$ and $\phi_F(\text{PYFPT, acetonitrile}) \approx 0.0019$. The fluorescence originates dominantly from the HPPT moiety. A fluorescence contribution from the 1-methylpyrene moiety is observed (structured emission in 350 to 420 nm range) with the quantum yields of $\phi_F(\text{pyrene moiety, dichloromethane}) \approx 5.5 \times 10^{-4}$ and $\phi_F(\text{pyrene moiety, acetonitrile}) \approx 2.9 \times 10^{-4}$. The corresponding fluorescence lifetimes are $\tau_F(\text{pyrene moiety, dichloromethane}) \approx 120$ ps and $\tau_F(\text{pyrene moiety, acetonitrile}) \approx 95$ ps using the relation $\tau_F = \phi_F \tau_{\text{rad}}$ (Equation 2.13) with $\tau_{\text{rad}}(\text{1-methylpyrene in dichloromethane}) \approx 221$ ns, and $\tau_{\text{rad}}(\text{1-methylpyrene in acetonitrile}) \approx 327$ ns (section 4.2). The fluorescence efficiency of 1-methylpyrene in the triad is reduced approximately a factor of 200 compared to the fluorescence efficiency of 1-methylpyrene in dichloromethane or acetonitrile (section 4.2). This fluorescence reduction will be interpreted below to be caused by oxidative electron transfer from the pyrene moiety to the flavin moiety (section 4.4), and Förster-type energy transfer to the phenyl-phenothiazine moiety.

The fluorescence polarisation spectra, $P_F(\lambda)$, of PYFPT are plotted in the lower parts Figures 4.48a and 4.48b, respectively, for the solvents dichloromethane and acetonitrile. The degree of fluorescence polarisation depends somewhat on the excitation wavelength. In the case of excitation at 428 nm the degree of fluorescence polarisation is low in the range of 0.08. This small value indicates the PYFPT fluorescence spectra are dominated by emission from a slowly relaxing excited state (formed charge-transfer state, see below) when the isoalloxazine moiety is excited. In the case of excitation at 365 nm the degree of fluorescence polarisation is small despite a low fluorescence lifetime (≈ 170 ps, see section 4.3). It is thought that the S_1 -state and the S_2 -state of the HPPT moiety are excited, while only the S_1 -state is emitting, and the orientation of the transition dipole moments of the S_1 -state and the S_2 -state is different. In the case of 311 nm excitation the degree of fluorescence polarisation is thought to be small because of the small degrees of fluorescence polarization of the phenyl-

phenothiazine moiety, of the flavin moiety and because of excitation transfer from the pyrene moiety to the phenothiazine part and the flavin part.

Temporal fluorescence traces of the triad PYFPT are shown in Figure 4.49. The samples are excited at $\lambda_{SH} = 400$ nm where only the flavin part of the triad is absorbing. The femtosecond fluorescence up-conversion measurements (part a for dichloromethane, and part c for acetonitrile) reveal the presence of a sub-picosecond component ($\tau_{F,1} \approx 600$ fs), while the real-time fluorescence measurements with micro-channel-plate photomultiplier and high-speed digital oscilloscope reveal a nanosecond component (Figures 4.49b and 4.49d, $\tau_{F,2} \approx 4$ ns). The obtained fluorescence lifetimes, $\tau_{F,1}$ and $\tau_{F,2}$, are listed in Figure 4.49 and Table 4.6. The fast component is thought to originate from the isoalloxazine part with radiative lifetime of $\tau_{rad,1} \approx 19.5$ ns (section 4.1). The fluorescence quantum yield of this contribution is $\phi_{F,1} \approx \tau_{F,1}/\tau_{rad,1} (\approx 3.2 \times 10^{-5})$. The slow component is thought to originate from the formed charge-transfer state (see below). Its fluorescence quantum yield is given by $\phi_{F,2} \approx \phi_F - \phi_{F,1} (\approx 2.5 \times 10^{-4})$. The radiative lifetime of the charge-transfer state is $\tau_{rad,2} \approx \tau_{F,2}/\phi_{F,2} (\approx 17 \mu s)$. The parameters are collected in Table 4.6.

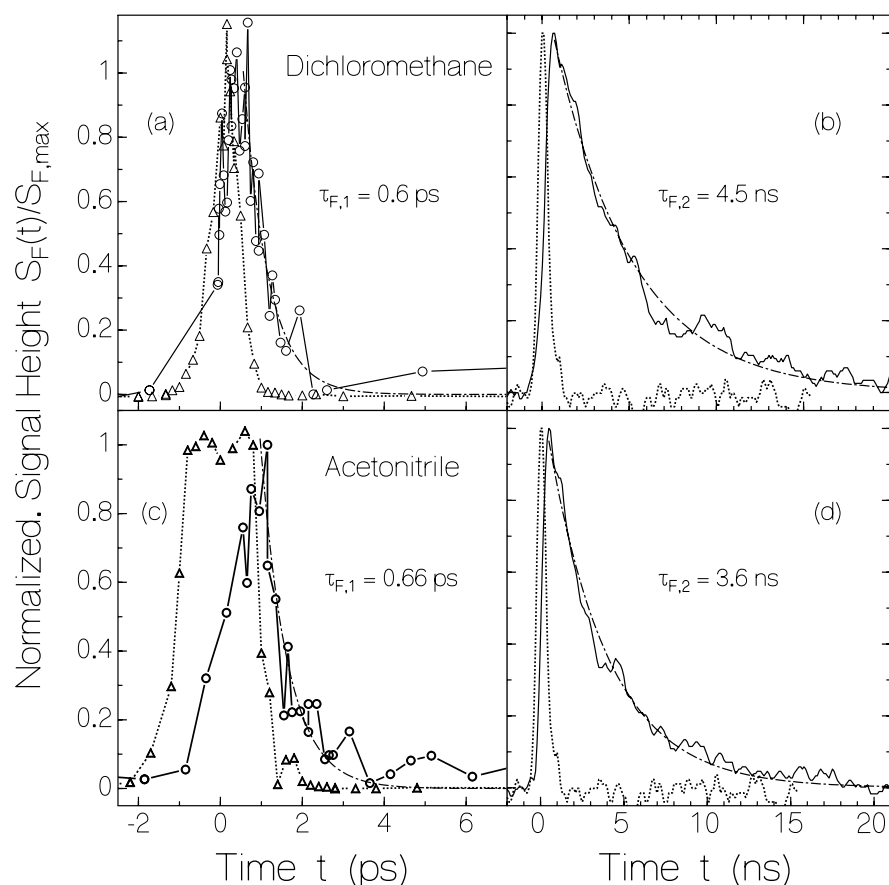


Figure 4.49: Temporal fluorescence traces of triad PYFPT. Line-connected circles: experimental data. Dash-dotted lines: single-exponential fits. Dot-connected triangles: response functions.

- (a) Solvent dichloromethane (up-converted fluorescence signal).
- (b) Solvent dichloromethane (oscilloscope trace).
- (c) Solvent acetonitrile (up-converted fluorescence signal).
- (d) Solvent acetonitrile (oscilloscope trace).

Absorption changes due to long-time blue-light excitation of triad PYFPT in dichloromethane (part a, excitation in range of 400 nm - 440 nm, excitation intensity $I_{\text{exc}} = 0.01 \text{ W cm}^{-2}$), and acetonitrile (part b, excitation at 428 nm, $I_{\text{exc}} = 0.0356 \text{ W cm}^{-2}$) are shown in Figure 4.50. Absorption coefficient spectra are depicted before exposure and after long-time of light exposure. Practically no absorption change is observed for the applied excitation intensities and exposure times. These findings indicate a high photo-stability.

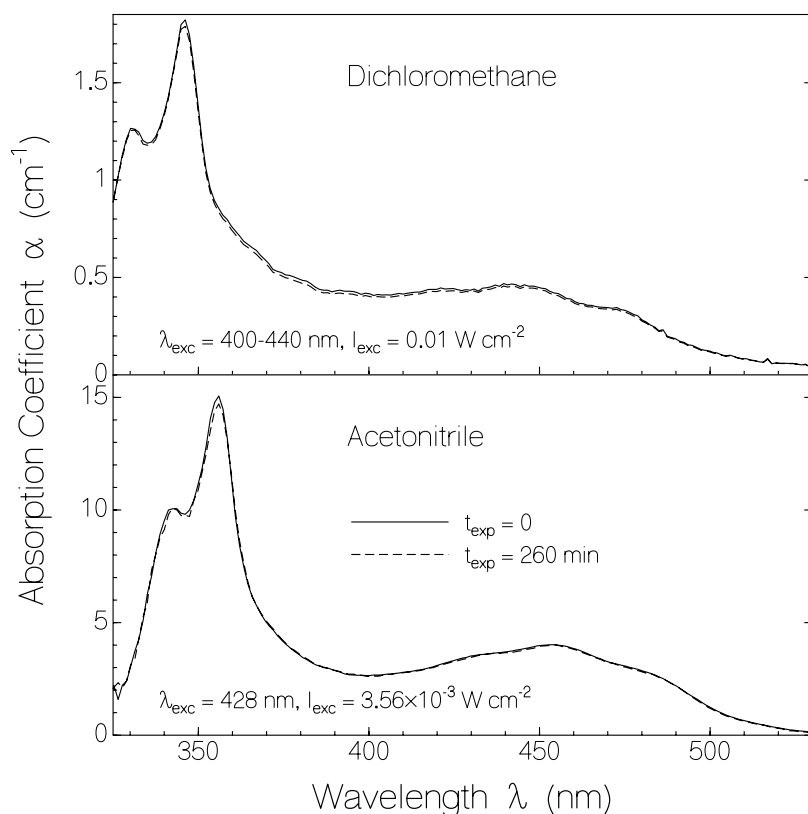


Figure 4.50: Absorption coefficient spectra of triad PYFPT before and after light exposure. Excitation wavelengths, λ_{exc} , excitation intensities, I_{exc} , and exposure times, t_{exp} , are listed in the figure.

(a) Solvent dichloromethane. Sample length $\ell = 5$ mm.

(b) Solvent acetonitrile. Sample length $\ell = 1.5$ mm.

4.6.2 Discussion

The fluorescence efficiency in the triad PYFPT is strongly reduced compared to the constituents, BrPF, 1-methylpyrene, and HPPT.

The photo-dynamics of the pyrene-flavin-phenothiazine triad is complex because it depends on which moiety of the triad is locally excited and on the interaction channels of this moiety with the other molecule constituents. The relaxation channels include besides normal radiative and non-radiative (internal conversion and intersystem-crossing) decay i) Förster-type energy transfer [För51] between pyrene and flavin or phenothiazine, as well as between phenothiazine and flavin, and ii) electron-transfer [Mar85] between phenothiazine-pyrene-flavin combinations. The electron transfer studies on dyads of pyrene-flavin (section 4.4),

4. Results and discussion: Pyrene-flavin-phenothiazine triad (PYFPT)

phenothiazine-flavin (section 4.5), and phenothiazine-pyrene [She03, Dau01] indicate an energetic ordering of the HOMO (highest occupied molecular orbital) and LUMO (lowest unoccupied molecular orbital) levels according to $E_{\text{LUMO}}(\text{phenothiazine}) > E_{\text{LUMO}}(\text{pyrene}) > E_{\text{LUMO}}(\text{flavin})$ and $E_{\text{HOMO}}(\text{phenothiazine}) > E_{\text{HOMO}}(\text{pyrene}) > E_{\text{HOMO}}(\text{flavin})$. This ordering allows ground-state reductive electron transfer from phenothiazine to unoccupied ground-state pyrene and flavin, and from pyrene to unoccupied ground-state flavin (HOMO-HOMO transfer). It also allows excited state oxidative electron transfer from phenothiazine to pyrene and flavin, and from pyrene to flavin (LUMO-LUMO transfer). In photo-induced reductive electron transfer the photo-excited molecule gets reduced while in photo-induced oxidative electron transfer the photo-excited molecule gets oxidized. In the charge recombination, neutralizing electron transfer from the anionic LUMO state of the electron donor moiety to the cationic HOMO state of the electron acceptor moiety takes place. Dexter-type excitation transfer [Dex53, Val02, Spe96] (concerted two-electron transfer, combined reductive and oxidative electron transfer) is not expected to occur since for the interaction of the excited moiety with the unexcited moieties either the reductive electron transfer or the oxidative electron transfer is energetically unfavourable (see Figures 4.51-53).

In the case of triad PYFPT irradiation at $\lambda_{\text{exc}} = 428$ nm the flavin part is involved. The photon absorption excites the isoalloxazine (flavin) part Fl. Reductive electron transfer from PT to Fl forms the intra-molecular charge-transfer complex PyFl^+PT^- . This process occurs with a time constant of $k_{\text{ET,r}}^{-1} \approx \tau_{\text{F},1} \approx 600$ fs. The charge-transfer complex recovers to the original ground-state dominantly by charge recombination (REC). During the charge-transfer-complex lifetime fluorescence emission occurs ($\tau_{\text{REC}} \approx \tau_{\text{F},2} \approx 4.5$ ns). Its efficiency is weak because of the long radiative lifetime ($\tau_{\text{rad}} \approx 17.1$ μs , low oscillator strength) of the charge-transfer complex. The process is illustrated in Figure 4.51. The dynamics is similar to the case of dyad PTFD excitation (phenothiazine-flavin-dyad) (section 4.5). Reductive electron

4. Results and discussion: Pyrene-flavin-phenothiazine triad (PYFPT)

transfer from pyrene to flavin is thought to be less important, since a lower rate of Py^+Fl^- formation was found for the pyrene-flavin dyad PFD than of Fl^-PT^+ formation for the phenothiazine-flavin dyad PTFD (section 4.4 and section 4.5).

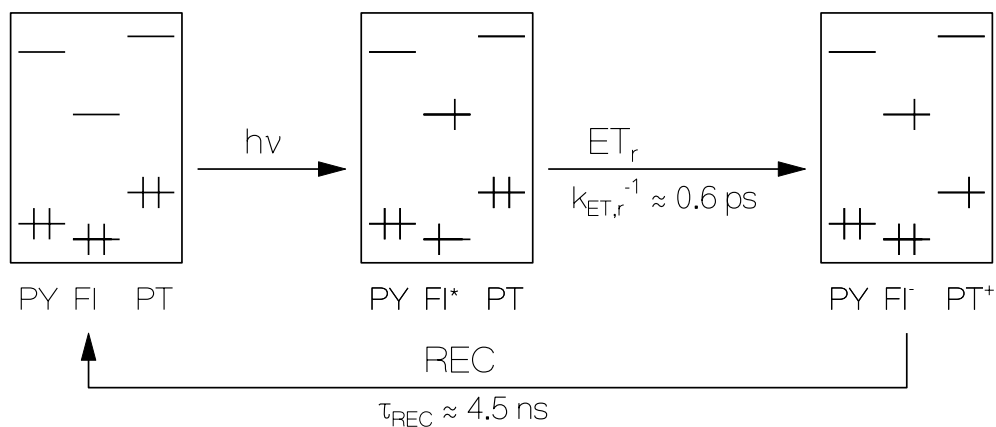


Figure 4.51: Illustrations of excitation and recovery dynamics of triad PYFPT in the case of excitation of the flavin part. Rates apply to solvent dichloromethane.

In the case of excitation at 365 nm the phenyl-phenothiazine moiety and the flavin moiety are excited while the excitation of the 1-methylpyrene moiety is small. From the absorption cross-sections in Figure 4.47a we expected the following excitation mole-fraction for isoalloxazine, phenothiazine, and pyrene: $x_{\text{Fl}} \approx 0.365$, $x_{\text{PT}} \approx 0.58$, and $x_{\text{PY}} \approx 0.055$. The fluorescence is dominated by emission of the locally excited phenyl-phenothiazine moiety. It is quenched by oxidative electron transfer from the phenothiazine part PT^* to the flavin part Fl and Förster-type energy transfer from PT^* to Fl. The relaxation dynamics is illustrated in Figure 4.52. The efficiency of Förster-type energy transfer was found in section 4.5 to be small (rate $k_{\text{FT}} \approx 1.7 \times 10^8 \text{ s}^{-1}$). The rate of oxidative electron transfer is estimated to be $k_{\text{ET},o} \approx k_{\text{ex}} \approx \tau_{\text{F}}^{-1}(365\text{nm}) = 1/[\phi_{\text{F}}(365\text{nm})\tau_{\text{rad,eff}}]$ with the effective radiative lifetime given by $\tau_{\text{rad,eff}}^{-1} = x_{\text{Fl}}\tau_{\text{rad,Fl}}^{-1} + x_{\text{PT}}\tau_{\text{rad,PT}}^{-1} + x_{\text{PY}}\tau_{\text{rad,PY}}^{-1}$. Using the above estimated mole-fractions and the radiative lifetime for flavin, $\tau_{\text{rad,Fl}} \approx 19.5 \text{ ns}$ (Table 4.1), $\tau_{\text{rad,PT}} \approx 22.5 \text{ ns}$ (Table 4.3) for phenyl-phenothiazine in dichloromethane, and $\tau_{\text{rad,PY}} \approx 221 \text{ ns}$ (Table 4.2) for 1-methylpyrene

4. Results and discussion: Pyrene-flavin-phenothiazine triad (PYFPT)

in dichloromethane, we estimate $\tau_{\text{rad,eff}} \approx 22.3$ ns and $k_{\text{ET,o}} \approx 2.0 \times 10^{10} \text{ s}^{-1}$. The higher rate of oxidative electron transfer observed here compared to section 4.5 may be due to two electron transfer paths, one directly from PT* to FI⁻ and one from PT* via PY⁻ to FI⁻ (both processes of similar effectiveness). The formed PYFI⁻PT⁺ charge transfer complex is the same as in the case of 428 nm excitation (Figure 4.51), and it recovers as described above.

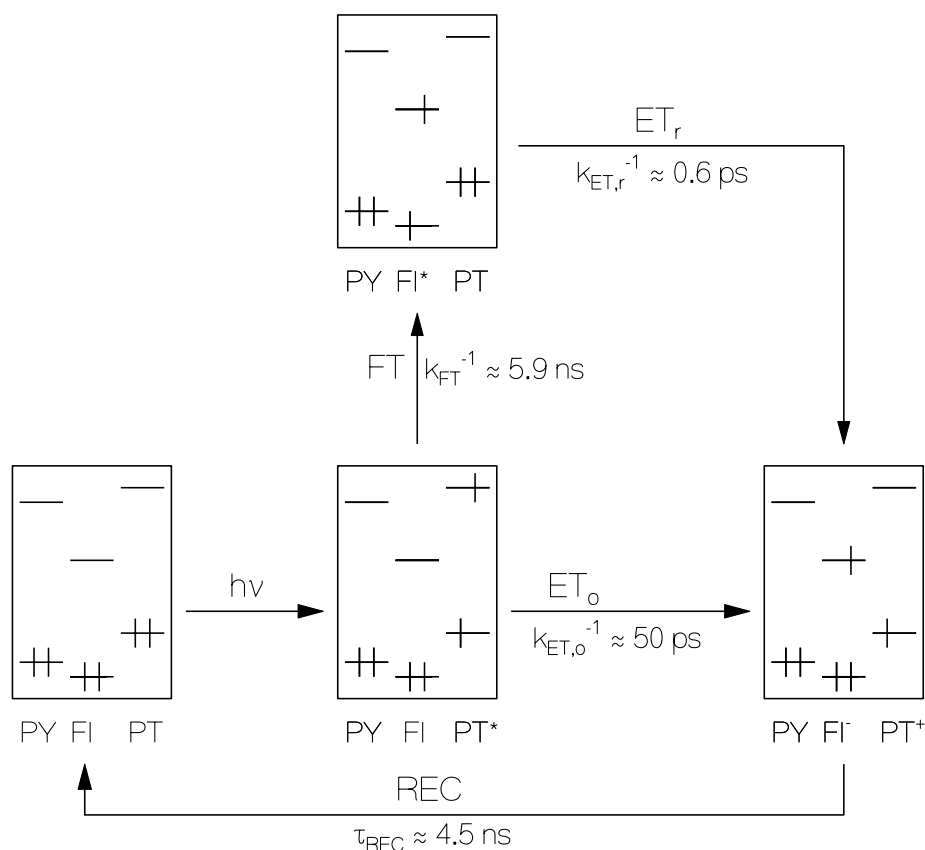


Figure 4.52: Illustrations of excitation and recovery dynamics of triad PYFPT in the case of excitation of the phenothiazine part. Rates apply to solvent dichloromethane.

In the case of excitation at 311 nm the flavin moiety, the phenothiazine moiety, and the pyrene moiety are excited with the mole-fractions: $x_{\text{FI}} \approx 0.20$, $x_{\text{PT}} \approx 0.55$, and $x_{\text{PY}} \approx 0.25$ (see Figure 4.47a). The excited flavin part is expected to behave as shown in Figure 4.51 (fast relaxation from S_n -state to S_1 -state, then dynamics the same as in Figure 4.51). The excited

4. Results and discussion: Pyrene-flavin-phenothiazine triad (PYFPT)

phenothiazine part is expected to behave as shown in Figure 4.52. The fluorescence lifetime of the pyrene part is estimated from Figure 4.48a and 4.48b to be approximately 100 ps. This agrees with the pyrene part fluorescence quenching of the dyad PFD by oxidative electron transfer from pyrene to flavin (Section 4.4.2 Figure 4.36). Therefore we think that this transfer is the dominant fluorescence quenching process for the pyrene moiety in the triad. The deactivation scheme for the locally excited pyrene part is shown in Fig 4.53. The Förster-type energy transfer processes, $PY^*FIPT \rightarrow PYFI^*PT$ and $PY^*FIPT \rightarrow PYFIPT^*$, with subsequent electron transfers, $PYFI^*PT \rightarrow PYFI^+PT^+$ (see Figure 4.52) and $PYFIPT^* \rightarrow PYFI^+PT^+$ (see Figure 4.52), are included. The allowed reductive electron-transfer from the phenothiazine part to the pyrene part is thought to be slower than the oxidative electron transfer from pyrene to flavin since the later rate known from the PFD dyad agrees with the here observed rate for the triad.

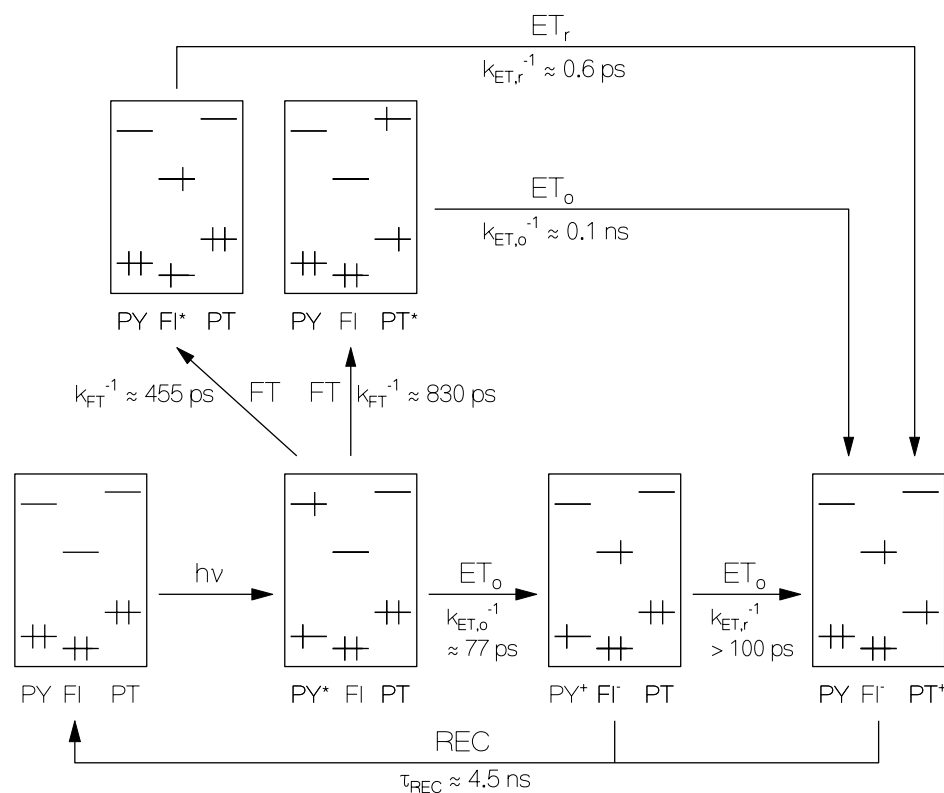


Figure 4.53: Illustrations of excitation and recovery dynamics of triad PYFPT in the case of excitation of the pyrene part. Rates apply to solvent dichloromethane.

4. Results and discussion: Pyrene-flavin-phenothiazine triad (PYFPT)

The relaxation of the PYFPT^+ charge transfer complex by dominant charge recombination is the same as in the case of 428 nm (Figure 4.51) or 365 nm excitation (Figure 4.52).

The photo-degradation of triad PYFPT was studied in Figure 4.50. No absorption decrease was observed with the applied experimental condition. For the experimental data upper limits of the quantum yield of photo-degradation were estimated using (Equations 3.2-3.4). These upper limits are listed in Table 4.6. For both the triad PYFPT in dichloromethane and in acetonitrile practically no change in the absorption coefficient spectra is observed for the applied excitation intensities and exposure times displayed in Figure 4.50. Taking experimental inaccuracy into account, one estimates an upper limit for the quantum yields of photo-degradation of $\phi_D < 1 \times 10^{-5}$ for both case.

Table 4.6: Spectroscopic parameters of investigated PYFPT triad at room temperature

Dye Solvent	PYFPT CH_2Cl_2	PYFPT CH_3CN	Comments
$\phi_F(428 \text{ nm})$	3×10^{-4}	2.4×10^{-4}	Figures 4.48a and 4.48b
$\phi_F(365 \text{ nm})$	0.0028	0.0022	Figures 4.48a and 4.48b
$\phi_F(311 \text{ nm})$	0.0036	0.0019	Figures 4.48a and 4.48b
$\tau_{F,1}$ (ps)	0.60	0.66	Figure 4.49
$\tau_{F,2}$ (ns)	4.5	3.6	$\tau_{F,2} = \tau_{\text{REC}}$
$\tau_{\text{rad},1}$ (ns)	≈ 19.5	≈ 19.5	of flavin [Drö03]
$\phi_{F,1}$	$\approx 3.1 \times 10^{-5}$	$\approx 3.4 \times 10^{-5}$	$\phi_{F,1} = \tau_{F,1} / \tau_{\text{rad},1}$
$\phi_{F,2}$	2.7×10^{-4}	2.1×10^{-4}	$\phi_{F,2} = \phi_F(428 \text{ nm}) - \phi_{F,1}$
$\tau_{\text{rad},2}$ (μs)	16.7	17.1	$\tau_{\text{rad},2} = \tau_{F,2} / \phi_{F,2}$
ϕ_D	$< 1 \times 10^{-5}$	$< 1 \times 10^{-5}$	Figure 4.50, Equations 3.2-4

5. Comparative discussion

The pyrene-flavin dyad (PFD) [Shi07a], the phenothiazine-flavin dyad (PTFD) [Shi07b], and the pyrene-flavin-phenothiazine triad (PYFPT) [Shi07c] and their constituents have been characterized by absorption and emission spectroscopy.

The absorption spectrum of PFD dyad resembles the superposition of the absorption of isoalloxazine (flavin) and 1-methylpyrene, indicating that both components retain their electronic structures and transition dipoles (Figure 4.29). Excitation of the long-wavelength absorbing isoalloxazine part led to reductive electron-transfer from the pyrene ground-state moiety to the isoalloxazine moiety (with time constant of ca 5 to 28 ps) followed by charge recombination (with time constant of ca. 70 ps to 150 ps) (Figure 4.54). Short-wavelength irradiation of PFD led to the excitation of both the isoalloxazine and the pyrene chromophore and caused –besides the relaxation dynamics of directly excited isoalloxazine part- the fluorescence quenching of the pyrene part by electron-transfer and Förster-type energy transfer from excited pyrene to isoalloxazine (Figure 4.55).

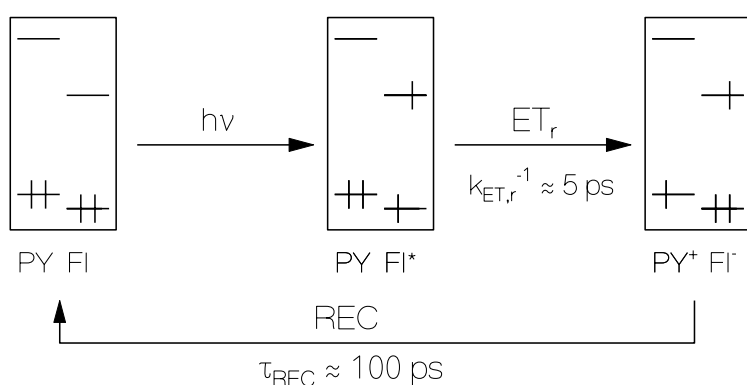


Figure 4.54: Illustrations of excitation and recovery dynamics of dyad PFD in the case of excitation of the flavin part. Rates apply to solvent dichloromethane. ET_r: reductive electron transfer. ET_o: oxidative electron transfer. REC: charge recombination (charge-transfer state relaxation).

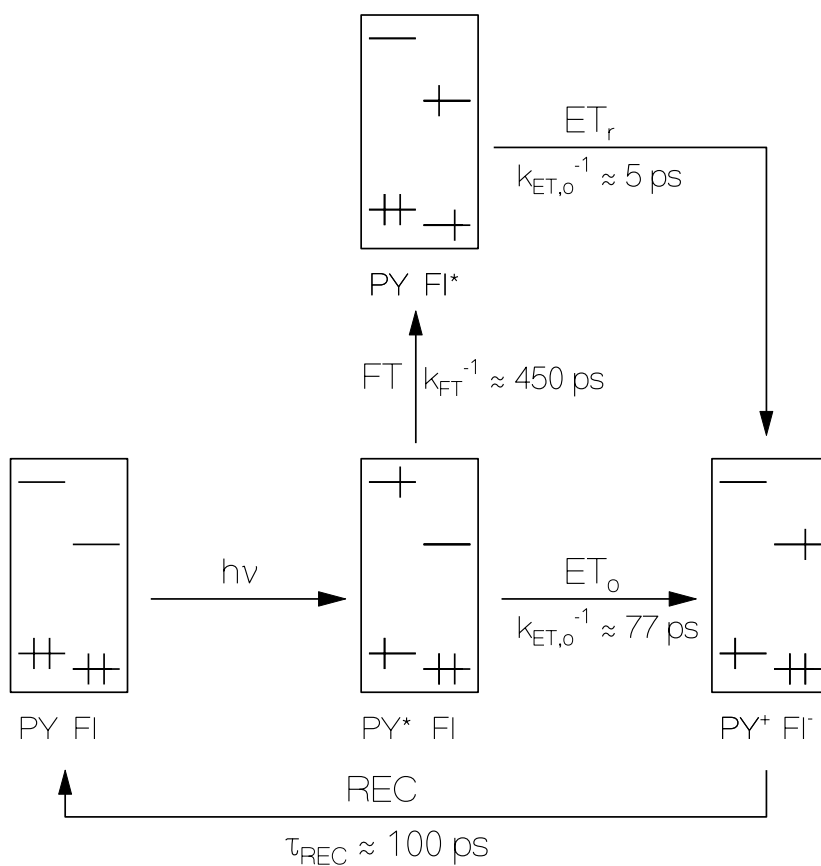


Figure 4.55: Illustrations of excitation and recovery dynamics of dyad PFD in the case of excitation of a) the flavin part, and b) the pyrene part. Rates apply to solvent dichloromethane. Parameters are taken from section 4.4. ET_r : reductive electron transfer. ET_o : oxidative electron transfer. REC: charge recombination (charge-transfer state relaxation). FT: Förster-type energy transfer.

The photo-stability of the PFD was measured by intense continuous photo-excitation of the S_0 - S_1 absorption band of the isoalloxazine part. Besides photo-degradation of the isoalloxazine part, the deposited energy also caused photo-degradation of the pyrene subunit. The quantum yield of photo-degradation has been obtained by analysis of the temporal absorption changes ($\phi_{D,0} \approx 10^{-4}$)

Also for the PTFD dyad the absorption identity of the isoalloxazine part and of the heptyl-phenyl-phenothiazine part remained in the dyad (Figure 4.37). Photo-excitation of the flavin moiety causes fluorescence quenching by ground-state reductive electron transfer from phenyl-phenothiazine to isoalloxazine (with time constant of ca. 700 fs) followed by charge recombination (with time constant of ca. 5 ns) (Figure 4.56). Photo-excitation of the phenothiazine moiety causes i) moderate Förster-type energy transfer followed by ground-state phenothiazine electron transfer and recombination, and ii) excited-state oxidative electron transfer from phenothiazine to isoalloxazine with successive recombination (Figure 4.57). The quantum yield of photo-degradation has been obtained by analysis of the temporal absorption changes ($\phi_{D,0} \approx 10^{-5} - 10^{-6}$). The photo-stability was found to be solvent dependent with higher stability in acetonitrile than in dichloromethane.

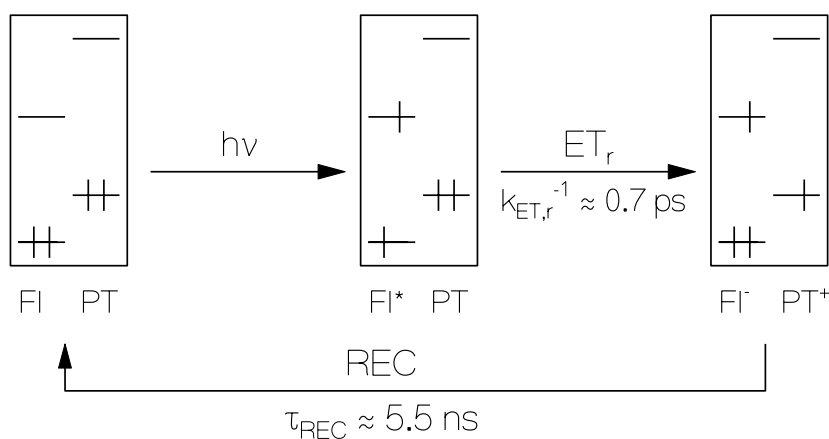


Figure 4.56: Illustrations of excitation and recovery dynamics of dyad PTFD in the case of excitation of the flavin part. Rates apply to solvent dichloromethane.

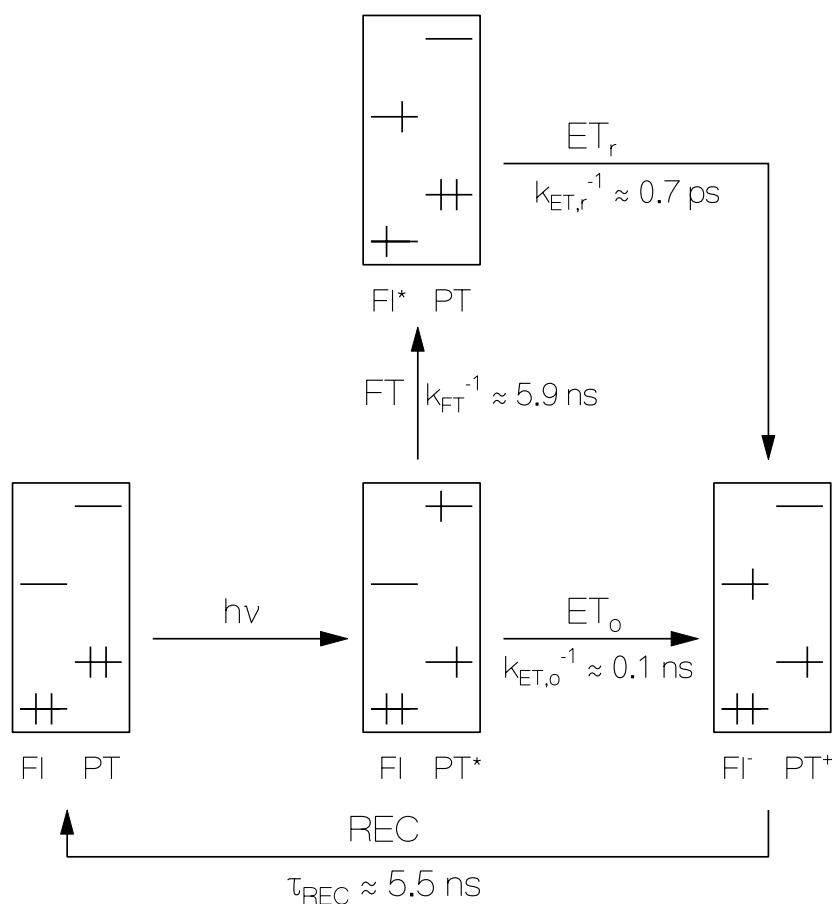


Figure 4.57: Illustrations of excitation and recovery dynamics of dyad PTFD in the case of excitation of the phenothiazine part. Rates apply to solvent dichloromethane.

The PYFPT triad absorption spectrum resembles the superposition of the absorption of the isoalloxazine moiety, the 1-methyl-pyrene moiety, and the phenyl-phenothiazine moiety (Fig 4.47). Excitation to the long-wavelength absorbing isoalloxazine part led to reductive electron-transfer dominantly from the ground-state phenothiazine moiety to the isoalloxazine moiety showing up in severe fluorescence quenching (Figure 4.51). The rate of charge-transfer state formation was resolved by locally excited state fluorescence measurement (≈ 0.6 ps). The charge-transfer state relaxation (charge recombination) was determined by charge-transfer state fluorescence measurement (≈ 4 ns).

Excitation to the short-wavelength region of combined isoalloxazine, phenothiazine, and pyrene absorption added to the relaxation dynamics of directly excited flavin i) the relaxation dynamics of locally excited phenothiazine (Figure 4.52) which was found to be dominated by oxidative electron transfer from the phenothiazine to flavin, both direct and via electron transfer to the pyrene part, and ii) the relaxation dynamics of the locally excited pyrene (Figure 4.53) which was found to be dominated by oxidative electron transfer from pyrene to flavin. Förster-type energy transfer between excited phenyl-phenothiazine and ground-state isoalloxazine and between 1-methylpyrene and ground-state phenothiazine and isoalloxazine is occurring but is less efficient than the electron-transfer processes.

For triad PYFPT in the case of flavin part excitation the reductive electron transfer from phenothiazine moiety to flavin part (see Figure 4.51) is similar to the case of dyad PTFD excitation (Figure 4.56). Reductive electron transfer from pyrene to flavin is thought to be less important, since a lower rate of Py^+Fl^- formation was found for the pyrene-flavin dyad PFD (Figure 4.54) than of Fl^+PT^- formation for the phenothiazine-flavin dyad PTFD (Figure 4.56).

In the case of phenothiazine part excitation of the triad PYFPT the rate of oxidative electron transfer from excited phenothiazine moiety to flavin part (see Figure 4.52) is higher than in the case of dyad PTFD excitation (see Figure 4.57). The observed higher rate may be due to two electron transfer paths, one directly from PT^* to Fl^- and one from PT^* via PY^- to Fl^- (both processes of similar effectiveness).

In the case of pyrene part excitation of the triad PYFPT (see Figure 4.53) the rate of oxidative electron transfer and rate of the Förster-type energy transfer from excited pyrene moiety to the flavin part are similar to the case of dyad PFD excitation (Figure 4.55)

A high photo-stability of the triad PYFPT with quantum yield of photo-degradation, $\phi_D < 1 \times 10^{-5}$, was determined. The high photo-stability is likely due to the short excited state life time of triad.

The photo-dynamics in the pyrene-flavin dyad, the phenothiazine-flavin dyad, and the pyrene-flavin-phenothiazine triad are speeded up compared to their building blocks (flavin, pyrene, and phenothiazine) because of mutual interaction (energy transfer and charge transfer) between their constituents. The optical absorption and emission spectra of the studied dyads and the triad are overlapping. Therefore Förster-type energy transfer between their moieties occurs. They mimic the antenna effect or light harvesting effect observed and applied in biological photosynthetic reaction centres [Mat96, Häd99, She02], and in some bi-chromophore biological photoreceptors like photolyases and cryptochrome [Mat96, Häd99, She02, She03, Pro04].

The photoionization potential (reduction state, HOMO-energy levels) and the electron affinity (oxidative state, LUMO-energy levels) of the studied dyads and the triad are so arranged ($E_{\text{HOMO}}(\text{phenothiazine}) > E_{\text{HOMO}}(\text{pyrene}) > E_{\text{HOMO}}(\text{flavin})$ and $E_{\text{LUMO}}(\text{phenothiazine}) > E_{\text{LUMO}}(\text{pyrene}) > E_{\text{LUMO}}(\text{flavin})$) that the fluorescence (even from lowest lying LUMO-state) is quenched by efficient electron transfer. The occurring electron transfer mimics the photo induced charge separation in photosynthetic reaction centres [Mat96, Häd99, She02] and electron transfer processes in flavin-based blue-light photoreceptors [Bat03, Bri05, Häd06].

Electron transfer plays an important role in the development of organic photovoltaic devices and generally in molecular electronics. The performed fundamental spectroscopy studies on the pyrene-phenothiazine-flavin dyads and triad may be of interest in the active field of molecular electronics.

6. Conclusions

In this thesis a pyrene-flavin dyad (PFD), a phenothiazine-flavin dyad (PTFD), a pyrene-flavin-phenothiazine triad (PYFPT), and their constituents -the phenyl-isoalloxazine (IAE), bromo-phenyl-isoalloxazine (BrPF), pyrene and 1-methylpyrene, heptyl-phenothiazine (HPT) and heptyl-phenyl-phenothiazine (HPPT)- have been characterized by absorption and emission spectroscopy. Absorption cross-section spectra, fluorescence quantum distributions, fluorescence quantum yields, degrees of fluorescence polarisation, and fluorescence lifetimes were determined. The photo-stability of the dyes has been investigated.

The two dyads and the triad retain the absorption spectral behaviour (spectral shape and absorption strength) of their constituents, indicating a weak coupling of their chromophores. The electron clouds of their constituents remain localized to them. The constituting moieties retain their identity. They may be considered as weakly coupled oscillators.

The dyads and the triad are electron donor-spacer-acceptor systems. Photo-excitation of one of the dyad or triad constituents brings the coupling between the constituent moieties strongly into action, quite similar to the excitation of one part of a coupled mechanical oscillator system. Due to the near distance between the dyad and triad constituents, exchange of excitation (Förster type energy transfer) occurs where the excited moiety gets deactivated and the adjacent moiety absorbing in the emission region of the excited moiety gets activated. Photo-excitation of the near distant chromophore in dyads or triad disrupts the lowest level population of the molecular orbitals of the constituents and a population re-equilibration by electron transfer sets in. Photo-excitation of the moiety with the lowest HOMO-level (HOMO=highest occupied molecular orbital) induces reductive electron transfer from the neighbouring moiety of higher lying HOMO-level. Photo-excitation of the moiety with the higher HOMO-level causes oxidative electron transfer if its LUMO level (LUMO=lowest

unoccupied molecular orbital) is energetically higher than of LUMO level of its neighbour moiety.

Both reductive and oxidative charge transfer quenches the fluorescence of the constituents. Depending on the coupling strength of the constituents after photo-excitation and depending on the solvent properties, either extremely fast charge-recombination, or charge-separation and charge-transfer-state stabilization may occur. This temporal behaviour determines the donor-acceptor system application in fast switching processes or in long-living bistable-state information storage devices.

In biology the photosynthetic apparatus is a refined electron donor-acceptor multi-molecular complex where energy-transfer, electron-transfer, charge separation stabilisation, and recovery to the initial state take place. The performed studies on a pyrene-flavin dyad, a phenothiazine-flavin dyad and a pyrene-flavin-phenothiazine triad may be considered as mimicry studies of the intricate dynamics occurring in photo-biological systems. Photoinduced energy transfer and electron transfer dynamics in biology [Mos92] is not limited to photosynthesis but also determines the photo-receptors dynamics [Häd99] of light driven biological process like vision, plant flowering or human circadian rhythm [Bri05, Bat03, Häd99].

7. References

- [Alb85]. T. A. Albright, J. K. Burdett, M. Whangbo, *Orbital interactions in chemistry*, (Willey, 1985).
- [Amm95]. F. Ammer, A. Penzkofer, P. Weidner, *Chem. Phys.* 192 (1995) 325.
- [Atk97]. P. W. Atkins and R. S. Friedman *Molecular Quantum Mechanics*, (Oxford University Press, Oxford, 1997).
- [Bal65]. C. J. Ballhausen, and B. G. Harry, *Molecular orbital theory*; (New York and Amsterdam: W. A. Benjamin, Inc. 1964).
- [Bat03]. A. Batschauer, *Photoreceptors and Light Signalling*, *Comprehensive Series in Photochemistry and Photobiology*, Vol. III, (The Royal Society of Chemistry, Cambridge, 2003).
- [Bau01]. H. Bauer, F. Stier, C. Petry, A. Knorr, C. Stadler, H. A. Staab, *Eur. J. Org. Chem.* (2001) 3255.
- [Ber71]. I. B. Berlman, *Handbook of Fluorescence Spectra of Aromatic Molecules* (Academic press, New York, 1971).
- [Bir69]. B. Birks, D. J. Dyson, *Proc. R. Soc. London A* 275 (1963) 135.
- [Bir70]. J. B. Birks, *Photophysics of Aromatic Molecules* (Wiley-Interscience, New York, 1970), p. 352.
- [Bod68]. C. Bodea, I. Silberg, in: *Advances in Heterocyclic Chemistry*, Vol. 9, edited by A. R. Katritzky and A. J. Boulton, (Academic Press, New York, 1968), pp. 321.
- [Bri05]. W. R. Briggs, J. L. Spudich, *Handbook of Photosensory Receptors*, (Wiley-VCH Verlag, Weinheim, 2005).

- [Car88]. F. L. Carter, R. F. Siatkowski, J. Wohltjen, *Molecular Electronic Devices*, (Elsevier, Amsterdam, The Netherlands, 1988).
- [Car93]. L. A. Carpino, *J. Am. Chem. Soc.* 115 (1993) 4397.
- [Cha88]. J. N. Chacon, J. McLearnie, R. S. Sinclair, *Photochem. Photobiol.* 47 (1988) 647.
- [Che06]. K.-Y. Chen, C.-C. Hsieh, Y.-M. Cheng, C.-H. Lai, P.-T. Chou, T. J. Chow, *J. Phys. Chem. A* 110 (2006) 12136.
- [Dau01]. J. Daub, R. Engl, J. Kurzawa, S. E. Miller, S. Schneider, A. Stockmann, M. R. Wasielewski, *J. Phys. Chem. A* 105 (2001) 5655.
- [Dex53]. D. L. Dexter, *J. Chem. Phys.* 21 (1953) 836.
- [Dmi91] V.G. Dmitriev, G.G. Gurzadyan, N.N. Nikogosyan, *Handbook of Nonlinear Optical Crystals*, (Springer Verlag, Berlin, 1991).
- [Dom77]. L. N. Domelsmith, L.L. Munchausen, K. N. Houk, *J. Am. Chem. Soc.* 99 (1977) 6506.
- [Dör66]. F. Dörr, *Angew. Chem.* 78 (1966) 457.
- [Drö03]. P. Drössler, W. Holzer, A. Penzkofer, P. Hegemann, *Chem. Phys.* 286 (2003) 409.
- [Eng99]. R. Engl, *Dissertation, Universität Regensburg*, 1999.
- [Fer01]. B.L. Feringa, *Molecular Switches*, (Wiley-VCH, Weinheim, 2001).
- [Fle86]. R. Fleming, *Chemical Applications of Ultrafast Spectroscopy* (Oxford University Press, New York, 1986).
- [För51]. Th. Förster, *Fluoreszenz organischer Verbindungen* (Vandenhoeck und Ruprecht, Göttingen, Germany, 1951).
- [Fri88]. W. Friedrich, *Vitamins*, (Walter de Gruyter, Berlin, 1988), pp. 445.
- [Ghi89]. S. Ghisla, V. Massey, *Eur. J. Biochem.* 181 (1989) 1.
- [Gra00]. H. Gratz, A. Penzkofer, *Chem. Phys.* 254 (2000) 363.
- [Häd06]. P. Häder, G. Jori, *Flavin Photochemistry and Photobiology*, (Elsevier, Amsterdam, The Netherlands, 2006).

- [Häd99]. D.-P. Häder, *Photosynthese*, (Thieme, Stuttgart, 1999).
- [Har80]. K. Hara, W. R. Ware, *Chem. Phys.* 51 (1980) 61.
- [Hee82]. P. F. Heelis, *Chem. Soc. Rev.* 11 (1982) 15.
- [Hee91]. P. F. Heelis, in: *Chemistry and Biochemistry of Flavoenzymes*, Vol. 1, edited by F. Müller, (CRC Press, Boca Raton, Fl. 1991), pp. 171.
- [Her67]. M. Hercher, *Appl. Opt.* 6 (1967) 947.
- [Her74]. A. H. Hertz, *Photographic Science and Engineering* 18 (1974) 323.
- [Hol99]. W. Holzer, M. Pichlmaier, A. Penzkofer, D. D. C. Bradley, W. J. Blau, *Chem. Phys.* 246 (1999) 445.
- [Hol05]. W. Holzer, J. Shirdel, P. Zirak, A. Penzkofer, P. Hegemann, R. Deutzmann and E. Hochmuth, *Chem. Phys.* 308 (2005)
- [Hop74]. J. Hopfield, *PNAS* 71 (1974) 3640.
- [Hus61]. N.S. Hush, *Trans. Faraday Soc.* 57 (1961) 557.
- [Isl03]. S D. M. Islam, A. Penzkofer, P. Hegemann, *Chem. Phys.* 291 (2003) 97.
- [Jor76]. J. Jortner, *J. Chem. Phys.* 64 (1976) 4860.
- [Jor97]. J. Jortner, M. A. Ratner, *Molecular Electronics*, (Blackwell, Oxford, 1997).
- [Kal77]. K. Kalyanasundaram, J. K. Thomas, *J. Am. Chem. Soc.* 99 (1977) 2040.
- [Kam71]. H. Kamin (Editor), *Flavins and Flavoproteins*, (University Park Press, Baltimore, 1971).
- [Kar80]. T. Karstens, K. Kobs, *J. Phys. Chem.* 84 (1980) 1871.
- [Kar95]. D. S. Karpovich and G. J. Blanchard, *J. Phys. Chem.* 99 (1995) 3951.
- [Kaw86]. Y. Kawanishi, N. Kitamura, S. Zazuke, *J. Phys. Chem.* 90 (1986) 2469.
- [Kaw86b]. Y. Kawanishi, N. Kitamura, S. Zazuke, *J. Phys. Chem.* 90 (1986) 6034.
- [Kir95]. P. Kirsch, A. Schönleben-Janás, R. H. Schirmer, *Liebigs Ann.* (1995) 1275.
- [Kir96]. P. Kirsch, R. L. Krauth-Siegel, A. Schönleben-Janás, P. R. E. Mittl, R. H. Schirmer, *J. Med. Chem.* 39 (1996) 1549.

- [Kna74]. W. R. Knappe, Ber. Dtsch. Chem. Ges. 107 (1974) 1614.
- [Kna76]. W. R. Knappe, in *Flavins and Flavoproteins*, edited by T. P. Singer, (Elsevier, Amsterdam, 1976), pp. 788.
- [Kön97]. B. König, M. Pelka, R. Reichenbach-Klinke, J. Schelter, J. Daub, Eur. J. Org. Chem. (2001) 2297.
- [Kop81]. B. Kopainsky, J. K. Hallermaier, W. Kaiser, Chem. Phys. Lett. 498 (83) 1981.
- [Kra01]. C. S. Kramer, K. Zeitler, T. J. J. Muller, Tetrahedon Lett. 42 (2001) 8619.
- [Kra91]. R. Krasnansky, J. Thomas, J. Photochem. Photobiol. A: Chem. 57 (1991) 81.
- [Lak99]. J. R. Lakowicz, *Principles of Fluorescence Spectroscopy*, Second Edition (Plenum press, New York, 1999).
- [Lan83]. F. W. Langkilde, E. W. Thulstrup, J. Michl, J. Chem. Phys. 78 (1983) 3372.
- [Lev59]. V.G. Levich, R.R. Dogonadze, Dokl. Akad. Nauk. USSR 124 (1959) 123.
- [Lia79]. P.Lianos, S. Georghiou, Photochem. Photobiol. 30 (1979) 355.
- [Lia80]. P. Lianos, B. Lux, D. Gerard, J. de Chimie Physique 77 (1980) 907.
- [Mah96]. G. Mahler, V. May, M. Schreiber, *Molecular Electronics – Properties, Dynamics, and Applications*, (Marcel Dekker, New York, 1996).
- [Mar56]. R.A. Marcus, J. Chem. Phys. 24 (1956) 966.
- [Mar85]. R.A. Marcus, N. Sutin, Biochim. Biophys. Acta 811 (1985) 265.
- [Mat96]. P. Mathis (Ed.), *Photosynthesis: From Light to Biosphere*, (Kluwer, Dordrecht, 1996).
- [McR64]. E. G. McRae, M. Kasha, in *Physical processes in Radiation Biology*, edited by R. Mason and B. Rosenberg, (Academic Press, New York, 1964), p. 23.
- [Mel61]. W. H. Melhuish, J. Phys. Chem. 65 (1961) 229.
- [Mos92]. C.C. Moser, J.M. Keske, K. Warncke, R.S. Farid, P.L. Dutton, Nature 355 (1992) 796.

7. References

- [Mül92]. F. Müller (Editor), *Chemistry and Biochemistry of Flavoenzymes*, Vol. 1-3 (CRC Press, Boca Raton, Fl. 1991-1992).
- [Mur93]. S. I. Murov, I. Carmichael, G. L. Hug, *Handbook of Photochemistry*, 2nd Edition (Marcel Dekker, New York, 1993).
- [Nak71]. A. Nakajima, *Bull. Chem. Soc. Japan* 44 (1971) 3272.
- [Nak73]. A. Nakajima, *Bull. Chem. Soc. Japan* 46 (1973) 2602.
- [Ots99]. J. Otsuki, K. Harada, K. Araki, *Chem. Lett.* 1999,269.
- [Pal97]. B. A. Palfey, V. Massey, in: *Comprehensive Biological Catalysis. A mechanistic Reference*, Vol. III: Radical Reactions and Oxidation / Reduction, edited by M. Sinnott, (Academic Press, San Diego, CA,1997), pp. 83.
- [Par68]. A. Parker, *Photoluminescence of Solutions* (Elsevier, Amsterdam, 1968).
- [Pen86]. Y. Lu, A. Penzkofer, *Chem. Phys.* 107 (1986) 175.
- [Per29]. F. Perrin, *Ann. Phys.* 12 (1929) 238.
- [Pet71]. O. G. Peterson, J. P. Webb, W. C. McColgin, J. H. Eberly, *J. Appl. Phys.* 42 (1971) 1917.
- [Pro04]. R. Procházka, *Dissertation*, Universität Regensburg, 2004.
- [Rag64]. J. B. Ragland, V. J. Kinross-Wright, *Anal. Chem.* 36 (1964) 1356.
- [Ram91]. V. Ramamurthy, *Photochemistry in Organized Constrained Media* (VCH Publishers Inc., New York, 1991).
- [Sad07]. K. Sadeghian, M. Schütz, *J. Am. Chem. Soc.* 2007, DOI: 0.1021/ja068536t.
- [Sai06]. M. Sailer, M. Nonnenmacher, T. Oesner, T. J. J. Müller, *Eur. J. Org. Chem.* (2006) 423.
- [Sai84]. M. Sainsbury, in: *Comprehensive Heterocyclic Chemistry*, Eds. A. R. Katritzky, C. W. Rees, (Pergamon Press, Oxford, 1984) Vol.3, p. 995.
- [Sai98]. M. Sainsbury, in *Rodd's Chem. Carbon Compd.* 2nd Edition, edited by M. Sainsbury (Elsevier, Amsterdam, 1998) Vol. 4, pp. 575-608

- [Sch01]. Schanz, S.A. Kovalenko, V. Kharlanov and N.P. Ernsting, *Appl. Phys. Lett.* 79 (2001), p. 566.
- [Sch90]. W. Scheidler, A. Penzkofer, *Opt. Commun.* 80 (1990) 127.
- [She02]. Z. Shen, J. Strauss, J. Daub, *Chem. Commun.* (2002) 460.
- [She03]. Z. Shen, R. Procházka, J. Daub, N. Fritz, N. Acar, S. Schneider, *Phys. Chem. Chem. Phys.* 5 (2003) 3257.
- [Shi06]. J. Shirdel, A. Penzkofer, R. Procházka, J. Daub, E. Hochmuth, R. Deutzmann, *Chem. Phys.* 326 (2006) 489.
- [Shi07a]. J. Shirdel, A. Penzkofer, R. Procházka, Z. Shen, J. Strauss, J. Daub, *Chem. Phys.* 331 (2007) 427.
- [Shi07b]. J. Shirdel, A. Penzkofer, R. Procházka, Z. Shen, J. Daub, *Chem. Phys.* 336(2007)1.
- [Shi07c]. J. Shirdel, A. Penzkofer, R. Procházka, Z. Shen, J. Daub, „Photo-induced Dynamics in a Pyrene-Isoalloxazine(Flavin)-Phenothiazine Triad” , *Chem. Phys.* (2007).
- [Son71]. P. S. Song, in: *Flavins and Flavoproteins*, edited by H. Kamin, (University Park Press, Baltimore, 1971), pp.37.
- [Spe87]. Sperber, M. Weidner, A. Penzkofer, *Appl. Phys. B* 42 (1987) 185.
- [Spe96]. Speiser, *Chem. Rev.* 96 (1996) 1953.
- [Sta94]. H. A. Staab, P. Kirsch, M. F. Zipplies, A. Weinges, C. Krieger, *Chem. Ber.* 127 (1994) 1653.
- [Ste97]. K. Stevenson, V. Massey, C. Williams (Editors), *Flavins and Flavoproteins*, (University of Calgary, Calgary, 1997).
- [Str02]. J. Strauss, *Dissertation*, Universität Regensburg, 2002.
- [Str04]. J. Strauss, J. Daub, *Organic Letters* 4 (2004) 683.
- [Str62]. J. Strickler, R. A. Berg, *J. Chem. Phys.* 37 (1962) 814.

7. References

- [Tri05]. C. Trieflinger, K. Rurack, J. Daub, *Angew. Chem. Int. Ed.* 44 (2005) 2288.
- [Val02]. B. Valeur, *Molecular Fluorescence. Principles and Applications.* (Wiley-VCH, Weinheim, 2002).
- [Van98]. D. A. Van Dyke, B. A. Pryor, P. G. Smith, M. R. Topp, *J. Chem. Ed.* 75 (1998) 615.
- [Vul05]. V. I. Vullev, H. Jiang, G. Jones, II, *Topics in Fluorescence Spectroscopy* 10 (2005) 211.
- [Wag05]. C. Wagner, M. Rist, E. Mayer-Enthart, H.-A. Wagenknecht, *Org. Biomol. Chem.* 3 (2005) 2062.
- [Wei93]. P. Weidner, A. Penzkofer, *Opt. Quant. Electron.* 25 (1993) 1.
- [Wei95]. P. Weidner, A. Penzkofer, *Chem. Phys.* 191 (1995) 303.
- [Win93]. F. M. Winnik, *Chem. Rev.* 93 (1993) 587.
- [Yag94]. K. Yagi, *Flavins and Flavoproteins*, (Walter de Gruyter, Berlin, 1994).
- [Zeg84]. M. van den Zegel, N. Boens, F. C. de Schryver, *Biophys. Chem.* 20 (1984) 333.

8. Acknowledgements

First of all, I would like to express my heartfelt gratitude to my supervisor, Prof. Dr. Alfons Penzkofer for giving me research opportunity under his guidance and then for his endless support, guidance and encouragement throughout my PhD.

I would also like to acknowledge Prof. Dr. J. Daub and Dr. R. Procházka, for synthesizing and providing samples which have been used in this work.

I am especially thankful to the secretaries of our group, Mrs. Elisabeth Schaffer and Mrs. Sigrid König for their kindness and help. I thank Anja Merkel for excellent technical assistance. I would also like to thank Dr. Wolfgang Holzer for his help during the initial stages of my PhD.

Special thanks to my friend and colleague, Peyman Zirak, for his friendship and encouragement during my studies and stay in Regensburg.

I also thank my friend, Keyarash Sadeghian for his friendship and many fruitful discussions during many of our coffee breaks.

I am also thankful to my colleagues and friends Ashu Kumar Bansal, for his friendship and his help and Amit Tyagi, for his help during writing my thesis. Also, my former colleagues Dr. Thomas Susdorf, Dr. Sang-Hun Song and my Spanish friend David Del Agua are gratefully thanked.

I also express my gratitude to my teacher in Iran, Prof. Habib Tajalli, for his wonderful guidance and encouraging me to go for research.

I am also thankful to DFG as this research was supported by Deutsche Forschungsgemeinschaft (DFG) under Graduate College, GK640/2, “Sensory photo-receptors in natural and artificial systems”.

Last but not the least, I am indebted to my parents and my whole family for their unconditional support and help during my studies.